REVIEW ON SYNTHESIS, CHARACTERIZATION AND ITS APPLICATION OF NANO PARTICLES

A THESIS SUBMITTED IN PARTIAL FULFILLMENT OF THE

REQUIREMENTS FOR THE DEGREE OF

Master of Philosophy (M.Phil)

CHEMISTRY

Submitted by

Mohd. Amish Khan

Under the Supervision of

DR. BIRENDRA PRATAP SINGH

UNIVERSITY INSTITUTE OF ENGEENRING TECHNOLOGY (U.I.E.T)

Chhatrapati Shahu Ji Mharaj (C.S.J.M) University Kanpur

Uttar Pradesh (208024) India 2015.

I DEDICATE

MY

DISSERTATION

WORK TO

MY GRAND

MATERNAL FATHER

BELOVED

DECLARATION

I Mohd Amish Khan hereby declare that, this dissertation thesis "**Synthesis, Characterization and its Application of Nano Particle",** submitted by me, under the guidance of **Dr. Birendra Pratap Singh**, **Ass. Professor**, (U.I.E.T) Kanpur, this University of my own and has not been submitted to any other University or Institute or Published earlier**.**

Mohd. Amish Khan

Date……

CERTIFICATE

This is to certify that the thesis entitled "**Synthesis, Characterization and its Application of Nano Particle,"** by Mohd. Amish Khan, submitted to the University Institute of Engineering Technology (U.I.E.T), Chhatrapati Shahu Ji Mharaj (C.S.J.M) University Kanpur for the Degree of Master of Philosophy (M.Phil) is a record of bonfide research work, carried out by his in the department of chemistry under my supervision.

I believe that the thesis fulfills part of the requirement for the award of Master of Philosophy. The results embodied in the thesis have not been submitted for the award of any other degree.

Date:

Place……

Dr. Birendra Pratap Singh
Dept. of Chemistry
(U.I.E.T), C.S.J.M.U, Kanpur

ACKNOWLWDGEMENT

"Little achievements often require long, tortuous effort and bitter experiences including some sacrifices. And this is only possible when the almighty God keep his Handful of blessings on the head of anybody, I would like to submit everything beneath the feet of God."

I would like to acknowledge my approbation and humility to my esteemed faculties and my admired guide **Dr. Birendra Pratap Singh, Ass. Professor, Dept. of Chemistry,** (U.I.E.T) C.S.J.M.U Kanpur, for his constant counseling and proper guidance throughout my dissertation Work.

I am extremely thankful to **Dr. Arpita Yadav, (H.O.D), dept. of Chemistry**, whose provide me for M. Phil. Course of Chemistry.

I am heartily thankful to Dr. Rashmi Dubey and Dr. Ratna Sukla for Special guidance dept. facultymember of Chemistry.

I am thanks to Liberian (I.I.T) Kanpur, (C.D.R.I.) and Science city of Lucknow for Understanding structure of Nano particle and center Library University campus Kanpur for providing necessary facilities for this research work my sincere thanks are due to Mrs. Shilpy Shigh, Dr. Abay krishna for Providing the healping hands and making for work on easy going task.

I would like to my Teachers Faculty Dr. N.P. Singh, (H.O.D) Y.D.P.G. College Lakhimpur Kheri and Associate Professor P.N. Tripathi, Dr. V.K. Dixit K.P.G. Colleg, Baharaich.

Now I would like to my respected friends circle Mr. Akhilesh Kumar SRF (C.D.R.I) Lucknow, Mr. Chandra Deo Pandey (NET,JRF) Central

University of Gujrat Mr. Muzib Khan (NET,JRF), Mr. Aniruddhra Chaudhari (NET,JRF) Lucknow University, Mis. Palvi (Ph.D.Scholers) I.I.T.Rurkee, Gazala khan (NET,JRF) Baba Saheb Bheemrao Ambedkar University Lucknow, Komodhi Yadav (Ph.D.Scholers) Centre University of Gujarat, Pragya Naulakha (Ph.D.Scholers) Centre University of (J.N.U) Delhi, Pardhi Singh (Ph.D. Scholers) ISOR Bhopal.

I carefully thank to my sister Shaziya khan Biotech. M. Tech, (G.B.T.U) Delhi for special helping hends.

I am also fathefull of my grand maternal father Mr. Haji Irshad Ahmad Khan retired Principle, for my great success and care.

Inadequate though in term of word and expression, this dissertation owes a lot to my beloved parents and my grand maternal father for their support, suggestion, inspiration, encouragement & good wishes for the success of my dissertation.

Lastl, I bow my head before my mother Smt. Najma Begam and my father Mr. Jalil Ahmad Khan for their supreme sacrifice & enernal benediction in evolving my personality .

PREFACE

This dissertation work is concerned with the representation of a newly discovered and modified Nanoparticle having nano scale dimention. It include many aspect such as introduction of the nano particle, synthesis and characterization, various new techniques for their presentation, modification for production hybrid Nano particle application in varies fields, their characterization using many spectroscopical, microscopical and scattering techniques such as IR, NMR, UV-Vis, Raman, SEM, TEM, AFM, STM, X-Ray, TGA, Zeta Potential etc, and focus on the future possibilities of their applications.

The Nano particles application over various field now a days and provides the advancement to the new technologies in the industrial as well as commercial field. It is now being used in chemical, physical as well as biological fields.

The nanoparticles are the miracle of nanotechnology which creates a miracle in the field of medical science especially in cancer cells. The engineered nanoparticles can be delivering to the target site which attracts by the diseased cells for allowing the direct treatment of the cells. The nanoengineered polymer matrix is used for light tubes with high efficiency which is shatter proof and has the capability of efficiency of compact fluorescence light bulbs. Engineered Nanoparticles are intentionally designed and created with physical properties tailored to meet the need as in the case of quantum dots or pharmaceutical drug.

The present dissertation work comprises of highlight of the review of synthesis, characterization and its application of the nanoparticles including

the literature work followed by references of the sans. The dissertation consists of four chapters. The first chapter is of the introduction of the nanoparticle, second chapter include the literature work of the review, the third chapter has conclusion of the literature and the end of the dissertation in the last chapter all the relative references are collectively listed.

CONTENTS

This dissertation consists of the following contents:-

LIST OF FIGURES

This dissertation consists of the following figures:-

ABBREVIATION

Techniques;

- SEM : Scanning electron microscope
- TEM : Transmuted electron microscope
- STM : Scanning tunneling microscope
- AFM : Atomic force microscope
- XRD : X – Ray diffraction
- UV- Visible : Ultra violate – Visible spectrophotometer
- NNR : Nuclear magnetic resonance
- FTIR : Fourier transform infrared spectroscope
- DLS : Dynamic light scattering

Units;

- nm : Nano Meter
- ns : Nanosecond
- µm : Micro Meter
- µL : Micro leter
- mV : Mili volt
- rpm : Rotation per Minute
- min : Minutes
- Hrs : Hours
- Å : Angstrom

Martials;

- ZnO : Zinc oxide
- TiO_2 : Titanium dioxide
- SiO_2 : Silicon dioxide
- MgO : Magnesium oxide
- $AgNO_3$: Silver Nitrate
- KBr : Potassium Bromide
- Ag NPs : Silver Nano Particle
- Au NPs : Gold Nano Particle
- Fe NPs : Iron Nano Particle
- Mo NPs : Molybdenum Nano Particle
- Al NPs : Aluminum Nano Particle

Historical background of Nano Science:

One of the historically important observations on the size dependent properties of materials came from the great scientist of 19th century. Many decades later in (1926) the first laboratory test proof on the size dependency of electronics properties of semiconductor had been published **[1].** Although nanotechnology is a relatively recent development in scientific research ,the development of its central concepts happened over a longer period of time .The emergence of nanotechnology in the 1980s was caused by the convergence of experimental advances such as the invention of the scanning tunneling microscope in 1981 and the discovery of fullerenes in 1985,with the elucidation and popularization of a conceptual framework for the goals of nanotechnology begging with the 1986 publication of the book Engines of Creation. The field was subjected to growing public awareness and controversy in the early 2000s, with prominent debates about both its potential implication as well as feasibility of the applications envisioned by advocates of molecular nanotechnology **[2].** In 1981 they were the first to see atoms and hence make nanotechnology a possibility .Scientist were soon able to pick up and move atom to build structures. Originally the term nanotechnology was restricted to these original experiments, which held no immediate practical use. However, as soon as the significance of the discovery was appreciated, interest increased, and the term has been more broadly used nanometer level **[3].** In recognition with this reality National Science and Technology Council (NSTC) of USA created an integration working group on Nano science, engineering and technology 1998th. Then in the year 2001 announced the National Nanotechnology Initiative (NNI) programme with a large amount of fund in the budgetary provision **[4]**.

Introduction:

Nano chemistry is a new branch of Nano science related with the production the reaction of nanoparticle and their compounds. It is concerned with the uniqes properties associated with assemblies of atoms or molecules or a scale between that of the individual building block and the bulk material from 1 to 1000 nm. His visionary paper Nano chemistry Synthesis in diminishing dimensions stimulated a whole new field it proposed how the principle of chemistry could be applied to the bottom up synthesis of materials 'overall length scales' through' building block hierarchical construction principle' that is by using molecular nanoscale building blocks **[5].** A micrometer also called a micron is one thousand times smaller than millimeter. It is equal to $1/1000000^{th}$ (one millionth of meter) things on this scale usually can't be seen with your eyes. The diameter of a hair which is 40 to 50 microns wide is very hard to discern without the use of a magnifying glass. A magnifying glass will help you see a dust nite. Dust mites are usually around 400 microns long **[6].** When Neil Armstrong first stepped onto the moon. He described it as a small step for a man and a giant leap for the mankind. Nanotechnology may represent another gint leap for the mankind but with a step so small that with respect to it Neil Armstrong would look like a solar system in size**.** In this Size range, the physical, chemical and biological properties of the nanoparticles changes in fundamental ways from the properties of both Individual atoms / molecules and of the corresponding bulk materials. Nanoparticles can be made of Materials of diverse chemical nature, the most common being metals, metal oxides, silicates, non-oxide ceramics, polymers, organics, carbon and biomolecules. Nanoparticles exist in several different morphologies Such as

spheres, cylinders, platelets, tubesetcetc **[7].** Metallic nanoparticles have different physical and chemical properties from bulk metals (e.g., lower melting points, higher specific surface areas, specific optical properties, mechanical strengths, and specific c magnetizations), When studying nanoparticles a distinction must necessarily be made between condensed "hard" matter nanoparticles, generally termed nanoclusters, and "soft" bio-organic nanoparticles and large molecules **[8].** There is emergent interest in developing biodegradable nanoparticle because of their application with small molecular drug, proteins or genes by either localized or targeted delivery to the tissue of interest. These biodegradable polymer based nanoparticles are conjugated with curative agents those are either entrapped or adhered chemically onto the polymer matrix. Although there are number of polymers that have been used for formulating biodegradable nanoparticles **[9].** Nano particles have size and shape dependent properties which make them totally different from bulk materials. Bulk materials have fixed properties regardless of their size but nanoparticles are totally different For example optical properties like refractive index and absorbance of a bulk material is fixed regardless of its mass or volume. But in nanoparticles optical properties are directly related to the size and shape of that specific nanoparticle. Quantum confinement is an important phenomenon in nanotechnology **[10].** Nanoparticles have a very high surface area to volume ratio. This provides a tremendous driving force for diffusion, especially at elevated temperatures. Sintering can take place at lower temperatures, over shorter time scales than for larger particles. This theoretically does not affect the density of the final product, though flow difficulties and the tendency of nanoparticles to agglomerate complicates matters. The large surface area to volume ratio also reduces the incipient melting temperature of nanoparticles

[11].Nanoparticles displays a wide variety of chemical and physical properties (e.g. mechanical properties, biological and sterile properties, catalytic properties, thermal and electrical conductivity, optical absorption and melting points) compared to the bulk of same substance. Thus, by modifying and controlling the size and shape at nano metric level, nanoparticles exhibit interesting dependence of properties like bio sensing, catalytic activity, optical activity, antimicrobial activity etc on the mentioned parameters **[12].** Nano Zinc Oxide particles have been found to have superior UV blocking properties compared to its bulk substitute. This is one of the reasons why it is often used in the sunscreen lotions. Clay nanoparticles when incorporated into polymer matrices increase re-enforcement, leading to stronger plastics, verified by a higher glass transition temperature and other mechanical property tests. These nanoparticles are hard, and impart their properties to the polymer (plastic). Nanoparticles have also been attached to textile fibers in order to create smart and functional clothing **[13].**

The different field of nanoparticle-

Quantumdots, Nanocluster, Liposomes, FunctionalizedNPs, IronoxideNPs, Ag, Fe, Al, Bi, Mo, Nanoparticle, Carbonnanotube, GoldNPs, PolymerNPs, Dendrimers, MicroandNanobubbles, UpconvertingNPs, Iron,platinumNPs, Nanodevices, Nanotransisters, Nanocell, Nanocapsules, Nanoforum, Nanosphere, Nanofibers, Nanoribbon, Nanopipette, Nanowires, Nanobds, Nanohorn, Nanospring, Nanoneedles, Nanoarray, Nanobelts, Nanopolymers, Nanobomb, Nanofluids, NanocompopsitsNanocontilever, Nanoplates, Nanoceramics, Nanochannels, anosensors, Nancages , Nanobeam, Nanobots, Nanoshell, Nanosim etc.

Application of Nano Science & Technology:

By Nanotechnology:-

Now-a-days nanotech solar cells are developed which are comparatively of lower cost than the conventional solar cell. Solar steam light is a successful invention of nanotechnology due to the scarcity of electricity which is useful in case of the wide application of water purification and disinfecting if the dental instruments. The fuel cells by changing the spacing between the platinum atoms which can be used in the fuel cells to increase the catalytic ability of the platinum. It allows the fuel cell to function with about 80% less platinum which can appreciably and considerably reduce the cost of the fuel cell. The wires with carbon nanotubes are lower resistance than the wires of electric transmission grid. The radical change of the electricity distribution grid is now possible by nanotechnology **[14].**

In Cancer Therapy:-

The nanoparticles are the miracle of nanotechnology which creates a miracle in the field of medical science especially in cancer cells. The engineered nanoparticles can be delivering to the target site which attracts by the diseased cells for allowing the direct treatment of the cells. For example, nanoparticles which deliver chemotherapy drugs directly to the cancer cells are under development. When the nanoparticles attach to cancer tumors, the nanoparticles release the biomarkers molecules known as the peptides. In this technique, the each nanoparticle carries several peptides of a very high concentration of these markers which will occur at very early stages of cancer and also allowing the early detection of the disease. The early

detection method for brain cancer under the development uses magnetic nanoparticles and NMR technology. The magnetic nanoparticles attach to the particles in the blood stream known as micro vesicles which originate in brain cancer cells. The NMR technique is used to detect these micro vesicles or magnetic nanoparticle clusters which allows the early diagnosis. The iron nanoparticles can be used to improve the MRI technique of the cancer cells. The nanoparticles coated with a peptide which binds to a cancer tumor cells. Once the nanoparticles are attached to the cancer tumor cells, then the magnetic property of the iron oxide enhances the images from the MRI scan. Bismuth nanoparticles are used for the radiation therapy for the treatment of cancer. The preliminary results specify the bismuth nanoparticles can increase the dose to the tumor by 90 percent. The carbon nanotubes and gold nanoparticles are being used in a sensor which detects proteins investigative of the oral cancer **[15].**

In Drug Delivery:

The diagnosis of early detection of the kidney damage is being developed by the use of gold nanorods which are functionalized to attach the proteins generated by the 36 damaged kidneys. The color of the nanorod changes when protein accumulates on the nanorod. The proteins can attach to damaged portions of the arteries. This technique provides the delivery of drugs to the damaged regions of arteries to fight against the cardiovascular disease. Functionalized metals with proteins have been used biolabels for ex antibody molecule coated gold particles of 10 – 40 nm size are routinely used in histology as biolabel. Nucleic acid coated nanoparticles can be used as sensors in biomedical digonosis such sensor can detect pathogenic nuclec acids. Burn dressings are treated by the nanocapsules containing antibiotics. The infection produced by the harmful bacteria in the wound causes the

breaking of the nanocapsules for the release of antibiotics which allows a quicker treatment of an infection and reduces the number of frequencies of dressing. The earliest nanomedicine application was the use of nanocrystal which acts as an antimicrobial agent for the treatment of wounds. The most common silver nanocrystal is used as an antimicrobial agent for the treatment of wounds **[16].**

In Engineering:

The nano engineered polymer matrix is used for light tubes with high efficiency which is shatter proof and has the capability of efficiency of compact fluorescence light bulbs. Engineered Nanoparticles are intentionally designed and created with physical properties tailored to meet the need as in the case of quantum dots or pharmaceutical drug. Electrodes made from nanowires that would enable flat penal displays to be flexible as well as thinner than current flat panel displays. Using MEMS techniques to control an arrays of probes when tip have a radius of a few nanometers. These probe are used to write and read data on to a polymer film. None engineered Nanoparticle, on the other hand are unintentionally generated or naturally produced such as atmospheric nanoparticle created during combustion **[17].**

Classification of Nano particle:-

Nanoparticles can be broadly grouped into two: namely organic and inorganic nanoparticles. Organic nanoparticles may include carbon nanoparticles (fullerenes) while some of the inorganic nanoparticles may include magnetic nanoparticles, noble metal nanoparticles (likegoldandsilver) and semiconductor nanoparticles (like titanium dioxide and zinc oxide). There is a growing interesting inorganic nanoparticle as they provide superior material properties with functional versatility. Due to their size features and advantages over available chemical imaging drugs agents and drugs, inorganic nanoparticles have been examined as potential tools formedical imaging as well as fortreating diseases. Inorganic nanomaterials have been widely used forcellular delivery due to their versatile features like wide availability, rich functionality, good biocompatibility, Capability of targeted drug delivery and controlled release of drugs **[18].** For example meso porous silica when combined with molecular machine sprove to be excellent imaging and drug releasing systems. Gold nanoparticles have been used extensively in imaging, as drug carriers and in thermo therapy of biological targets. Inorganic nanoparticles (such as metallic and semiconductor nanoparticles) exhibit intrinsic optical properties which may enhance the transparency of polymer – particle composites. For such reasons, inorganic nano particles have found special interest in studies devoted tooptical properties in composites. For instance, sizedependant colour of gold nanoparticles has been used to colour glass for centuries **[19].**

Scale of Nanoparticle:

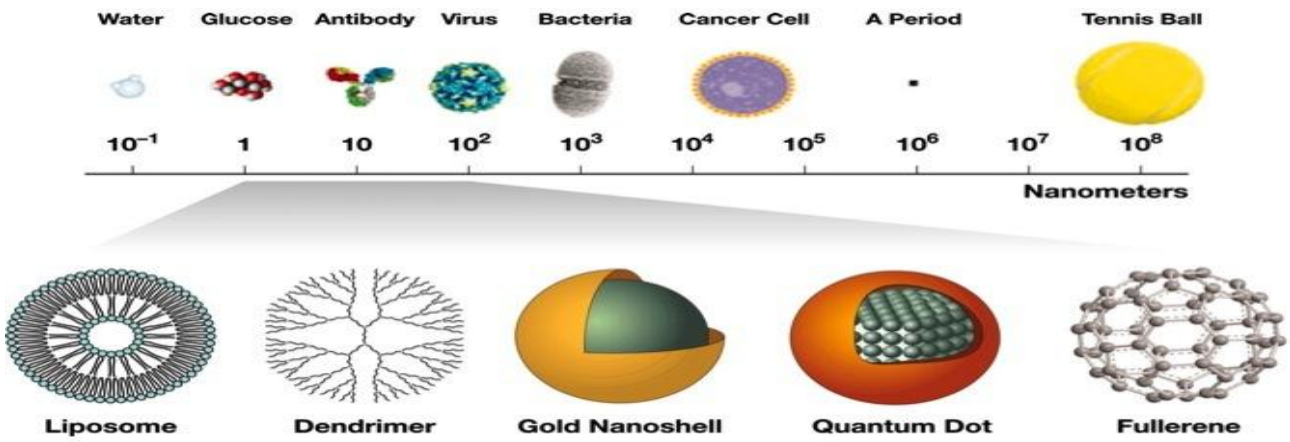

Synthesis of Nano Particle:-

Nanoparticles can be synthesized using various approaches including chemical, physical, and biological. Although chemical method of synthes is requires short period of time for synthesis of large quantity of nanoparticles, this method requires capping agents for size stabilization of then anoparticles. Chemicals used for nanoparticles synthesis and stabilization are toxic and lead to non – ecofriendly by products. The need for environmental non-toxic synthetic protocols for Nanoparticles synthesis leads to the developing interest in biological approaches which are free from the use of toxic chemicals as by products **[20].** Among them simple-solution based methods, chemical precipitation, sol-gel, solvothermal or hydrothermal, electrochemical and photochemical reduction method are preferable methods **[21].** Traditionally nanoparticles were produced only by physical and chemical methods. Some of the commonly used physical and chemical methods are ions puttering, salvo thermal synthesis, and reduction, sol gel technique. Basically there are two approaches for nanoparticle synthesis namely the Bottom up approach and the Top down approach **[22].** In

general, top-down approaches are easier to use and less expensive but have less control over the size distribution and also could be destructive. Among others, the biggest problem with top-down approach is the imperfection of the surface structure. It is well known that the conventional top-down techniques such as lithography can cause significant crystallographic damage to the processed patterns and additional defects may be introduced even during the etching step **[23].** The bottom-up approach usually employs solution-phase colloid chemistry for the synthesis. In a typical colloidal synthesis, atoms of the desired component are produced in the solution at very high super saturation to induce the assimilation of these atoms into particles to reduce the system Gibbs free energy. Due to the flexibility in selecting different reducing agents, particle capping agents, solvent systems as well as synthesis conditions, colloidal synthesis offers a great variety of options for composition, shape, size and surface chemistry control. The bottom-up approach is also suitable for controlling mono dispersity of the nanoparticles. With all these advantages, the bottom-up approach has become the main route to nanomaterial production **[24].**

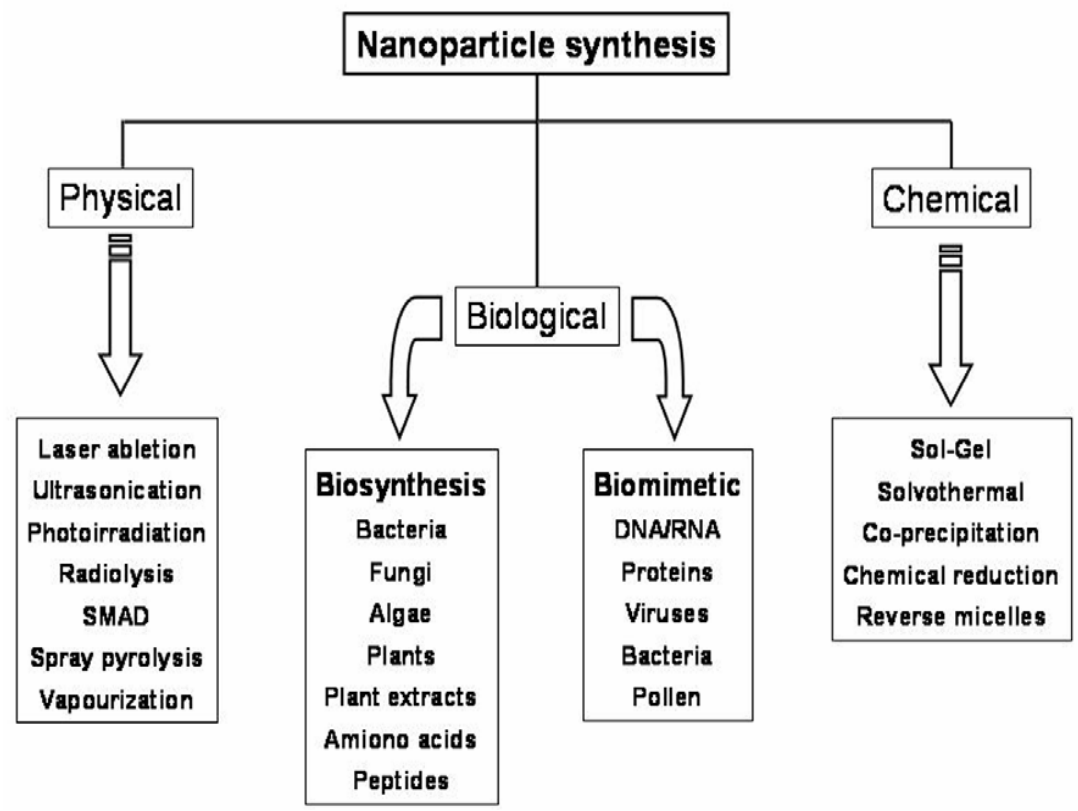
Nanoparticle synthesis
Physical
Biological
Chemical
Laser ablation
Ultrasonication
Photoirradiation
Radiolysis
SMAD
Spray pyrolysis
Vapourization
Biosynthesis
Bacteria
Fungi
Algae
Plants
Plant extracts
Amiono acids
Peptides
Biomimetic
DNA/RNA
Proteins
Viruses
Bacteria
Pollen
Sol-Gel
Solvothermal
Co-precipitation
Chemical reduction
Reverse micelles

The synthesis routes of Nanoparticle are following.

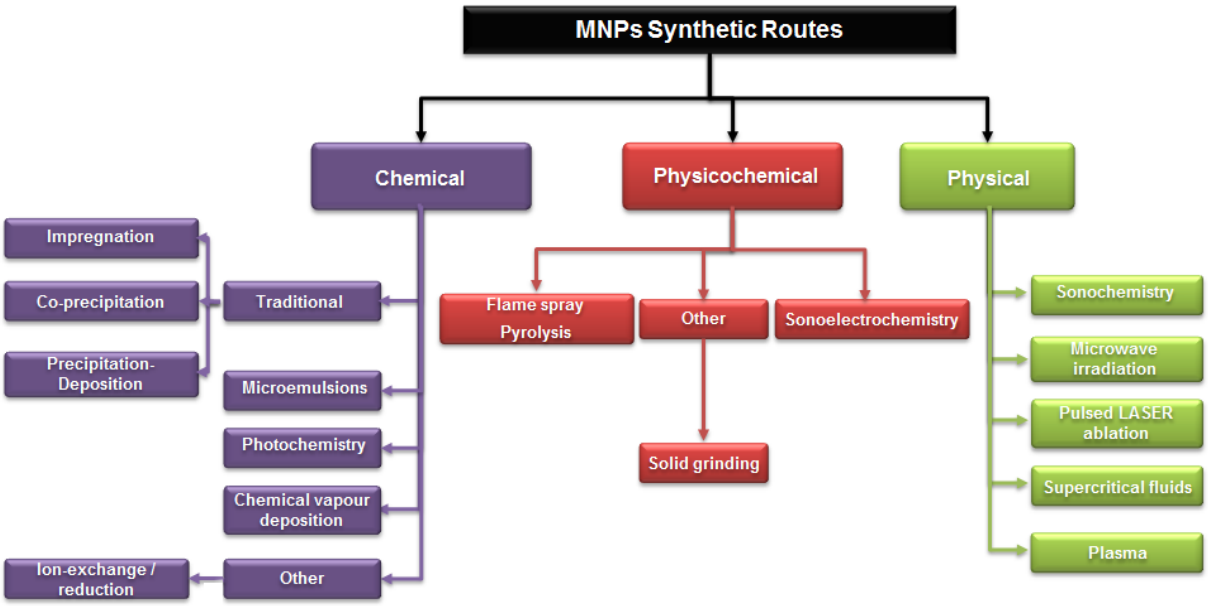

By Physical method:-

Physical methods developed for synthesis of ZnO nanoparticles of ten require special equipments or operational control. The physical method often called top - down approach which includes methods like diffusion, irradiation, thermal decomposition and arc discharge etc. The thermal decomposition method is one of the significant top -down approach. It is used for the creation of mono disperse nanoparticles. These approaches use larger initial structures or macroscopic units which can be externally controlled in the processing of nanostructures. Etching through the mask; Ball milling and application of severe plastic deformation are common examples of physical top - down method of synthesis of nanoparticles. The top - down method of synthesis is a model which generates on a larger scale for further reduction of Nano scale. Mostly the top - down methods are not

cheap and quick to manufacture. This method is slow and not suitable for large scale production **[25].**The synthesize nanostructure utilizes a vapour transport process. There are several ways to generate Zn and oxygen vapor. Decomposition of ZnO is a direct and simple method; however, it is limited to very high temperature .The indirect methods to provide Zn vapor include metal organic vapour epitaxy, in which organ metallic Zn compound, diethyl zinc for example is used under appropriate oxygen or N_2O flow. According to the difference on nanostructure formation mechanism, the extensively used vapour process can be categorized into the catalyst free vapour solid (VS) process and catalyst assisted vapor liquid solid (VLS) process **[26].**

By chemical method:-

Moderate reaction conditions and convenient synthetic manipulation have rendered Chemical methods an attractive option for accessing ZnO nanoparticles. Traditional chemical routes that are frequently used in recent years include sol-gel approach, chemical precipitation and colloidal synthesis. Surfactants or polymer based preparative method for ZnO nanomaterials are also quite popular to avoid agglomeration and achieve better control of ZnO nanoparticles. Removal of surfactants or polymers, however, poses serious limitations to such methods. Hence, delicate and precise control of experimental factors for the synthesis of nanoparticles with desired morphologies is a cherished goal for future device applications. Homogeneous chemical precipitation method is often considered economically viable for preparation of mono disperse metal oxide particles of different shapes and sizes. The method also provides better control of chemical and morphological characteristics **[27].** The wet chemical method of synthesis of nanoparticles in detail which is most widely used technique

as far as antibacterial property is concerned. These chemical methods may be based on the kinetic control of nucleation and growth of the particles on electrostatic stabilization in aqueous suspense on or on the introduction of constraints. The former category however includes “the bottom-up” method of salt reduction known as wet-chemical method **[28].** During the synthesis of inorganic nanoparticles by chemical precipitation method, the kinetics of nucleation and particle growth in homogeneous solutions can be adjusted by the controlled release of anions and captions. Careful control of precipitation kinetics can result in mono disperse nanoparticles. Once the solution reaches a critical super saturation of the species forming particles, only one burst of nuclei occurs. Thus, it is essential to control the factors that determine the precipitation process, such as the pH and the concentration of the reactants and ions. Organic molecules are used to control the release of the reagents and ions in the solution during the precipitation process. The particle size is influenced by the reactant concentration, pH, and temperature. By engineering these factors, nanoparticles with narrow size distributions, such as $Zr(OH)_4$, Ba-TiO_3, $YBaCu_3Oy$, CdS, HgTe, and CdTe, have been produced. Although the method of using precipitation to prepare nanoparticles is very straight forward and simple, very complicated nanostructures can also be constructed using this method such as CdS/HgS/CdS, CdS/(HgS)2/CdS and HgTe/CdS quantum well systems and other core/shell structures **[29].**

By Biological method:-

Green synthesis method is proved as beneficial over other methods which are. Implemented for the synthesis of nanoparticles. Green synthesis methods are ecofriendly approach and compatible for pharmaceutical and other biomedical applications, as the toxic chemicals are not used in these methods. Besides, this method does not require high pressure, temperature. Synthesis of various nanoparticles by microorganisms is used more than the other techniques due to its ecofriendly nature. The use of environmentally beneficial materials like plant leaf extract, bacteria, fungi and enzymes for the synthesis of zinc nanoparticles proposes abundant benefits of Eco friend lines and compatibility for pharmaceutical and many other biomedical applications **[30].** Synthesis of inorganic nanomaterials can be effected by using different biomolecules. One of the fundamental processes involved in the regulation of mineral deposition in biological organisms is the organic matrix composed of proteins or other biological macromolecules that controls the nucleation and growth of inorganic structures. Realization of this fact has led many materials scientists to explore proteins identified from biomineralizing organisms as 'enzymes' for materials synthesis in vitro. In such systematic attempts a limited success has been achieved in synthesizing inorganic nanoparticles with specific compositions, sizes and shapes. Since, proteins are known to initiate, catalyze and fabricate nano/micro structures, attempts have been made to synthesize various nanostructures using the proteins isolated from biominerals, with which they are associated **[31].** In recent times, the plant extracts are widely used

as a viable and facile alternative strategy for the synthesis of metal nanoparticles rather than physical and chemical methods. The presence of various secondary metabolites, enzymes, proteins and/or other reducing agents with electron-shuttling compounds are usually involved in the synthesis of metal nanoparticles by plant components. In bioaccumulation, the localization of nanoparticles is based on the presence of particular enzymes or proteins involved in it. The recovery of these nanoparticles from plant tissues is not only tedious but expensive and also needs enzymes to degrade the cellulosic materials. Thus, the synthesis of various metal nanoparticles using plant extracts is easy in downstream processing and in scaling up of nanoparticles **[32].**

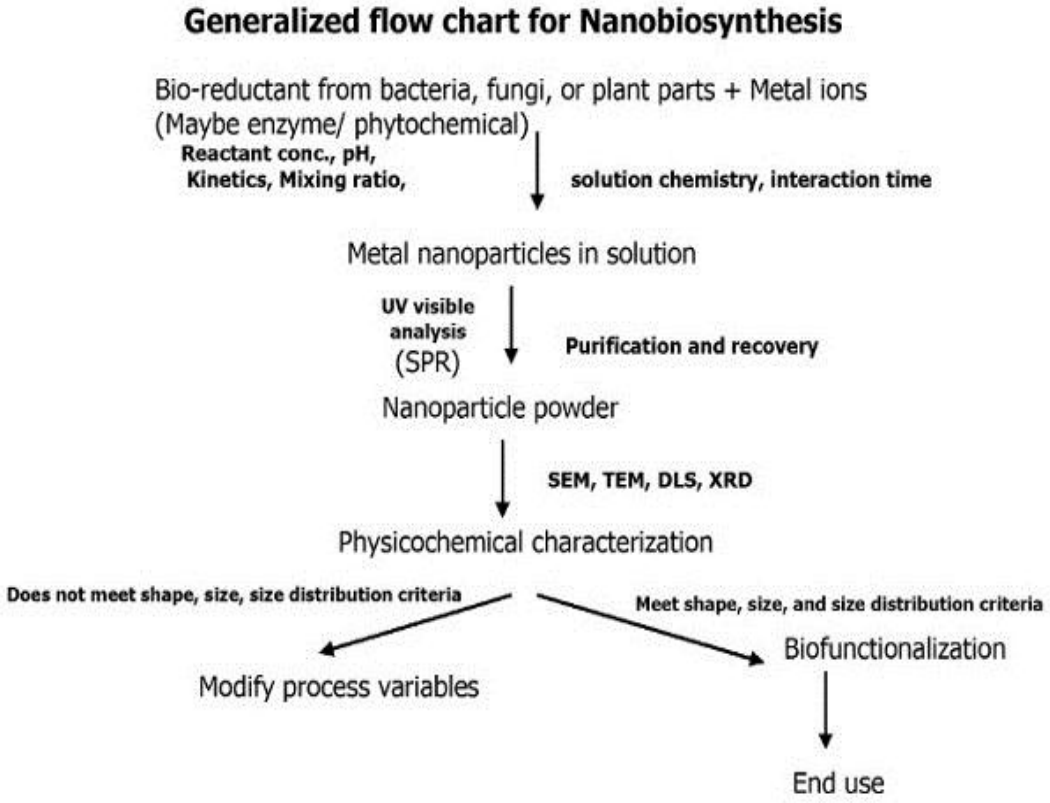

Top down approach:-The top–downapproach is a subtractive process starting from bulk materials to make nanomaterials. This approach involves division of bulk material or miniaturization of bulk fabrication process to produce the desired structure with the appropriate properties. This includes some of the following commonly used methods: Attrition or Ball milling, Photolithography, Electron beam lithography, Machining. In general, top-down approaches are easier to use and less expensive but have less control over the size distribution and also could be destructive. Among others, the biggest problem with top-down approach is the imperfection of the surface structure. It is well known that the conventional top-down techniques such as lithography can cause significant crystallographic damage to the processed patterns and additional defects may be introduced even during the etching steps. For example, nanowires made by lithography are not smooth and may contain a lot of impurities and structural defects on surface. Such imperfections would have a significant impact on physical properties and surface chemistry of nanostructures and nanomaterials, since the surface-to-volume ratio in nanostructures and nanomaterials is very large. The surface imperfection would result in a reduced conductivity due to in elastic surface scattering, which in turn would lead to the generation of excessive heat and thus impose extra challenges to the device design and fabrication. Regardless of the surface imperfections and other defects that top-down approaches may introduce, this is the method of choice when highly complex structures are made. This is the case in the integrated circuit industry, where nanosized structures are cut in plain silica wafers using laser **[33].**

These seek to arrange smaller components into more complex assemblies. DNA nanotechnology utilizes the specificity of Wastson – Crick base

pairing to construct well –define structures out of DNA and other nucleic acids. Approaches from the field of 'Classical' chemical synthesis (Inorganic and organic synthesis) also aim at designing molecules with well – defined shape (bio peptides) More generally ,molecular self – assembly seeks to use concepts of supra molecular chemistry ,and molecular reaction in particular ,to cause single- molecule components to automatically arrange themselves into some useful conformation. Atomic force microscopic tips can be used as a nanoscale 'write head' to deposit a chemical upon a surface in a desired pattern in a process called dip pen nanolithography. This technique fits into the large subfield of nanolithography **[34].**

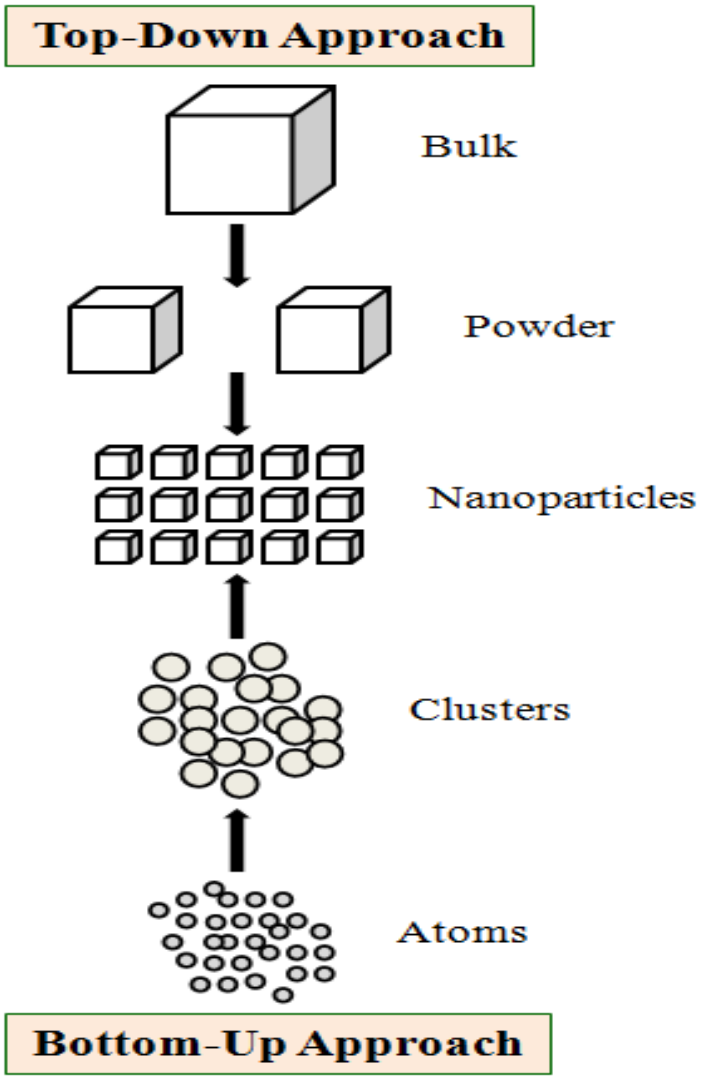

Bottom up approach:-

Bottom-up approach is a controlled additive process that deals with the assembly of precursor Atoms or molecules to make nanomaterials. In this approach, atoms, molecules or clusters are used as the building blocks for the creation of complex nanostructures. Though the bottom-up Approach mostly used in nanotechnology, it is not a newer concept. All the living beings in nature observe growth by this approach only. Bottom-up methods are chemically controllable and non-destructive. The synthesis of nanoparticles from molecular solutions is a good

Example of a bottom - up approach. The size of the nanostructures, which can be obtained with a bottom-op approach, spans the full nano scale. An advantage of the bottom-up approach is the better possibilities to obtain nanostructures with less defects and more homogeneous Chemical compositions. This is due the mechanisms utilized in the synthesis of nanostructures reducing the Gibbs free energy, so that the produced nanostructures are in a state closer to a thermodynamic equilibrium .Some of the important methods involved are: Sol-gel method, Vapour phase deposition method, Chemical reduction method. The bottom-up approach usually employs solution-phase colloid chemistry for the synthesis. In a typical colloidal synthesis, atoms of the desired component are produced in the solution at very high super saturation to induce the assimilation of these atoms into particles to reduce the system Gibbs free energy. Due to the flexibility in selecting different reducing agents, particle capping agents, solvent systems as well as synthesis conditions, colloidal offers a great variety of options for composition, shape, size and surface chemistry control. The bottom-up approach is also suitable for controlling mono dispersity of the nanoparticles. With all these advantages, the bottom-up approach has become the main route to nanomaterial production. Among all bottom-up methods, the chemical reduction of the metal salt in an aqueous, an organic phase or two phases, is one of the most popular routes as nanoparticles of a wide range of sizes and shapes can be prepared by controlling the reaction conditions. The reduction of gold salts in existing of a stabilizing agent is a facile and easy technique to produce desired sizes of nanoparticles **[35].**

These seek to create smaller devices by using larger ones to direct their assembly. Many technologies that descended from convention al solid state silicon methods for fabricating microprocessors are now capable of creating

features smaller than 100 nm ,falling under the definition of nanotechnology .Giant magneto resistance based hard drives already on the market fit this description , as do atom layer deposition techniques. Solid state techniques can also be used to create devices known as nanoelectromechanical systems or NEMS, which are reacted to micro electro mechanical systems on MEMS. Focused ion beam can directly remove material, or even deposit material when suitable pre – cursor gasses are applied at the same time .Atomic force microscope tips can be used as a nanoscale 'write head' to deposit a resist, which is then followed by an etching process to remove material in a top down method **[36].**

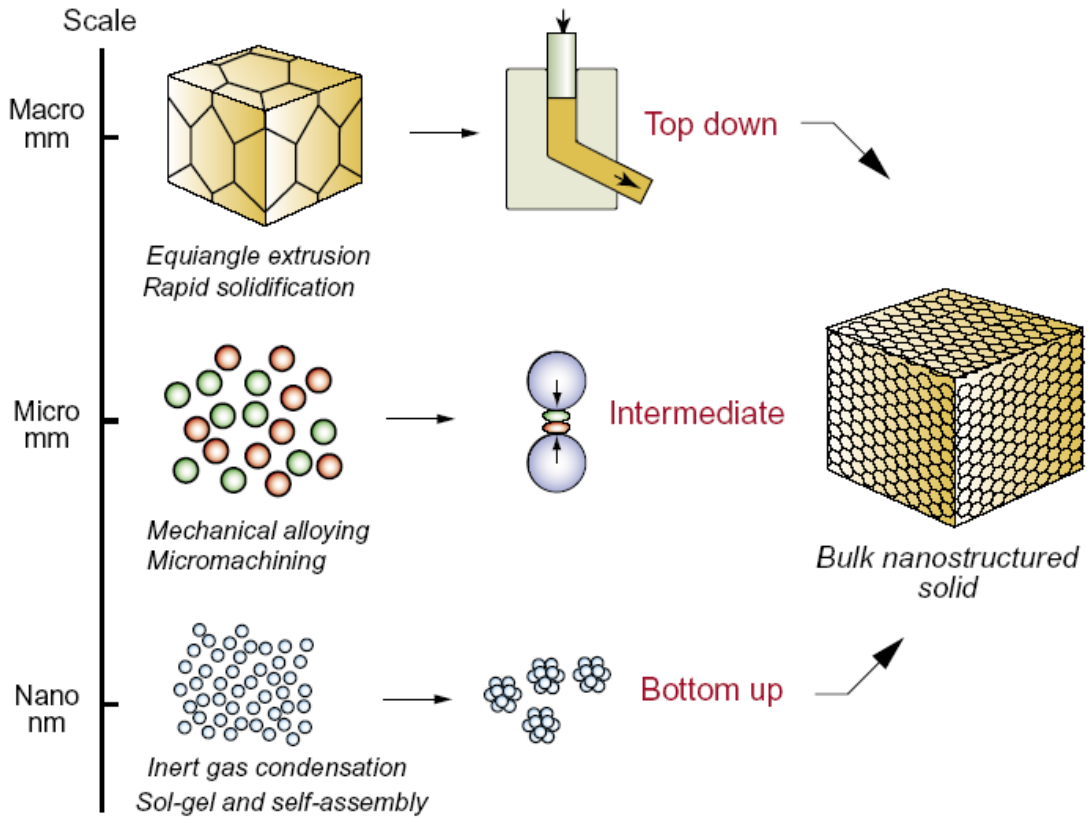

Different type Method to Preparation of Nano Particle:-

Physical Methods:-

Evaporation methods: Physical vapor depositions (PVD), sputtering and chemical vapor deposition (CVD) are the commonly used methods to form thin films of inorganic nanomaterials **[70].** PVD involves condensation from the vapor phase. The PVD process is composed of three main steps: (a) generating a vapor phase by evaporation or nanowire, ZnO nanorod, GaO nanobelt and nanosheet, SnO_2 nanowire, nanoribbon, nanotube, etc., have been synthesized using PVD. In CVD, the carrier gases containing the elements of the desired compound flow over the surface to be coated. This surface is heated to a suitable temperature to allow decomposition of the carrier gas and to allow the mobility of the deposited atoms or molecules on the surface. The CVD process consists of three steps: (a) mass transport of reactants to the growth surface through a boundary layer by diffusion, (b) chemical reactions on the growth surface, and (c) sublimation of the material, (d) transporting the material from the source to the substrate, and (e) formation of the particle and/or film by nucleation and growth. Different techniques have been used to evaporate the source such as electron beam, thermal energy, sputtering, cathodic arc plasma, and pulsed laser.

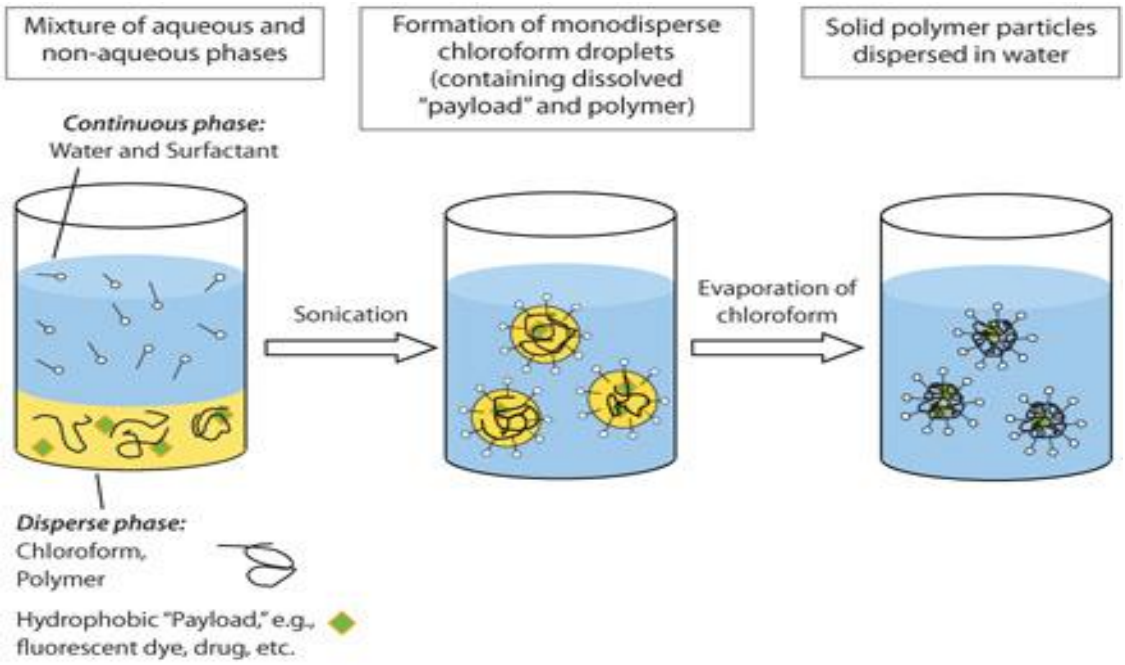

***Solvated metal atom deposition (SMAD)*:** Most metals vaporize as atoms, which are highly reactive as a result of the input of the heat of vaporization and the lack of steric interactions. The basic strategy in this process is to co–deposit the metal atoms with a large excess of reactant, thereby promoting reaction between the metal atom and the substrate and suppressing recombination to the bulk metal. In SMAD, a bulk metal is evaporated under vacuum and the vapors of the metal are co-condensed with vapors of organic solvents like acetone to form nanoparticles in solution using a physical method **[71].** Evaporation of metal is achieved by electrically heating a metal wire under vacuum. The resulting solution would consist only of colloids and solvent with no byproducts of gold salt. Polar protic or aprotic solvents yield generally stable colloids but those with nonpolar organic solvents and water yielded large gold particles that undergo irreversible

precipitation. SiO_2, Co-Mn and Pt-Sn alloys, metallic nanoparticles like Au etc have been synthesized using SMAD.

Laser ablation: When intense laser pulses are focused on a metal target, metal atoms present in the exposed region will be desorbed. In a Laser ablation experiment, a bulk metal is immersed in a solvent containing surfactant. During the laser irradiation, the metal atoms will vaporize and are immediately solvated by the surfactant molecules to form nanoparticles in solution **[72].** The intensity of the laser pulse and time of exposure are two parameters, which control the size of the nanoparticles formed during laser ablation. Metal nanoparticles such as gold, silver and platinum nanoparticles are prepared by this way with good control over size.

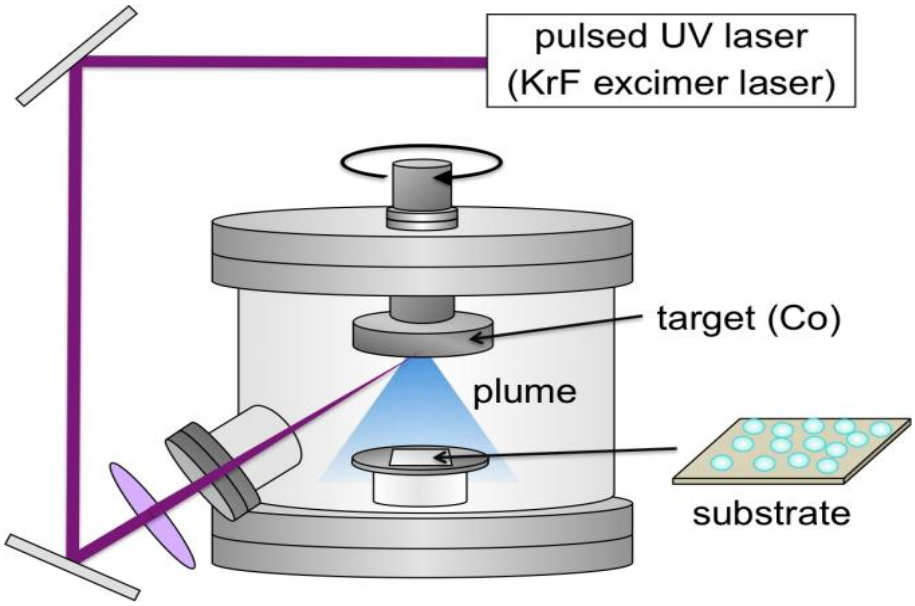

Photolytic and radiolytic methods: - These methods involve the reduction of metal salts by radio lytically produced reducing agents such as solvated electrons and free radicals and the photolysis of metal complexes in the presence of some donor ligands **[73].** Radiolysis of aqueous solutions of metal ions gives solvated electrons that may directly react with the metal ions or with other dissolved materials to produce secondary radicals, which then reduce the metal ions to form nanoparticles. Alcohols are known to form radicals when they are irradiated with UV light. Radicals thus generated by this way can reduce the metal ions to form nanoparticles when UV light is irradiated on mixture of aqueous metal ions and alcohols metallic nanoparticles like gold and silver has been synthesized by this method.

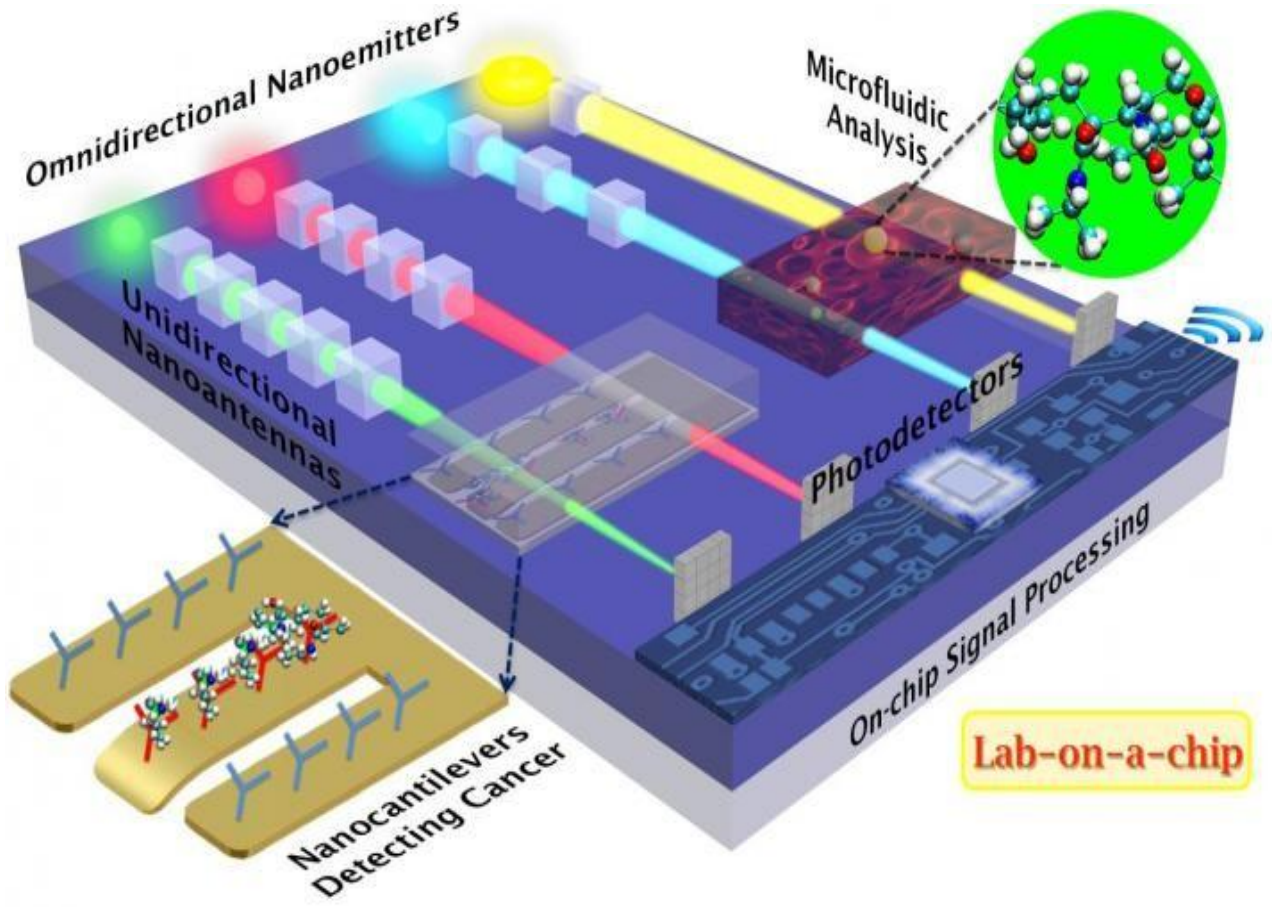

Electrochemical discharges Method:-

Electrochemical discharges occur under extreme current densities in an aqueous electrolyte. The phenomenon is characterized by a sudden breakdown of the conductivity accompanied by the formation of an insulating gas layer around the electrode. Discharges or sparks occur across this gas film. If the electrolyte contains metal salt and if the working electrode is the cathode, while most of the discharge current is used up for production of H_2 bubbles, a part of it converts M^+ to M which group to form clusters. The clusters are prevented from depositing on the electrode surface by the gas film. The method has been used for several metals and allows to create particles from 10-150nm. A mechanism to control the size has been

developed based on rotation speed of the working electrode. It is estimated that this method should allow controlling the size of particles to ≈ 10 nm quite easily **[74].**

Polymerization Method:-

In this method, monomers are polymerized to form nanomaterials in an aqueous solution. Drug is incorporated by adsorption onto the nanoparticles or by dissolving in the polymerization medium after polymerization has been completed. The suspension is then puried to remove stabilizers and surfactants which were used for polymerization by ultracentrifugation and then re-suspending the particles in a medium free of isotonic surfactants. This technique is suitable for making poly (alkylcyanoacrylate) or polybutylcyanoacrylate nanoparticles. The particle size depends on the concentration of the stabilizers and surfactants used **[75].**

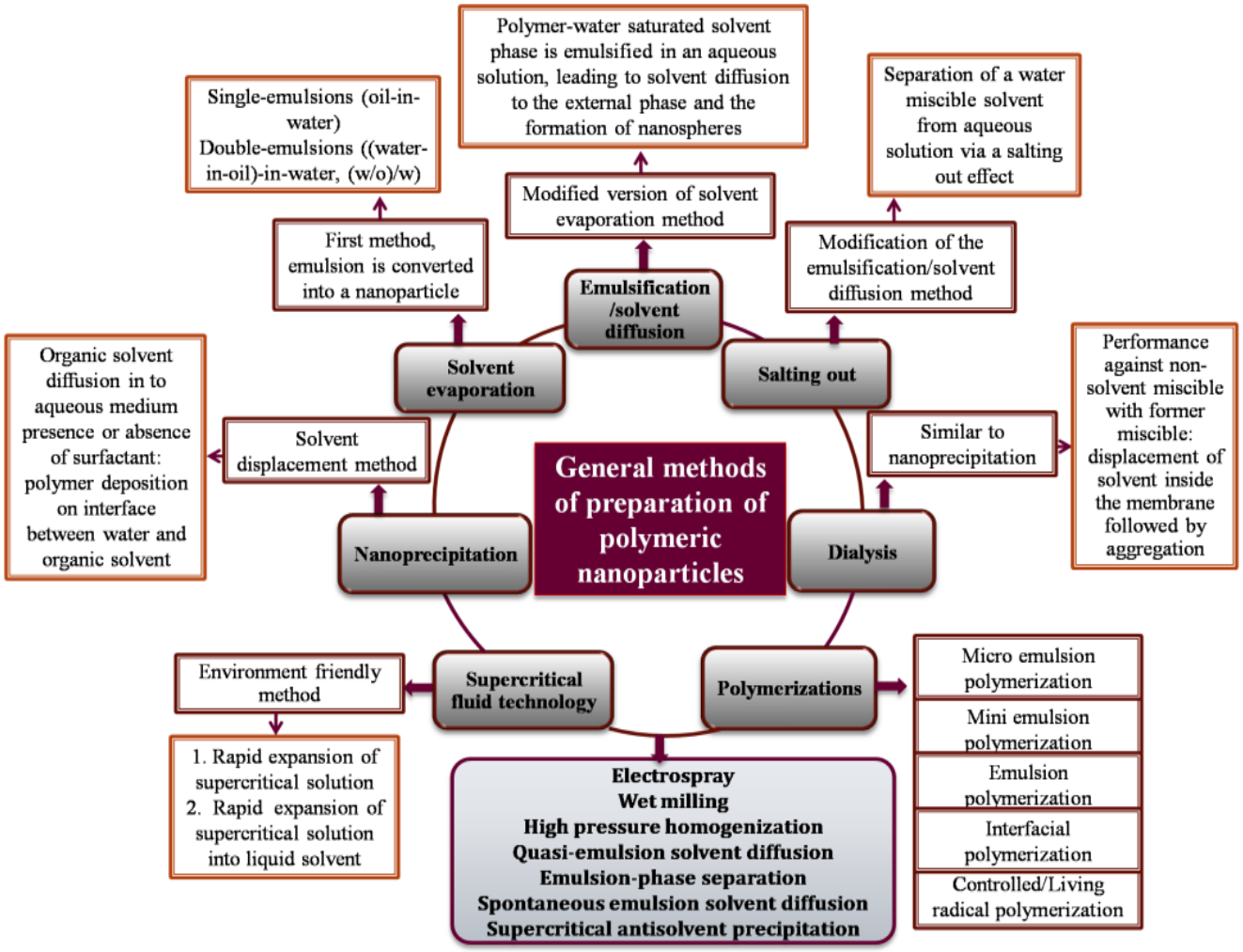

Chemical Methods:-

Sol- gel Techniques: - Sol –gel techniques used for the fabrication of metal oxides from a chemical solution which acts as a precursor for integrated network (gel) of discrete particle or polymers. The precursor sol can be either deposited on the substrate to from a film, acts into a suitable container with desired shape or used to synthesize powder **[80].**

The sol-gel method is based on inorganic polymerization reactions. The sol-gel process includes four different steps: hydrolysis, polycondensation, drying, and thermal decomposition **[81]**

After the solution has been condensed to a gel, the solvent must be removed. Higher temperature calcinations is needed to decompose the organic precursor. The size of the sol particles depends on the solution composition, pH, and temperature. By controlling these factors, one can tune the size of the particles. This method has been used to synthesize metal oxide nanostructures, such as TiO_2, UO_2, TnO_2, ZrO_2, CeO_2, SnO2, SiO_2, CuO, SnO_2, ZnO, Al_2O_3, Sc_2O_3, $ZnTiO_3$, $SrTiO_3$, $BaZrO_3$, $CaSnO_3$, and other nanostructures.

This is a wet-chemical method that allows high purity, high homogeneity nanoscale materials to be synthesised at lower temperatures compared to competing high temperature methods. A significant advantage that sol-gel science affords over more conventional materials-processing routes is the mild conditions that the approach employs **[82].** Two main routes and chemical classes of precursors have been used for sol-gel processing:

The **inorganic route** (“colloidal route”) uses metal salts in aqueous solution (chloride, oxychloride, and nitrate) as raw materials. These are generally less costly but their reactions are more difficult to control and the surfactant that is required by that process might interfere later in downstream manufacturing and end use. The **metal-organic route** (“alkoxide route”) in organic solvents. This route typically employs metal alkoxides M (OR)Z as the starting materials, where M is Si, Ti, Zr, Al, Sn or Ce; OR is an alkoxy group and Z is the valence or the oxidation state of the metal. Metal alkoxides are preferred because of their commercial availability and the high

lability of the M-OR bond. In general, the sol-gel process consists of the following steps: Sol formation, Gelling, Shape forming, Drying, and Densification **[83].**

Chemical precipitation: During the synthesis of inorganic nanoparticles by chemical precipitation method, the kinetics of nucleation and particle growth in homogeneous solutions can be adjusted by the controlled release of anions and cations. Careful control of precipitation kinetics can result in monodisperse nanoparticles. Once the solution reaches a critical supersaturation of the species forming particles, only one burst of nuclei occurs. Thus, it is essential to control the factors that determine the precipitation process, such as the pH and the concentration of the reactants and ions. Organic molecules are used to control the release of the reagents and ions in the solution during the precipitation process. The particle size is influenced by the reactant concentration, pH, and temperature. By engineering these factors, nanoparticles with narrow size distributions, such as $Zr(OH)_4$, $Ba\text{-}TiO_3$, $YBaCu_3O_3$, CdS, HgTe, and CdTe, have been produced. Although the method of using precipitation to prepare nanoparticles is very straightforward and simple, very complicated nanostructures can also be constructed using this method such as CdS/HgS/CdS, CdS/$(HgS)_2$/CdS and HgTe/CdS quantum well systems and other core/shell structures **[81,84].**

Hydrothermal synthesis: Hydrothermal synthesis is a common method to synthesize zeolite/molecular sieve crystals. This method exploits the solubility of almost all inorganic substances in water at elevated temperatures and pressures and subsequent crystallization of the dissolved

material from the fluid. Water at elevated temperatures plays an essential role in the precursor material transformation because the vapor pressure is much higher and the structure of water at elevated temperatures is different from that at room temperature. The properties of the reactants, including their solubility and reactivity, also change at high temperatures. The changes mentioned above provide more parameters to produce different high-quality nanoparticles and nanotubes, which are not possible at low temperatures. During the synthesis of nanocrystals, parameters such as water pressure, temperature, reaction time, and the respective precursor- product system can be tuned to maintain a high simultaneous nucleation rate and good size distribution. Different types of oxides and sulfides nanoparticles such as TiO_2, $LaCrO_3$, ZrO_2, $BaTiO_3$, $SrTiO_3$, $Y_2Si_2O_7$, Sb_2S_3, CrN, α-SnS_2, PbS, Ni2P, and SnS_2 nanotubes, Bi_2S_3 nanorods, and SiC nanowires have been successfully synthesized in this way. The solvent is not limited to water but also includes other polar or nonpolar solvents, such as benzene, and the process is more appropriately called solvo thermal synthesis in different solvents **[81, 84].**

Micelles or microemulsion based Method: In this method, the synthesis of nanoparticles can be achieved by confining the reaction volume in a restricted place. When the surfactant concentration exceeds the critical micelle concentration (cmc) in water, micelles are formed as aggregates of surfactant molecules. In normal micelles, the hydrophobic hydrocarbon chains of the surfactants are oriented toward the interior of the micelle, and the hydrophilic groups of the surfactants are in contact with the surrounding

aqueous medium. On the other hand, reverse micelles are formed in non aqueous medium where the hydrophilic head groups are directed toward the core of the micelles and the hydrophobic groups are directed outward. A micro emulsion is a dispersion of fine liquid droplets of an organic solution in an aqueous solution. Such a micro emulsion system can be used for the synthesis of nanoparticles. The chemical reactions can take place either at the interfaces between the organic droplets and aqueous solution, when reactants are introduced separately into two immiscible solutions or inside the organic droplets when all the reactants are dissolved into the organic droplets. This method is particularly useful for the synthesis of semiconductor, oxide and metal nanoparticles such as CdSe, CdTe, CdS, ZnS, ZrO_2, TiO_2, SiO_2, $Fe_2O_{3,}$ Pt, Au, Cu etc respectively **[81,84].**

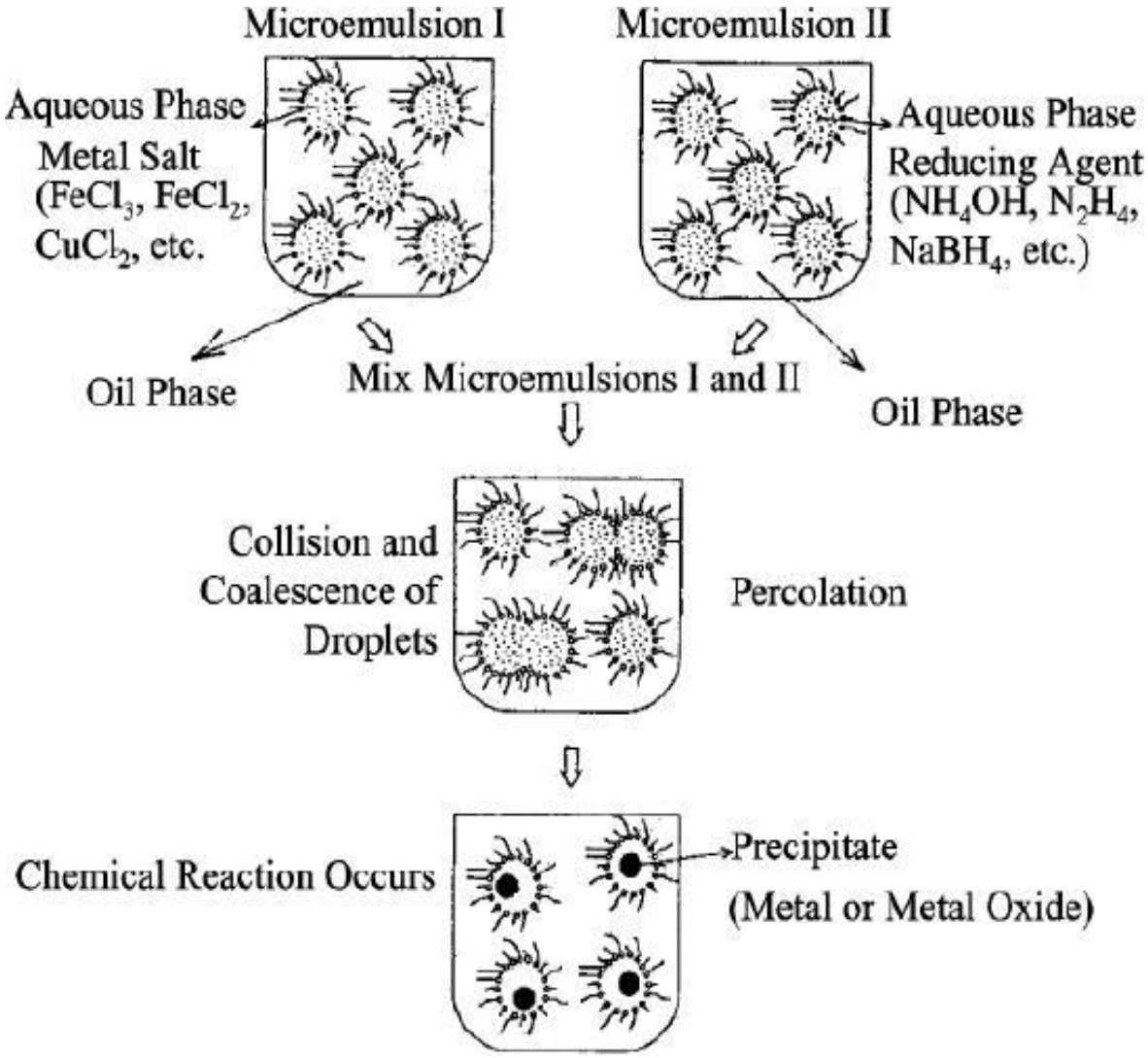

Gas-Phase Method:-

Several gas-phase synthetic techniques have been used to prepare nanoparticles. These methods use both inert and reactive atmospheres at a variety of pressures. Gasphase nanoparticle synthesis methods include electrospray, flame pyrolysis, vaporization and condensation using lasers and other heat sources, laser ablation, and plasma synthesis. These methods feature the rapid cooling of evaporated material to induce nucleation and growth of nanoparticles, typically within a confined region. Depletion of the

supersaturated vapor prevents excessive growth of the particles, which tend to show a log-normal size distribution. Particle size depends on material properties as well as the evaporation conditions. Coalescence of particles can result in particle growth, or the formation of aggregates which complicated the post-synthetic required for some applications. While product control (size, morphology, crystallinity) in gas-phase synthetic methods can be complex, many materials can be synthesized without contaminants such as solvents or stabilizers. In addition, many vapor-phase particle growth methods are adaptable for use in continuous, industrial reactors that are compatible with mass production **[85].**

Biological Methods:-

By Bacteria: The first evidence of bacteria synthesis silver nanoparticles was established using the pseudomonas stutzeri AG259 strain that was isolated from silver mine. There are some microorganism that can survive metal ion concentration and can also grow under those condition, and this phenomenon is due to their resistance to that metal .The mechanisms involved in the resistance are efflux system, alter of solubility and toxicity via reduction or oxidation, boisorption, bioaccumulation, extracellular complex formation or precipitation of metals, and lack of specific metal transport systems **[90].** There is also another aspect that thought these organisms can grow at lower concentration, their exposure to higher concentration of metal ions can induce toxicity. The most widely accepted mechanism of silver biosynthesis is the presence of the nitrate reductase enzyme. The enzyme converts nitrate into nitrite. In in- vitro synthesis of

silver using bacteria , the presence of alpha – nicotinamide adenine dinucleotide phosphate reduced from (NADPH) – depend nitrate reductase would remove the downstream processing step that is required in other case **[91].**

By Plants:-

The major advantages of using plant extract for silver nanoparticle synthesis is that they are easily available, safe, and nontoxic in most case, have a broad variety of metabolites that can aid in reduction of silver ions, and are quicker than microbes in the synthesis . The main mechanism considered for the process is plant- assisted reduction due to phytochemical. The main Phytochemical involved are terpenoids, flavones, ketones, aldehydes, amides, and carboxylic acids. Flavones, organic acids, and quinines are water – soluble phytochemicals that are responsible for the immediate reduction of the ions. Studies have revealed that xerophytes contain emodin, an anthraquninone that undergoes tautomerization, leading to the formation of the silver nanoparticle, In the case of mesophytes, it was found that they contain three types of benzoquinones, cyperoquinone, dietcchequinone, and remirin. It was suggested that the photochemicals are involved directly in reduction of the ions and formation of silver nanoparticle **[92].** In recent times, the plant extracts are widely used as a viable and facile alternative strategy for the synthesis of metal nanoparticles rather than physical and chemical methods. The presence of various secondary metabolites, enzymes, proteins and/or other reducing agents with electron-shuttling compounds are usually involved in the synthesis of metal nanoparticles by plant

components. In bioaccumulation, the localization of nanoparticles is based on the presence of particular enzymes or proteins involved in it. The recovery of these nanoparticles from plant tissues is not only tedious but expensive and also needs enzymes to degrade the cellulosic materials (Marshall et al. 2007). Thus, the synthesis of various metal nanoparticles using plant extracts is easy in downstream processing and in scaling up of nanoparticles **[93].**

By fungi: - When in comparison with bacteria, fungi can produce larger amounts of nanoparticles because they can secrete larger amounts of proteins which directly translate to higher productivity of nanoparticles **[94].**The mechanism of silver nanoparticle production by fungi is said to follow the following steps, trapping of Ag+ ions at the surface of the fungal cells and the subsequent reduction of the silver ions by the enzymes present in the fungal system **[95].**

Characterization of Nanoparticles:-

Microscopic Techniques:-

Scanning Electron Microscopy (SEM):

Scanning Electron Microscope is used to image and analyze materials of sizes that are less then micrometer range. The electrons are accelerated by the potential difference between cathode and anode. The electrons emitted are secondary electrons, back scattered electrons and auger electrons which decide upon the energy spectrum that is available by the interaction of electrons and specimen. During SEM the signal is developed when electrons are interacted with the atoms that are at the surface of the material. The signals are secondary electrons, back scattered electrons, characteristic X-ray etc**. [100].** The signals show information about the sample including chemical composition, and crystalline structure, external morphology (texture) and orientation of materials which make up the sample. SEM analysis is normally considered to be non-destructive because the x-rays generated do not lead to loss of volume of the sample, so it becomes possible to repeatedly analyze the same materials. A scanning electron microscope is a kind of electron microscope which images a sample by scanning it using a high-energy electron beam. The electrons then interact with the atoms making up the sample, thus producing signals which reveal information about the sample's composition, surface topography and other properties such as electrical conductivity. Various types of signals produced by a SEM include back-scattered electrons (BSE), secondary electrons, characteristic X-rays, specimen current; light (Back-scattered electrons (BSE). These characteristic X-rays are in turn used to and out the composition of the material and also measure the presence of elements in the sample as well as

the level of impurities. Magnication in a scanning electron microscope technique can be controlled over a range of about 6 orders of magnitude from approximately 10 to 500,000 times. Assuming that the display screen has axed size, higher magnication is obtained by reducing the raster size of the specimen, and vice versa. Magnication is hence controlled by the voltage supplied to the x, y detector plates or the current supplied to the scanning coils and not by objective lens power **[101].**

Transmission electron microscopy (TEM):-

A transmission electron microscope probes the internal structure of solids to givean access to the morphological fine structural details. In TEM, the transmitted electrons are used to create an image of the sample. Electron beam instruments are operated under high level of vacuum to avoid scattering of electrons from their molecules and arcing due to high voltage. A TEM is operated under vacuum in the order of 10-7 torr, equipped with an electron gun capable of accelerating electrons through a potential difference in the range of 60 to 300kV. A thin sample fixed on the grid is illuminated by an electron beam to perform analysis in the TEM. These electrons contribute towards formation of a diffuse halo around the transmitted beam, the diffracted beam and to the general background intensity between the diffraction spots. Most of the intensity at the exit surface of the crystal is in the transmitted and diffracted beam. In the bright field imaging mode, electrons transmitted through the sample are used to form image while intensity of scattered electron is filtered out **[102].**

Atomic force microscopy (AFM):-

AFM can be used for the precise study of nanoscaled materials. AFM works by scanning an ultrafine ceramic or semiconductor probe over the surface of

the material being analyzed. The tip is positioned at the end of a cantilever spring. As the probe tip moves over the sample surface, from left to right and top to bottom it measures the forces (at the atomic level) between the probe tip and the sample. The data from the photodiode sensor are translated into digital form and are processed using specialized software. A plot of the laser deflection versus probe tip position on the sample surface provides a highly resolved picture of the peaks and valleys of the sample surface, which constitutes, essentially, an atom-by-atom topographical visualization of the material surface **[103].** Atomic force microscopy (AFM) or scanning force microscopy (SFM) is a very high-resolution type of scanning probe microscopy, with demonstrated resolution on the order of fractions of a nanometer, more than 1000 times better than the optical diffraction limit. The information is gathered by "feeling" the surface with a mechanical probe. In some variations, electric potentials can also be scanned using conducting cantilevers. In more advanced versions, currents can be passed through the tip to probe the electrical conductivity or transport of the underlying surface. Electron micrograph of a used AFM cantilever image width ~ 100 micrometers and ~ 30 micrometers. The AFM consists of a cantilever with a sharp tip (probe) at its end that is used to scan the specimen surface. The cantilever is typically silicon or silicon nitride with a tip radius of curvature on the order of nanometers **[104].**

Scanning Tunneling Microscope:-

A **scanning tunneling microscope** (**STM**) is an instrument for imaging surfaces at the atomic level. For an STM, good resolution is considered to be 0.1 nm lateral resolution and 0.01 nm depth resolution. With this resolution, individual atoms within materials are routinely imaged and manipulated.

The STM can be used not only in ultra-high vacuum but also in air, water, and various other liquid or gas ambients, and at temperatures ranging from near zero Kelvin to a few hundred degrees Celsius **[105].**The STM is based on the concept of quantum tunneling. When a conducting tip is brought very near to the surface to be examined, a bias (voltage difference) applied between the two can allow electrons to tunnel through the vacuum between them. The resulting *tunneling current* is a function of tip position, applied voltage, and the local density of states (LDOS) of the sample. Information is acquired by monitoring the current as the tip's position scans across the surface, and is usually displayed in image form. STM can be a challenging technique, as it requires extremely clean and stable surfaces, sharp tips, excellent vibration control, and sophisticated electronics, but nonetheless many hobbyists have built their own **[106].**

Scanning Probe Microscopy:-

SPM- extensively applied to characterize nanostructures with atomic or subatomic spatial resolution. A common characteristic of these techniques is that an atom sharp tip scans across the specimen surface and images are formed by either measuring the current flowing through the tip or the force acting on the tip. SPM can be operated in a number of environmental conditions, in a variety of different liquids or gases, allowing direct imaging of nanoparticle surfaces. It allows viewing and manipulation of objects on the nanoscale and its invention is a major milestone in nanotechnology **[=].**

Spectroscopic Techniques:-

U-V spectrophotometer:

Ultraviolet-Visible spectrophotometer is designed to use light of ultraviolet and visible spectral region. This technique is used to determine the concentrations of unknown solutions and determination of transition metals whose electron transition energy that fall under UV or visible regions. Beer-Lambert law is used to determine the concentration of unknown solutions. When a beam of electromagnetic radiation strikes an object it can be absorbed, transmitted scattered, reflected or it can excite fluorescence. The processes concerned in the absorption spectroscopy are absorption and transmission. The conditions under which sample is examined for absorption are chosen to keep reflection, scatter and fluoresces to a minimum. An optical spectrometer records the wavelength at which absorption occurs together with the degree of absorption at each wavelength. UV- visible spectroscopy is used for quantitative analysis of the samples **[107].** Nanoparticles dispersed in a solvent or embedded in the insulator matrix. The absorption of the incident radiations takes place due to surface plasmon resonance of the metal nanoparticles. Surface plasmons are essentially the light waves that are trapped on the surface because of their interaction with the free electrons of the metal.

Raman Spectroscopy:-

Raman spectra are another vibrational technique and differ from the infrared spectroscopy by an indirect coupling of high-frequency radiation with vibrations of chemical bonds. When the incident photon interacts with the chemical bond, the chemical bond is excited to a higher energy state. The

scattering process is inelastic and thus the scattered light can have a lower (Stokes, by depositing energy into the molecule) or higher energy (anti-Stokes, by gaining energy from the molecule) than the incident light (Rayleigh scattering). The energy shift is characteristic for the chemical structure where the scattering occurred and complex molecules have therefore a characteristic Raman spectrum that allows for detection and identification. A Raman spectrum serves as a "molecular fingerprint" of a sample, yielding information on molecular bonds, conformations, and intermolecular interactions. In spite of its advantages, its practical uses have been significantly limited because the Raman scattering signal is intrinsically weaker than most other fluorescence signals. Methods of enhancement have been developed to extend the detection limit. Among various methods, enhancement with noble metal nanostructures, a technique termed surface-enhanced Raman scattering (SERS), has been found to enhance the efficiency dramatically. Using this method, it is possible to probe single molecules adsorbed onto a single gold nanoparticle **[=].**

Infrared Spectroscopy:-

The mechanical molecular and crystal vibrations are at very high frequencies ranging from10^{12} to 10^{14} Hz (3–300 μm wavelength), which falls in the infrared (IR) region of the electromagnetic spectrum. In infrared Spectroscopy, the oscillations induced by certain vibrational frequencies provide a means for matter to couple with an impinging beam of infrared electromagnetic radiation and to exchange energy with it when the frequencies are in resonance. These absorption frequencies represent excitations of vibrations of the chemical bonds and thus, are specific to the type of bond and the group of atoms involved in the vibration. In Fourier

transform infrared spectroscopy, the intensity-time output of the interferometer is subjected to a Fourier transform to convert it to the familiar infrared spectrum (intensity-frequency) and atomic arrangement, surrounding environments and concentrations of the chemical bonds that are present in the sample can be determined. The studies relating the quantification of the coverage and binding strength of ligands, surfactants etc **[=]**.

Scattering Techniques:-

Dynamic Light Scattering (DLS):

Differential scanning calorimetry or DSC is a thermo-analytical technique in which the difference in the amount of heat required to increase the temperature of a sample and reference are measured as a function of temperature. Both the sample and reference are maintained at nearly the same temperature throughout the experiment. Generally, the temperature program for a DSC analysis is designed such that the sample holder temperature increases linearly as a function of time. The reference sample should have a well-defined heat capacity over the range of temperatures to be scanned. The main application of DSC is in studying phase transitions, such as melting, glass transitions, or exothermic decompositions. Whether more or less heat must flow to the sample depends on whether the process is exothermic or endothermic. This is due to the absorption of heat by the sample as it undergoes the endothermic phase transition from solid to liquid. Likewise, as the sample undergoes exothermic processes (such as crystallization) less heat is required to raise the sample temperature. By observing the difference in heat flow between the sample and reference, differential scanning calorimeters are able to measure the amount of heat

absorbed or released during such transitions. DSC may also be used to observe more subtle phase changes, such as glass transitions. DSC is widely used in industrial settings as a quality control instrument due to its applicability in evaluating sample purity and for studying polymer curing. Since DSC is more sensitive to phase transition temperature (with a precision of 0.01oC) and is capable of monitoring the exact rate of energy exchange or reaction rate. Positions of all these peaks depend on heating rate. Increasing the heating rate caused every peak shift toward higher temperatures, with the first two endothermic peaks merged into one broad one. This is due to activation energy involved in such transition **[108].**

X-RAY Diffraction method:-

X-ray diffraction is a versatile, non-destructive analytical method for identification and quantitative determination of various crystalline forms, known as ‘phases’ of compound present in powder and solid samples. Diffraction occurs as waves interact with a regular structure whose repeat distance is about the same as the wavelength. The phenomenon is common in the natural world, and occurs across a broad range of scales. For example, light can be diffracted by a grating having scribed lines spaced on the order of a few thousand angstroms, about the wavelength of light. It happens that X-rays have wavelengths on the order of a few angstroms, the same as typical inter-atomic distances in crystalline solids. That means X-rays can be diffracted from minerals which, by definition, are crystalline and have regularly repeating atomic structures. When certain geometric requirements are met, X-rays scattered from a crystalline solid can constructively interfere, producing a diffracted beam. **[109].**

Light Scattering:-

Light scattering is a form of scattering in which light is the form of propagating energy which is scattered. Light scattering can be thought of as the deflection of a ray from a straight path, for example by irregularities in the propagation medium, particles, or in the interface between two media. Deviations from the law of reflection due to irregularities on a surface are also usually considered to be a form of scattering. When these irregularities are considered to be random and dense enough that their individual effects average out, this kind of scattered reflection is commonly referred to as diffuse reflection.

Most objects that one sees are visible due to light scattering from their surfaces. Indeed, this is our primary mechanism of physical observation. Scattering of light depends on the wavelength or frequency of the light being scattered. Since visible light has wavelength on the order of a micrometre, objects much smaller than this cannot be seen, even with the aid of a microscope. Colloidal particles as small as 1 μm have been observed directly in aqueous suspension **[110].**

Other Techniques:-

Zeta Potential analysis by electrophoresis:-

Environmental fate and reactivity of NPs can be controlled by their dispersion and Agglomeration behavior. NPs are affected by the weak physical forces of attractive Vander Waals forces and repulsive electrostatic charges. The zeta potential (ζ) is an important parameter for a number of applications. The ζ is a function of the surface charge of a particle or any adsorbed layer at the interface and the natural composition of the

surrounding medium, Particles that are sterically stabilised can remain well dispersed even at high salt concentrations or where ζ is close to zero. When a solid surface is in contact with an aqueous solution, ions of opposite charge to that of the particle are strongly attracted to the surface; termed the stern layer. The arrangement of the charges at the solid-liquid interface and the balancing counter ions in the liquid is usually referred to as the EDL. The ions in the stern layer are immobile due to the strong electrostatic attraction where ions outside the compact layer (diffuse layer) are mobile,. The ζ is the electrostatic potential at the boundary dividing the compact layer and the diffuse layer, called the slipping plane. When an electric field is applied across an aquatic dispersion, charged particles will move toward the electrode of opposite polarity **[=].**

Thermograviometric Analysis:-

(TGA) is a type of testing that is performed on samples to determine changes in weight in relation to change in temperature. Such analysis relies on a high\ degree of precision in three measurements: weight, temperature, and temperature change. As many weight loss curves look similar, the weight loss curve may require transformation before results may be interpreted. A TGA is commonly employed in research and testing to determine characteristics of materials such as polymers, to determine degradation temperatures, absorbed moisture content of materials, the level of inorganic and organic components in materials, decomposition points of explosives, and solvent residues. It is also often used to estimate the corrosion kinetics in high temperature oxidation. The analyzer usually consists of a high-precision balance with a pan (generally platinum) loaded with the sample. The pan is placed in a small electrically heated oven with a thermocouple to accurately measure the temperature. The atmosphere may

be purged with an inert gas to prevent oxidation or other undesired reactions. The temperature in many testing methods routinely reaches 1000°C or greater, but the oven is so greatly insulated that an operator would not be aware of any change in temperature even if standing directly in front of the device. After the data is obtained, curve smoothing and other operations may be done such as to find the exact points of inflection. A method known as hi-res TGA is often employed to obtain greater accuracy in areas where the derivative curve peaks. In this method, temperature increase slows as weight loss increases. This is done so that the exact temperature at which a peak occurs can be more accurately identified. Several modern TGA devices can vent burnoff to a fourier-transform infrared spectrophotometer to analyze composition **[111].**

Properties of Nano Particle:-

Optical Properties; Zinc oxide is generally transparent to visible light but strongly absorbs ultra violet light below 3655 A°. The absorption is typically stronger than other white pigments. In the region of visible wavelengths, regular zinc oxide appears white, but, rutile and anatase titanium dioxide have a higher reactive index and thus has a superior opacity. ZnO is a wide band gap of 3.4 eV semiconductors with a large exciton binding energy of 60 meV and also considered as one of themost promising semiconductor material for electronic, photonic, optical and biological applications **[A].** The band gap energy occurs between the between valence and conducting bands corresponds to the energy of 3655 photons. Zinc oxide is considered as the photoconductive under the analytical study of ultra violet light. The arrangement of optical and semiconductor properties construct a doped zinc oxide which is a contendor for new generations of devices. Solar cells require transparent conductive coating like indium tin oxide and zinc oxide are the finest materials. Intrinsic optical properties of ZnO nanostructures are being intensively deliberated for the implementing photonic devices. Photoluminescence (PL) spectra of ZnO nanostructures have been extensively reported. Excitonic emissions have been examined from the photoluminescence spectra of the ZnO nanorods. It is shown that quantum size confinement can significantly enhance the exciton binding energy. Strong emission peak at 380 nm due to band-to-band transition and green-yellow emission band related to oxygen vacancy are observed. Photoluminescence spectra show that the ZnO nanowire is a capableand promising material for the UV emission. Its UV lasing property is

additionally more significant and interesting. Due to its near-cylindrical geometry and large refractive index of nearly about 2.0, ZnO nanowire or nanorod is a natural candidate for the optical waveguide. The additional advantages of ZnO nanowire lasers are that the excitonic recombination lowers the threshold of lasing, and quantum confinement yields a substantial density of the band edges and enhances radiative efficiency. Optical wave guiding using dielectric nanowire also achieved considerable progress. In recent times, ZnO nanowires were stated as sub-wavelength optical waveguide. Optically forced light emission was guided byZnO nanowire and coupled into SnO**2** nanoribbon. These discoveries show that the ZnO nanostructures can be potential building blocks for integrated optoelectronic circuits. Optical properties have a great interest towards the vast application of optoelectronics, photovoltaics and biological sensing **[B].**

Mechanical Properties;

The mechanical properties of materials involve various concepts such as hardness, stiffness, and piezoelectric constants, Young‟s and bulk moduli, and yield strength. Although the wurtzite ZnO crystal is acoustically anisotropic, there is only a very small difference between the shear sound velocities vTA1 and vTA2 propagating along the (001) and (100) directions, respectively (vTA2/vTA1) = 0.98. Piezoelectricity is the electric charge that accumulates in certain solid materials in response to applied mechanical stress. The word piezoelectricity means electricity resulting from pressure. The piezoelectric effect is understood as the linear electromechanical interaction between the mechanical and the electrical state in crystalline materials with no inversion symmetry. The piezoelectric effect is a reversible process in those materials exhibiting the direct piezoelectric effect

(the internal generation of electrical charge resulting from an applied mechanical force)

also exhibit the reverse piezoelectric effect (the internal generation of a mechanical strain resulting from an applied electrical field). The inverse piezoelectric effect is used in production of ultrasonic sound waves. Among the tetrahedrally bonded semiconductors, it has been stated that ZnO has the highest piezoelectric tensor. This property makes it a technologically important material for many applications, which require a large electromechanical coupling. The piezoelectric tensor has three independent components in hexagonal wurtzite phase and one in the cubic zinc-blende phase, which characterize the full piezoelectric tensors of such crystals.108.Two of these components in wurtzite phase measure the polarization induced along the *c* axis, at zero electric field, by a uniform strain either along the *c* axis or in the basal plane **[C].**

Electrical Properties;

The fundamental study of the electrical properties of ZnO nanostructures is crucial for developing their future applications in nanoelectronics. ZnO has a quite large band gap of 3.3 eV at room temperature. The advantages of a large band gap include higher values of breakdown voltages, sustaining large electric _elds, high-temperature and highpower operations. ZnO has n-type character, in the absence of doping. Nonstoichiometry is usually the origin of n-type character. Due to defects such as oxygen vacancies and zinc interstitials, ZnO nanowires are reportedly show n-type semiconductor behavior. The main impediment of ZnO for wide-ranging applications in electronics and photonics rests with the di_culty of p-type doping. Successful p-type doping for ZnO nanostructures will greatly enhance their

future applications in nanoscale electronics and optoelectronics. P-type and n-type ZnO nanowires can serve as p-n junction diodes and light emitting diodes (LED). **[D].**

Magnetic Property;

The hysteresis loops of the nanocomposites were collected at RT. Ms values at room temperature were obtained by extrapolation to infinite field in M versus 1/H2 plot. The increase in the density of magnetization with the increase in the Fe/Si molar concentration can be observed very clearly. The changes in the magnetic properties of the Nanocomposites can be accounted for by the modification of the average size of nanocrystallites with the Fe/Si molar concentration. The magnetic behavior of this sample is caused by its small crystallite size as revealed by XRD characterization. Ms increases with the increasing of the diameters of $CoFe_2O_4$

Nanocrystallites and its maximum value is 16.6 emu g-1. Considering only the ferrite mass and assuming that the final composition was equal to that of the as-prepared gel, the maximum value of density of magnetization is about 55 emu g-1. The density of magnetization is lower than the reported values for bulk cobalt ferrite (80 emu g-1) **[E],** but it is in fairly good agreement with the values measured in $CoFe_2O_4$ particles of similar size. The decrease in the density of magnetization with the decrease in the average diameter of the nanocrystallites can be attributed to surface effects and core-shell morphology. The surface effects are the result of finite-size scaling of nanocrystallites, which in turn leads to a non-collinearity of magnetic moments on their surface. These effects are more intense in ferromagnetic system, where the exchange interaction occurs through the oxygen ion O2 - (superexchange). The absence of the oxygen ion at

the surface or the presence of another atom (ion) in the form of an impurity leads to a break of the superexchange bonds between the magnetic cations which induce surface spin disorder. Due to the above-mentioned effects, the density of magnetization in the nanocrystallites is lower than that of bulk cobalt ferrite. The decrease is more pronounced with the increase in the surface– volume ratio of the nanocrystallites and the decrease in the average diameter of nanocrystallites, respectively. The observed behavior is conditioned by the magnetic structure that corresponds to a single-domain configuration of the crystallites. The maximum value of Hc is as high as 2000 Oe, which is much higher than the coercivity of bulk cobalt ferrite.

Limitations of Nanoparticles;

In spite of these advantages, nanoparticles do have limitations.

For example, their small size and large surface area can lead to particleparticle aggregation, making physical handling of nanoparticles dicult in liquid and dry forms. In addition, small particles size and large surface area readily result in limited drug loading and burst release. These practical problems have to be overcome before nanoparticles can be made commercially available. The present review details the latest development of nanoparticulate drug delivery systems, surface modication issues, drug loading strategies, release control and potential applications of nanoparticles [1]

Literature Review

Xu. Bing She., and Tanaka. S., [1] were observed that, In situ in metastable oxide particles on the room temperature stage of TEM under an electron beam intensity of 10^{19} e/cm^2 sec particles of 10-15 nm diameter $\alpha - Al_2O_3$ and 5 nm diameter Al metal were obtained from 100 nm metastable θ-Al_2O_3 particle by a process dependent on the electron beam intensity. Al nanoparticles were bonded by continuous irradiation via surface diffusion of Al atom and the formation of 2 nm sized cluster. The effects of the electron beam are the irradiation induced increases of the oxygen mobility and localized heating.

Encapsulation of foreign materials within a hollow graphitic cage was carried out for rareearth and irongroup metals by using an electric arc discharge. It was produced by Saito.Y., [2] The rare- earth metals with low vapor pressures, Sc. Y, La, Ce, Pr, Nd, Gd, Tb, Dy, Ho, Er, Tm, and Lu, were encapsulated in the form of carbides, whereas volatile Sm, Eu, and Yb metals were not, for Iron-group metals, particles in metallic phases (α-Fe, -γ-Fe; HCP.Co, FCC-Co; FCC-Ni) and in a carbide phase (M_3C, M- Fe Co, Ni) were wrapped in graphitic carbon. The excellent protective nature of the outer graphitic cages against oxidation of the inner materials was demonstrated. In addition to the wrapped nanoparticles, exotic carbon materials with hollow structures, such as single-wall nanotubes. Bamboo-shaped tubes, and nanochains, were produced by using transition metals as catalysts.

The existence of short-range interlayer stacking correlations demonstrated by Reznik. D., et al [3] our calculations show that such correlations should not be observable in idealized models of nanotubes. The observation of short-range interlayer correlations can be explained if many of the nanotubes and nanoparticles have polygonal cross sections, largely consisting of flat regions having graphitic interlayer correlations. This polygonization is almost certainly driven by the van der Waals interactions responsible for the *AB AB* stacking in crystalline graphite.

The morphology of graphitic boron nitride nanometric particles was produced [4] by Boulanger. L., and Andriot. B., from the reaction between ammonia and borontrichloride heated by a CO_2 laser is investigated by high resolution electron microscopy. A variety of roughly spherical particles are revealed, consisting of concentric graphitic shells and ranging in size from 20 to more than 100 nm and in shape from hollow to filled-to-the center. This onion-like configuration is very similar that observed in carbon materials. Another morphology made of stockings of a few perfectly flat graphitic sheets (10 to 50 layers. 50 nm in length) is developed after heat treatment.

The Brewster angle technique on samples constituted by Pb and Sn nanoparticles embedded in an amorphous SiO matrix, the extended comparison with different effective medium is models gives clear indications on (i) the structural composition of the samples and **(ii)** the spatial distribution of the metallic particles in these systems, pointing to a quasi-two-dimensional arrangement was reported by Tognini.P., et al [5]

The microstructure of agglomerate can be characterized [6] by Weber. A. P., et al the coordination number. The relationship between the fractal dimension and the coordination number of agglomerates of nanometer particles was investigated in experiments and computer insulations. The results for silver agglomerates formed by laser ablation agreed well with the simulations. The coordination number is low for low density fractals because of the large fraction of surface particles which have fewer bonds. The sensitivity of the coordination number to the fractal dimension increases with increasing fractal dimension.

The shape of copper metal particles is demonstrated to depend on the structure of the mesosphere (cylindrical reverse micelles, interconnected networks of surface aggregates or lamellar phases) in the surfactant system used as a micro reactor for their synthesis. An understanding of this correlation is of great importance for magnetic recording technology that was demonstrated by Pileni. M. P., and Tanori. J., [7]

The Silicon nanoparticles were discoverded [8] by Li. Ping., and Sattler. K., the particle are formed by deposition of silicon vapor onto silicon wafers and highly oriented pyrolytic graphite (HOPG). On silicon substrates, the particles are close to spherical with relatively narrow size distributions and they are randomly located. On graphite substrates the particles are arranged in chains, within the chains they show strong deformations in the contact areas relate this to covalent interparticle interactions.

Silicon nanoparticles was produsedby Borsella. E., et al [9] To optimize the process, in order to reduce the particle size, a wide angle X-ray diffraction (WAXS) investigation method has been developed to rapidly and easily characterizes the produced powder batches, The method is based on a Monte Carlo interference function (MIF) fitting of the experimental peaks. The results of the application of the MIF procedure on powder batches with different particle sizes are presented and compared with Brunauer-Emmett-Teller specific surface measurements and transmission electron microscopy.

XPS spectra of core levels, valence bands and Auger transitions were reported by Putten. D. van der., et al [10] on the molecular cluster compound $Cu_{146}Se_{73}(pph_3)_{30}$ and on Cu_2Se bulk phase obtained - from the cluster after heat treatment. The photoemission features of both species are reported and commented in the tight of a cluster-to-bulk transition.

Morphology and crystallography of nano particle were investigated [11] by Allard. L.F., et al. That Profiles of intensity over the phase image are, in particularly advantageous cases, directly related to particle morphology, since the phase intensity for materials that are essentially kinematic scatters and are of homogeneous composition is directly related to thickness, Holograms at high revolution can also be used for many other analyses of a material's structure; they provide, for example, a method for precise calibration of lattice spacing's in nanometer size areas, that allows for the correlation of structure to processing parameters. Examples of the use of holography for studies of nanoparticles of oxides and model catalyst are given.

The different type of application were discussed by [12] Groza. J.R., The key characteristic of the nanopowder consolidation process is to achieve densification without microstructural coarsening. The nanocrystalline nature of the consolidating particulates. The theoretical issues that affect the thermodynamics and kinetics of the atomic processes involved in nanopowder densification are related to higher driving force, enhanced interfacial energy and diffusion, and full density values. The experimental aspects cover powder compressibility and differential shrinkage, heating rate and pressure effects, and grain growth. Meaningful results in terms of final density values and grain growth are presented with the emphasis on processes that have demonstrated the capability to form dense specimens with retention of fine grain sizes.

Gold nanoparticles, within AOT reversed micelles, have been imaged by an atomic force microscope (AFM) operating in the contact mode in air at room temperature .The AFM images show an attractive interaction among gold nanoparticles leading to the formation of well distinct aggregate where however each nano particle retains its individualy. Moreover the AFM, images show that the mean size of gold nanoparticle is a fuction of the size of the AOT reverse micelles and offer evidence of a stabilization mechanism of the nanoparticle due, most probly to the formation of an adsorbed layer of surfactant molecules at the nanoparticle surface, This stabilization mechanism results in being active even at high nanoparticle concentration. The AFM of Gold nanoparticle was investigated by [13] Arcoleo. V., and Liveri. V. T.,

1997

The measurement of optical absorption was made on the nanoscale silver particles dispersed in silicon oil and silicon oil with added dressing agent was reported by Fei. G. T., et al [14] an absorption peak appears in the nanoscale silver particles dispersed in silicon oil, but the absorption peak disappears when the dressing agent is added. The interaction between external molecules and the surface of small silver particles seems to have strong influence on the absorption peak of small silver particles.

The optical properties of nanoparticle were reported by Averitt. D.A., et al [15] these structures naturally in the form of Au-coated Au_2S nanoparticles. During the course of nanoparticle growth, the plasmon-related absorption peak undergoes very large wavelength, from - 650 to - 900 nm. That this plasmon peak shift is classical inorigin and is determined solely by the relative thickness of the Au size and the Au_2S core diameter. This understanding of the optical properties of Co nanoparticies is used to elucidate the nanoparticle growth kinetics.

In an attempt to identify the driving force for the formation of chains composed it nanometer size Fe alloy particles that were recently reported, experiments have been carried out with the magnetic metals Fe, Co, and Ni and a nonmagnetic metal.The samples obtained by a reduction of aqueous metal chloride solutions with polysium borohydride have been characterized by x-ray diffraction, transmission, electron , microscopy, and superconducting quantum interference device magnetometer mm surements. The results reveal that the magnetic interaction between the adjacent particles plays a determining role in the chain structure formation. Although

both crystallinity and boron content do not play a direct role, they influence significantly magnetic properties, and thereby, have an indirect role in the formation of the chelaty structures. That chains composed of nanosize metal particles was investigated by [16] Zhang. L., and Manthirama. A.,

Carbon anions are found along with carbon nanotubes and other carbon nanoparticls in the cathodic deposit in the arc-vaporization of graphite was investigated by [17] Raina. G., and Sen. R., The Atomic force microscopes has been used to characterize these particles on the basis of their sizes and shape Onion-like particles have three-dimensional, near spherical structure and are distier from two-dimensional graphitic particles. The spherical shape and height to diameter ratios obtained using atomic force microscope, afford a distinction between onion like structures and other carbon nanoparticles.

The behaviour of atomic species and of growing nano-particles in the laser-ablated plume was observed by laser-induced fluorescence (LIF) and Rayleigh scattering (RS) imaging techniques, and the results on the ablation of silicon (Si) in a He ambient were presented by Muramoto. J., et al [18]. The particles were formed in a limited region in the plume with a characteristic spatial distribution. The growth of the particles was completed about 20 ms after ablation at a helium (He) ambient pressure of 1.33 kPa and 50 ms at 0.67 kPa. The spatial distributions of the particles were retained for more than one second.

The formation of Si nanoparticles in a SiH_4-Ar plasma discharge generated in a helical resonator type inductively coupled plasma reactor was reported by Gorla. C.R., et al [19] that Si particles vary in sizes from 5 to 15 nm under

different conditions. The particles were mostly spherical and made up of a crystalline core with a 1-2 nm thick amorphous shell. The size distribution was narrow for particles formed at a pressure of 200 mTorr, plasma power of 400 W and silane flow rate of 20 sccm (+980 sccm Ar). The effect of a dc bias applied to the particle collecting grids has also been studied. It is found that a negative bias (-25 to —100 V) applied to the grids used for particle collection results in a large increase in the number of Si nanoparticles collected, while a positive bias does not change the collection efficiency considerably, suggesting that the particles are positively charged. Under very low flow rates and under high plasma powers, the Si particle density decreases considerably and a film like deposition occurs on transmission electron microscopy grids placed in the reactor for collecting the particles. We have also studied the formation of Ge particles (50-200 nm) in a GeH_4-Ar plasma generated in the same reactor. These particles are crystalline with a spherical morphology.

The potential of the arc discharge technique for the growth of complex nanocrystaline systems is demonstrated by Maser. K. W., et al. [20] with the formation of quaternary superconducting nanoparticles belonging to the recently discovered intermetallic boron carbide family RNi_2B_2C (R=Y, Lu). The nanoparticles, which were embedded in a glassy carbon matrix and had Tc-15 K, are reported to exhibit magnetic behavior characterized by finite size effects and weak Josephson links between the particles. The formation and characterization of the nanoparticles are detailed.

The analysis of selected, individual nanoscale particles represents the limit of performance for the most advanced micro analytical techniques was discussed by [21] Newbury. D.E., Ion beam methods are inadequate for

objects with dimensions below 100 nm because of limitations on the number of atoms that can be ionized and collected. By using near-field optical techniques, photon beam methods are just beginning to gain the spatial resolution necessary to penetrate the 100 nm barrier. Electron beam techniques such as low voltage (<5 kV) scanning electron microscopy and high voltage (2100 kV) analytical electron microscopy are highly effective in the sub-100 nm size regime. Electron-excited X-ray spectrometry can provide accurate elemental analysis in both energy regimes. At high energy, electron energy loss spectrometry (EELS) can also be utilized augmenting elemental analysis with molecular (compound) information. Analytical masses as small as 1 zg can be characterized with EELS.

A novel Si nanoparticle (SNP) system of spatially coherent distribution was synthesized by Ishikawa. Y., et al. [22] low energy oxygen ion implantation during Si molecular beam epitaxy. Highly oriented Si nanoparticles embedded in a SiO_2, matrix of dimensions d of 4-100 nm with log-normal size distribution are demonstrated. The singlecrystal character of the SNPs is revealed by transmission electron microscopy and the preferred crystalline axis is oriented to the substrate normal, [100] retaining the epitaxial character compared with dispersive SNPs. The morphology of individual nanoparticles is significantly faceted towards [100] and [111] as opposed to regular polyhedra with the crystal habit of [31l], [111] characteristic of thermodynamically stabilized dispersive SNIPs. Visible luminescence bands are observed at room temperature.

Schiffmann. K.I., et al [23] prepared a metal containing amorphous hydrogenated carbon films are protective coating materials with very low friction coefficients, high hardness and wear resistance, combined with an adjustable electrical conductivity. The structure of these films, consisting of nanometer size metallic particles in a hydrogen-carbon matrix, was investigated by means of scanning tunneling microscopy (STM) in order to determine particle size and particle distance distributions. In doing so, tip convolution effects lead to apparent particle enlargement and particle hiding, falsifying radii and distance determination. In order to correct these errors (1) a statistical method is presented which allows off-line tip radius determination by analyzing apparent particle radii, (2) a simple Monte Carlo model is proposed to compute fractions of hidden particles and their influence on particle distance distributions. Both methods are applied to STM measurements of Au-C: H and Pt-C:H samples of different metal content and the result is compared with results of small angle X-ray scattering (SAXS), transmission electron microscopy (TEM) and X-ray diffraction (XRD).

[24] Gao. Y. H., and Zhang. Z., was investigated a high-resolution electron microscopy study of β-SiC nanoparticles formed by C^+- implantation of single crystal silicon with subsequent annealing has been carried out, the as-implanted sample had a trilayered structure, in which the surface layer, A, and the bottom layer, C, were crystalline but damaged, and the middle layer, B, was amorphous. After annealing this structure, β-SiC particles were formed throughout the trilayered structure but with different forms: a few epitaxial β-SiC nanoparticles in layers A and C, and more random nanoparticles in layer B. The β -SiC nanoparticles, in the size range 2-8 nm,

should be responsible for the blue-emitting effect of the silicon-based porous β-SiC.

Fluorescence and light – scattering were reported by Mei Li. And Ming Jiang [25] the lightly sulfonated polystyrene ionomer is only soluble in some organic solvents, such as toluene and tetrahydrofuran (THF). The mixture of its organic solution with water normally leads to macroscopic phase separation, namely precipitation. In this study, using steadystate fluorescence, nonradiative energy transfer and dynamic laser light scattering, demonstrate that the sulfonated polystyrene ionomers can form stable colloidal nanoparticles if the THF solution of the ionomers is dropwisely added into an excessive amount of water, or vice versa, water is added in a dropwise fashion into the dilute ionomer THF solution under ultrasonification or fast stirring. The hydrophobic core made of the polystyrene backbone chains is stabilized by the ionic groups on the particle surface. Such formed stable nanoparticles have a relatively narrow size distribution with an average diameter in the range of 5-12 nm, depending on the degree of sulfonation, the initial concentration of the ionomer THF solution, and the mixing order. This study shows another way to prepare surfactant-free polystyrene nanoparticles.

Dutta. J., et al. [26] produced the Cluster – induced crystallization of nano – silicon particles. The possibility of producing from 20 nm to 100 nm sized silicon powders by plasma-induced reactions of silane including the formation of high-mass hydrogenated silicon anion clusters has been recently demonstrated. Careful HREM imaging showed circular contrast features, 1.5 to 2.5 nm in size, embedded in the amorphous particles which were attributed to the presence of medium range order in these regions. This

non homogeneous atomic distribution with partially ordered regions of a couple of nanometer dimension became more pronounced upon annealing up to the onset of crystallization. This observation and the formation of fivefold crystallite thereafter indicate that the clusters serve as seeds in the amorphous-to-crystalline transition.

Ultrafine oxidized tin particles with particle size about 6 nm have been prepared by Shek. C. H., et al. [27] inert gas condensation deposition under low oxygen pressure. The nanostructure, hyperfine parameters, and chemical stability of the particles have been studied by means of TEM, XRD and Mossbauer spectra analysis. The results show that the nanostructure of particles can be divided into a crystalline component and a disordered component. Nanopowders have high chemical activity and can be oxidized into stable SnO_2 compounds at ambient temperature: XRD measurements indicate that post-annealing at temperatures of 300-600°C for 2 h in air produced orthorhombic and tetragonal SnO2 phases. Orthorhombic SnO_2 phase may be an intermediate phase during the transformation of disordered SnO_2 to tetragonal SnO_2 (rutile) which is the high temperature stable phase under oxygen deficiency conditions.

The morphology of nanometer-sized cobalt granules in a granular $Cu_{88}Co_{12}$ alloy was directly determined by Wendog. Wang., et al [28] utilizing an atom probefield ion microscope. The granules are spherical in shape, and exhibit a size distribution. Giant magneto resistance (GMR) was observed in alloys with an average granule size ranging from 1.5 to 6 nm in diameter. A well-known theoretical model of general GMR behavior in magnetgranular

systems was confirmed based on measurement of size distribution pi the granules.

Photoinduced electron transfer at the surface of TiO_2 nanoparticles in ethanol were investigated by Martino. D. M., et al [29] studied with Fourier transform EPR (FT-EPR). Measurements were performed on three systems: (1) a solution of coumarin 343 (C343) dye and methyl viologen (MV^{2+}) in ethanol, (2) a colloidal solution of TiO_2 in ethanol containing MV^{2+}, and (3) a colloidal solution of TiO_2 in ethanol containing both C343 and MV^{2+}. In the C343/MV^{2+} system, pulsed-laser (355 nm) excitation of the dye results in MV^{2+} reduction. The rate constant of the photoinduced electron-transfer reaction, derived from the time profile of the FT-EPR spectrum of the MV^{+} radical, was found to be —$5x10^{9}$ M^{-1} s^{-1}, consistent with a near diffusion controlled reaction. Bandgap excitation (308 nm) of the semiconductor particles in the TiO_2/MV^{2+} system also gives rise to MV^{+} formation. In this case the FT-EPR signal growth can be described by a single exponential with rate constant kf =0.41 $x10^{6}$ s^{-1}. The kinetics indicates that MV^{2+} reduction involves photogenerated electrons trapped on the TiO_2 particles and is controlled by interfacial charge transfer rather than diffusive encounters of acceptor molecules with TiO2 particles. Dye-sensitized formation of MV^{+} radicals is observed as well following laser (355 nm) excitation of the C343/MV2+/TiO2 system. However, whereas the MV^{+} spectrum produced by the C343/MV^{2+} system reaches its maximum intensity around 100 ns after laser excitation, in the presence of TiO_2 the maximum is found tens of microseconds after the laser pulse. The time profile of MV^{+} formation in this case follows first-order kinetics with a time dependent rate constant, $kf = k_0 t^{\alpha-1}$, where both k_o and α are a function of the degree of dye

adsorption onto the TiO_2 particles and the pH of the solution. In this system, the trapped electrons responsible for MV^{2+} reduction are generated by excitation of adsorbed dye molecules, which leads to electron injection into the conduction band of the semiconductor. Dye-sensitization of the TiO_2 particles strongly increases the free radical yield. However, as the surface coverage by dye molecules approaches saturation level, the rate of electron transfer from semiconductor particles to acceptor molecules in solution is strongly attenuated.

Carbon encapsulated nanoparticle of Ni, Co, Cu, and Ti., was reported by Seraphin. S., [30] the encapsulation of metal nanoparticles into carbon clusters deposited by arc discharge, the detailed pathways of the formation of novel forms of materials remain unclear. The growth of a rich variety of morphologies is not well understood. Studies are reported here on the growth phenomena different metals encapsulated into carbon cages that emphasize the effect of carbon and metal supply on the size of particles. Postdeposition annealing was introdused as a process that induces structural rearrangements, and thus enables changes in morphologies. A set of carbon encapsulated Ni, Co, Cu, and Ti particles were prepared by an arc discharge process modified in the geometry of the anode and flow pattern of helium or methane gas. The samples were then annealed under flowing argon gas. Three annealing temperatures were used (600, 900, and 1100°C). Samples were characterized by transmission and scanning electron microscopy. Particles made under the same experimental conditions are of roughly the same size. When the supply of metal in the reactor space was increased by using a larger diameter of the metal pool the average diameter of the

particles is bigger than those of produced from the smaller metal pool. The thickness of the carbon cages of Ni and Co particle increased during the annealing. The carbon cages of Cu particles, however, did not change their thickness, while some carbon coatings of Ti particles disappeared under annealing. This suggests that the addition of layers for the Ni and Co cages results from a precipitation of carbon previously dissolved in the metal, while the much lower solubility of C in Cu prevents this possibility. The Ti of high reactivity, on the other hand, may further react with the available carbon under annealing to form TiO_2 is suggested that annealing provides additional thermal energy that makes structural rearrangement possible long after the initial deposition process was terminated This may explain the rich variety of morphologies of deposit obtained at different locations of the reaction chamber.

Polar solvation dynamics of a 95:5% (v/v) water/acetone mixture have been meausered at the ZrO_2 nanoparticle surface by timeresolved fluorescence of a probe molecules adsorbed to the particle surface that was synthesized by **[31]** Pant. D., and Levinger. N. E., interfacial solvent response displays two mb-picosecond diffusive components with the same time constants as bulk solution. However, the relative amplitudes for the individual relaxation-components are significantly different, leading to a faster average salvation response for molecules at the ZnO_2 surface. Furthermore, the overall fluorescence Stokes shift is approximately three times smaller for dye molecules adsorbed to the nanoparticle surface. Implication wits for electron injection into semiconductor nanoparticles are discussed.

A new method was developed by [32] Harris. P. J., and Tsang. S. C., for the production of filled carbon nanoparticles, which has many advantages over the usual arc-evaporation technique. The method involves high-temperature heat treatment of a microporous carbon which has been impregnated with a compound of the material to be encapsulated. In this study, this technique is used to synthesis nanoparticles filled with molybdenum, uranium and cobalt.

Particles with a diameter in the range of 1 to 100 nm are in a state intermediate between the solid and the molecular ones. When the number atoms in the particle are in the thousand ranges or above, properties evolve gradually from the molecular to the solid ones. In the limit where thermodynamical arguments remain valid, it was theoretically deduced by Wautelet. M., [33] that the melting temperature of small particles decreases with decreasing size. In the literature, such dependence is calculated for spherical particles. It is shown here that the radius-dependence of the melting temperature might be larger for the matter between particles than for the spherical particles.

Structural transition of bismuth nanoparticles observed by Oshima. Y., et al. [34] Bismuth nanoparticles with sizes ranging from 2 to 17 nm were found to be trans-, formed among three different structural phases using ultra high-vacuum TEM. Below 8.5 nm, the structure fluctuated among cubic, rhombic and twin structure like a quasiliquid phase. Between 8.5 and 11 nm, bismuth particles had a core-shell structure: the core of the cubic structure is surrounded by eight crystallites of the rhombic structure:-each rhombic

crystallite has (111), (110) and (112) facets of low surface energies; and have dislocations at the boundaries between them. Above 11 nm, the particle .had rhombic structure.

The sintering of copper nanoparticles deposited on a clean (001) copper surface has been studied in real time using a novel in-situ ultrahigh vacuum (UHV) transmission: electron microscope with a UHV DC sputtering attachment. The particles were found to assume an initially random orientation on the foil, reorienting upon heating to assume the orientation of the substrate by a mechanism involving classical sintering and grain growth, contrary to expectation. The experiment was inspired by that of Gleiter, where rotation of macroscopic copper balls to low energy configurations was observed upon annealing. It presents the results of our study and discusses the differences in reorientation mechanisms in the case of macro- and nano-scale particle sintering that were reported by Yeadon. M., et al. [35]

Layer-by-layer self-assembly of composite thin films of cadmium sulfide (CdS) nanoparticle and alkanedithiol were achieved by Nakanishi. T., et al [36] on a gold substrate by an alternate immersion into solutions of dithiols (1,6-hexanedithiol and 1,10-decanedithiol) and solution containing CdS nanoparticles (ca. 3 nm in diameter). The layer-by-layer structure was confirmed by angle-resolved X-ray photoelectron spectroscopy (XPS) at each composite-film preparation step. The proposed structure and mechanism of self-assembly were in agreement with our previous results obtained by Fourier trans-form infrared reflection-absorption spectroscopy.

Zink oxide nanoparticles are produced by the laser vaporization-controlled condensation technique were prepared by Silvers. S. J. S. Li. And El-Shall.

M. S., [37] these particles are connected in a web-like agglomeration. Their proper-ties are compared to those of ZnO nanoparticles produced by solution sol-gel and reverse micelle techniques. All particles have the bulk crystal structure and show quantum size effects in absorption and emission. They show emissions that consist of a blue bandgap feature with a subnanosecond lifetime and a green feature with mul-tiexponential lifetime decays. Emission from the stearate coated particles produced by the reversed micelle method is particularly intense.

The average particle size of 40-100 nm was observed by [38] Kezuka. H., and Zhang Qiang. Z. Xi., for ultrafine YBCO particles by TEM. From the analysis of nanostructures by high resolution electron microscopy, characteristic periodic patterns are estimated to be in [011]-image with calculated lattice parameters with a=3.84 Å and b=3.90 Å.

Electron microscopy of mesoscale arrays of quantum – Confined CdS Nanoparticles formed by Pinizzotto. R.F., et al [39] CdS nanoparticles using DNA as a template for the overall shape. Three DNAs were used: the circular and linear forms of the plasmid pUCLeu4 and circular ϕX 174 RF in all three cases, the mesoscale lengths are consistent with the A-form of DNA. The structural signatures and crystallography were confirmed using conventional and high resolution transmission electron microscopy, and electron diffraction. Optical spectroscopy demonstrated that the particles display quantum-confinement effects. This research is a fundamental demonstration of the power of combining biochemical and solid-state processing tech-niques.

Arrays of metal nanoparticles with well-defined two- or three-dimensional ordered structures in a solid matrix have many potential applications, e.g., novel optical gratings, data-storage systems, and microelectronics. A synthetic method is described for preparing multilayer composite thin films with metal nanoparticles in porous ceramic matrices through colloidal adsorption and sol-gel processing. Techniques for the control of the interparticulate distance, the number of particles in each layer, the interlayer distance, and the pore structure are outlined that were characterized by Hongyou. Fan., et al. [40]

Preliminary tests of plasma torches for the production of carbon-coated nanoparticles were synthesysed by Majetich. S. A., et al [41] a summary of carbon-coated nanoparticle synthesis using a carbon arc and other methods, we describe two types of plasma torches, used to prepare nanoparticles. In a plasma torch, the plasma can be generated either using a DC arc or through RF inductive coupling. Based on our transmission electron microscopy results, we have identified RF plasma torch synthesis as the better means of scaling up carbon coated nanoparticle production. The RF plasma is crucial to developing the carbon coatings because it can provide enough power to vaporize the car bon feedstock.

A thin $Ti_{73}Fe_{27}$ ribbon was prepared by Lee. C. L., et al [42] rapid quenching from the melt. The asquenched ribbon was in a metastable condition with a small amount of nanoparticles of TiFe, of a size of 138±31 nm, embedded in the β-Ti matrix. The β-Ti matrix was supersaturated with Fe, and the fraction of the matrix was higher than that in the equilibrium state. High-resolution imaging of the interface of the TiFe/β-Ti showed that a periodic array of dislocations was present in the interface to accommodate tht lattice

mismatch. The spacing between the dislocations in the as-quenched specimer was 5.0±0.5 nm. When the ribbon was heated to 700°C, growth of the TiFe nanopar-ticles to a size of 228±37 nm took place in the β-Ti matrix. The amount of β-Ti was reduced, as well as the Fe content in β-Ti. The interface between the TiFe and β-Ti remained semicoherent, except that the spacing between the interfacial dislocations was reduced to 3.5±0.6 nm. The persistence of the semicoherent interface was ascribed to the same crystal structure and close lattice parameters shared by TiFe and β-Ti. The growth kinetics of the TiFe nanoparticles during heating was examined based on the modified theory of isothermal heating. It can be considered to be con-trolled by the diffusion of Fe atoms in the β-Ti matrix to the TiFe phase. Prolonged heating of the ribbon below the eutectoid temperature led to partial transformation of β-Ti to α-Ti.

The size and shape of silver and indium nanoparticles embedded in a plasma polymer matrix formed from benzene or styrene monomer were characterized by Uan. D.N., [43] transmission electron microscopy (TEM) in lateral direction and by cross-sectional transmission electron microscopy (XTEM) in vertical direction. In multilayer assemblies consisting of plasma polymer/plasma polymer metal composite/plasma polymer (ABA), silver as well as indium nanoparticles were embedded only in one plane. XTEM micro-graphs on samples before and after appropriate thermal annealing (450 K) showed, that the multilayer [ABA] structure was not destroyed. At a higher annealing temperature and time (570 K, 3 h) only parts of the plasma polymer matrix were left. With all thermal annealed samples, reshapening and coalescence of the embedded silver particles was found. For multilayers with embedded indium particles, the second plasma polymer layer was

formed mainly as a shell around the large particles. During thermal annealing in the electron microscope, the formation of indium oxide particles inside these shells was observed.

Silicon carbide nanoparticle for advanced materials was produced by Viera. G., et al [44] nanometric powder of silicon carbide has been produced in a radiofrequency square wave-modulated glow discharge of SiH_4 and CH_4 gases. The transient behavior observed in the power absorbed during the discharge has been related to the various steps of the formation of particles. At the transmission electron microscope, two populations of particles were found: around 70 and 300 nm.'Electron diffraction pat-terns showed that the particles were amorphous although the short-range order was similar to that of β-SiC micrometric powder. The atomic concentrations of Si, C and H were determined by elemental analysis. The chemical composition was determined by X-ray photoelectron spectroscopy. The polymeric character of the powder was evident from the presence of CH_2 and CH_3 species as indicated by RAMAN and FTIR spectroscopies.

Irons. S. H., et al [45] synthesizing small metal particles for the catalytic growth of carbon nanofibers via chemical vapor deposition (CVD). We also found that abrasion of metals on a rough aluminum oxide surface will produce metal particles that will catalyze nanofiber growth. Ferritin, a biomolecule, also shows promise as a source of small iron particles for fiber growth. We also discuss our preliminary results involving the synthesis of. a nanoparticle array and the use of Co as a carbon precursor for the CVD synthesis of carbon nanofibers.

Small metal and semiconductor particles with a size of a few nanometers are one of the important systems in modern materials science. Nanoparticles have found applications in many fields, ranging from catalysis to magnetic storage that were reported by [46] Yacaman. M. Jose., and Mehl. R.F., In the present work, discuss some of the methods to characterize the structure of nanoparticles using electron microscopy, also discuss some of the exciting novel applications of nanoparticles in nanoelectronics and nanophotonics. Finally, show that nanoparticles play an important role in producing atmospheric pollutants.

Kineticly controlled growth and shape formation mechanism of platinum nanoparticles wes reported by Petroski. J. M. et al [47] transmission electron microscopic (TEM) results on the time-dependent shape distribution of platinum nanoparticles during the growth period and its dependence on the concentration of the capping polymer as well as the pH of the solution. The results suggest a shape-controlled growth mechanism in which the difference between the rate of the catalytic reduction process of Pt^{2+} on the (11 1) and (100) faces, the competition between the Pt^{2+} reduction and the capping process on the different nanoparticle sur-faces, and the concentration-dependent buffer action of the polymer itself all control the final distribution of the different shapes observed.

Nanorods and nanoparticles of NbC and TaC have been synthesized by Fukunaga. A., et al [48] reacting carbon multilayer tubes with NbC and Ta vapor in evacuated and Ar back filled quartz. ompoules, at various temperatures. As a function of the temperature, it is possible to stynthesize

an equiatomic superconducting carbide phase. After reacting at lower temperatures. —25 nm nanorods are observed in TEM and SEM. At higher temperature nanorods coarsen and eventually facet to form more equiaxed particles. Interesting hysteretic superconducting properties are observed which differ from known, bulk properties of the superconducting carbides. It suggests that in nanocrystalline lodshaped particles the influence of surfaces on the vortex lattice is considerable, .leading to interesting features in both the equilibrium and pinning-related hysteretic: response in high fields.

Nanotubes filled with pure Cu formed by Setlur. A. A., et al [49] using an arc discharge with metal/graphite composite anodes in a hydrogen atmosphere. These nanotubes are found in the soot deposited on the chamber walls instead of on the redeposited rod on the cathode as is the case with experiments in He, Since Cu and Ge do not form stable carbide phases, catalyze carbon fiber growth or have significant carbon solubility, a new mechanism is needed to explain the formation of these nanowires. It is proposed that polycyclic aromatic hydrocarbon molecules, produced by the hydro-gen arc are the precursors to the graphitic layers encapsulating the Cu or Ge nanowire. Direct evidence for this mechanism is given by evaporating pyrene ($C_{16}H_{10}$) and Cu or Ge together to form filled nanotubes. When evaporating a com-posite anode in hydrogen using ferromagnetic elements, such as Co, encapsulated nanoparticles are formed instead of nanowires. Encapsulated nanoparticles are also obtained when evaporating pyrene and cobalt, supporting the assertion that PAH molecules are precursors to nanostructure formation. Reasons for the' difference between nanoparticle

and nanowire formation are attributed to differences in reactivity of the metal with carbon.

Ion implantation of calcium and yttrium into high-purity, single crystalline alumina has resulted in the formation of metallic aluminum nanoparticles in the implanted regions that was synthesized by Hunt. E. M., et al [50] the calcium implantations were carried out at accelerating energies of 50 and 70 keV and resulted in particles with average diameters of approximately 8.2±1.4 nm. The yttrium was implanted at an accelerating energy of 150 keV and resulted in particles of approximately 10±1.8 nm in diameter. The ion fluence for all implantations was $5x100^{16}$ ions cm^{-2}. Differential optical absorption measurements support the presence of nanoparticles in these samples. The spectra from the Ca implanted samples show absorption features at —245 nm. The spectrum from the Y implanted sample shows a similar, but more intense, absorption feature at 239 nm. The particles are face-centered cubic with a calculated lattice parameter of a_o.0.41 nm and are randomly oriented and aluminum-rich with respect to the surrounding amorphous alumina matrix. Energy filtering transmission electron microscopy (EFTEM) results confirm that the particles contain metallic aluminum, which is formed as a result of the reduction of the alumina matrix.

Effect of nanoparticles size on the internal structure of copolymer nanoparticles composite were investigated by Lauter. Pasyuk. Y., et al [51] neutron reflection was used for the study of the composite films made of

symmetric (d-PS-PBMA) diblock copolymer (molecular weight Mw=170 and 135 K). With nanoparticles of γ-Fe2O_3 (4 and 6 nm in diameter) incorporated in the deuterated PS-domains with different concentrations. From the neutron reflection experiment we determined the period of the lamellar structure and the position of the nanoparticles in the PS-layers. It is important to examine the effect of the particle size on the lamellar structure. We determined that the small nanoparticles (4 nm) concentrate close to d-PS-PBMA interfaces while larger nanoparticles (6 nm) localize in the center of PS domains. This effect is of considerable interest in the elaboration of new composite materials since it will give a control on the particle distribution inside the host domains.

Silver nanoparticles encapsulation in carbon cages obtained by sputtering of the metal and graphite was reported by Babonneau. B.D., et al [52] synthesized C-Ag thin films by co- sputtering of a silver-graphite target. The, eposition temperature ranged from 77 K to 773 K, the silver concentration varying; from 10 to 71 at%. The microstructure of the films has been characterized by transmission electron microscopy (TEM) and small-angle X-ray scattering under grazing I ncidence (GISAXS) experiments. It is shown that homogeneousl:' distributed silver lanoparticles, having an elongated shape along the direction of the thin film growth, are formed within a more or less graphitized carbon n matrix. After liquid nitrogen and room temperature depositions, a preferential crystallography orientation is observed, lense (1 l l) silver planes being at 90° with respect to the surface layer whereas the .carbon matrix is amorphous. A graphitization leading to the encapsulation of the silver nanoparticles in graphite-like

carbon has been obtained when the depositor were performed at 773 K for lower silver concentrations without ion-beam assistance and below 573 K for upper silver concentrations with ion-beam assistance. 'We propose that the demixing of carbon and silver occurs during the co-deposition process) by surface diffusion of C and Ag atoms. It is inferred that the presence of silver imply serves as a "catalyst" for the graphitization process at these relatively low emperatures. Furthermore, we have investigated the tribological properties of our C-Ag coatings: a substantial increase in the wear resistance and a significant decrease in friction relative to an austenitic stainless steel substrate are observed.

The importance of the longrange Lifshitz-van der Waals interaction energy between: condensed bodies are well known. However, its implementation for interacting bodies hat are highly irregular and separated by distances varying from contact to micromeers has received little attention. As part of a study of collisions of irregular aerosol)articles, an approach based on the Lifshitz theory of van der Waals interaction has seen developed to compute the interaction energy between a sphere and an aggregate) of spheres at all separations. In the first part of this study, the iterated sum-over -dipole interactions between pairs of approximately spherical molecular clusters are :ompared with the Lifshitz and Lifshitz-Hamaker interaction energies for continuum spheres of radii equal to those of the clusters' circumscribed spheres and of the same nasses as the clusters, The Lifshitz energy is shown to converge to the iterated dipolar energy for quasispherical molecular clusters for sufficiently large separations, vhile the energy calculated by using the Lifshitz-Hamaker approach does not. Next, the interaction energies between a contacting pair of these molecular clusters and a hird cluster in

different relative positions are calculated first by coupling all molecules in the three-cluster system and second by ignoring the interactions between the molecules of the adhering clusters. The error calculated by this omission is shown to x very small, and is an indication of the error in computing the long-range interaction energy between a pair of interacting spheres and a third sphere as a simple sum) ver the Lifshitz energies between individual, condensed-matter spheres. This Lifshitz energy calculation is then combined with the short-separation, nonsingular van kr Waals energy calculation of Lu, Marlow, and Arunachalam, to provide an integrated picture of the van der Waals energy from large separations to contact that were oblised by Arunachalam. V., et al. [53]

The alloying behaviour in nanometer (nm)-sized particles was characterized by Mori. H., and Yasuda. H.,[54] transmission electron microscopy (TEM). When solute atoms are vapour-deposited.onto sin sized particles at room temperature. rapid dissolution of solute atoms into partitci occurs, and solid solution or compound particles are successfully formed. Such spoor. taneous alloying occurs even between nm-sized particles of different elements. Our results can he summarized as: (i) spontaneous alloying takes place via a solid-state

Alkaline earth oxide nanoparticle as destructive absorption for environmental toxins was reported by Moscovici. J., et al [55] Sc and Ca oxide nanoparticles are very reactive materials used to mitigate atmos fheric.pollution and to sequester polluting molecules. It studied the structure SrO nanoparticles using Sr K-edge and Fe K-edge XAFS. that was prepared with 'various reactivities. with or without a Fe_2O_3 coating. And before and after reaction CCl_4, or SO_2. For CCl_4, the polluting fraction of the reagent is

totally absorbed in the bulk particle for SO_2. the results show a total reaction for the aerogel preparation' (AP) compound. For the coated particles before reaction, the iron oxide has a very disordered structure and it is mixed with small metallic iron clusters for conventional preparation (CP) compounds.

A micromechanism-based model is developed by Lyer. R., and Sastry. M. L. [56] for nanoparticle densification during uniaxial and hydrostatic pressing. The model takes into account the effects on densification of agglomeration, bulk and surface impurities, fewer dislocations per particle and low stability of dislocations due to fine size, and other factors unique to nanoparticle systems. The model is applicable to a general nanoparticle system, and is capable of predicting density.'densitication rate(s), dominant densification mechanisms. and microstructural features. as a function of consolidation parameters. The Present model is the first rigorous and comprehensive attempt to extend the HeIle -Easterling-Ashby model to the nanocrystalline grains-size regime. Predictions of the model were compared with experimental data on nanocrystalline copper and nanocrystalline molybdenum disilicide and observations reported in literature. A good agreement of model predictions with experimental data for a wide range of material and processing variables was observed.

The ion beam synthesis of group IV (SiC) and II-VI (ZnS) compound nanoparticles in SiO_2 layers was synthesized by Perez Rodringuez. A., et al [57] these systems are potentially interesting for optoelectronic applications such as electroluminescent devices emitting in the visible and UV range. The combination of structural (transmission electron microscopy. electron

and X-ray diffraction), optical (infrared and Raman spectroscopies, optical absorption and photoluminescence) and physico-chemical (X-ray photoelectron spectroscopy, secondary ion mass spectroscopy) techniques have been used to identify the phases formed and to correlate the optical behaviour of the layers with their microstructure. The first part is dedicated to the synthesis of luminescent SiO_2 layers coimplanted with Si and C. The presence of regions with different composition in terms of C content gives rise to the formation of 3 types of nanoparticles (Si,C and SiC) leading to three intense. Simultaneous and independent emission bands covering the whole visible range. A second part is dedicated to the synthesis of Mn doped ZnS nanocrystals. We have succeeded in synthesizing ZnS nanocrystals by sequential ion implantation in SiO_2. The structural characterization of the annealed layers shows ZnS precipitates having a wurtzite-2H structure and with a quite narrow distribution of sizes. This population of nanocrystals is organized in two layers parallel to the free surface, as a consequence of a pure Ostwald ripening process or as a result of the implantation damage distribution. The optical analysis of samples coimplanted with Mn shows the presence of a yellow-green and intense photoluminescence corresponding to an intra-Mn^{2+} transition, which demonstrates the effective doping with Mn of the ZnS precipitates.

The γ-Fe_2O_3 nanoparticles coated with DBS and CTAB were prepared by Liu. T., et al **[58]** by the microemulsion method. The coated samples show enhanced nonlinear optical properties compared with their bulk counterpart. The Mossbauer spectra at room temperature were measured for the coated ferric oxides. The monolayers of the organic molecules are found to have a

strong chemical bond with the surface atoms and thus have a significant influence on the electron structure of the particle surface.

Fivefold twinning in thin films and small particles of nanometer dimensions is origin of metastable structures the ubiquitous presence of which in a whole class of nanocrystalline materials results from the great variety of materials and fabrication processes involved. These are reviewed and discussed together with the formation mechanisms of such structures and their stability including the role of lattice defect various illustrative examples are aimed to emphasise the importance of this phenomena in the area of nanocrystalline materials that was investigated by Hofmeister. H., [59]

Polymer composites of nano sized particle were characterized by Dzhardimalieva. G. I., and Pomogailo. A.D., [60] the kinetics and mechanism of thermal decay of transition metal acrylates or its collides are studied. At 200-300^0 C the rate of thermal decay can he described by first order rate equations. The thermal transformations of the metal-containing monomers order study involve dehydration. solid-phase polymerization and thermolysis process. The compositions of products of the thermal transformations are studied. The products of the decay are analyzed by optical and electron microscopy as well as magnetic measurements. IR and mass spectroscopy. The main solid-state products decomposition are nanometer-sized particles of metal or its oxide and features with a narrow size distribution stabilized by' the polymeric matrix. The average particles sizes are 6.0-13.0 nm in the case of $FeAcr_3$ and 6.0 nm for cocrystallites for CoAcr and Fe_2CoAcr.

EXAFS of cobalt nanoparticles embedded in a coper matrix was characterized by Cezar. J. C., et al. [61] In this work samples with different

microstructures, departing from as-quenched Con-xCox(x = 3. 10 and 25) meltspun ribbons,. were studied using the X-ray absorption, specctroscopy (XAS) technique. The spectra (XANES. EXAFS) of these samples, as well as of pure fcc Cu and hcp Co used as reference. were measured in the XAS line of LNLS. As a function of heat treatment, the spectra in the Co K edge shift, in terms of average Co-metal distances. from FCC Cu towards pure FCP Co a detailed analysis of this evolution could, in principle. give indications of the cluster size.

Argon – saturated aqueous solution of $NaAuCl_4$ and $PdCl_2$ or K_2PtCl_4 were reduced simultaneously by ultrasound irradiation to prepare noble metal alloy nanoparticle were prepared by Oshima. R., et al [62] droplets recovered from colloidal dispersions were placed on carbon-supported cop-per grids, and dried in a vacuum. They were examined by TEM, HRTEM, and nano-area energy dispersion X-ray spectroscopy (EDX). The Au-Pd nanoparticles exhib-ited monodispersive distribution (8 nm), and consisted of a gold core and a palladium shell. Au-Pt alloy nano-particles could not be produced from NaAuCl4 and K2Ptai aqueous solutions either by simultaneous or successive reduction.

Hofmeister. H., and Kodderitzsch. P., [63] were explored the possibilities of inert gas arc evaporation for fabrication of nanosized Si partic es and studied agglomeration, size, shape, crystallinity, surface roughness and internal structure of these particles by conventional and high resolu-tion electron microscopy. The rarely used technique yielded single crystalline, spher-ical Si particles 3-16 nm in size completely free of planar lattice defects. The parti-cles, covered by thin amorphous oxide shells. are agglomerated into chains and tangles. The lattice of diamond cubic type exhibits contractions

which decrease as with, decreasing particle size the oxide shell thickness is reduced. This effect is ascribed to compressive stress at the Si/oxide interface.

Opyical and electrical properties of embedded silver nanoparticles was reported by Heilmann. A., et al [64] silver nanoparticles which are embedded in a polymer matrix exhibit an optical absorption in the visible and near-infrared region due to plasma resonance excitation. The spectral position, the half width and the intensity of the plasma resonance absorption depend on the particle size, particle shape as well as on the optical behavior of the host material. The particle size and shape distribution was determined by transmission electron microscopy (TEM). Optical extinction and d. c. conductivity at one and the same silver particle assembly with large particles ($D_m \approx 50$ nm) were measured 'simultaneously at 4.2 and 1.2 K as well as at room temperature. A significant blue shift of the plasma resonance absorption was found at low temperatures. The D.C. conductivity decreases up to two orders of magnitude and a significant photocur-rent was measured.

Glasses containing nanoparticles of $CulnS_2$ dispersed in a silicate matrix were fabricated. Absorption and luminescence spectra of glasses containing nanocrystals with size of 10-70 nm were studied. The possible reasons for the long-wavelength shift of the fundamental absorption edge and the non-chalcopyrite structure of $CuInS_2$ nanoparticles are discussed. Anomalous crystal structure and some optical properties of small particles were reported by Gurinovich. I.J., et al. [65]

Nanosized ceramic powders (Cu/SiC. Y_2O_3 -stabilized cubic ZrO_2) were produced by Lutzenkirchen – Hecht. D., et al [66] evaporation of coarsely

grained powders of the respective materials in an inductively coupled thermal plasma process and rapid quenching of the vapor. The atomic short range order of these nanoparticles with an average diameter of about 10 nm was investigated ex situ with EXAFS. The results are compared to crystalline reference neterials.

Hematite nanoparticles which were coated, respectively, with sodium dodecyl benzene sulphonate (DBS) and cetyltrimethyl ammonium bromide (CTAB) were synthesized by Zhonghua. Wu., et al [67] using microemulsion method in the system of water/toluene. The particle size and shape were characterized with transmission electron microscopy TEM. The TEM results show that the nanoparticles take the shape of sphere with diameter of 5.0 nm and 6.0 nm for modified DBS and CTAB respectively. The local atomic structures of these nanoparticles were probed by using XAFS technique. Fe-K absorption spectra were collected at beam line 4W I B of BSRF. The local atomic structure in DBS-coated hematite was found to be similar with that in bulk hematite except the anharmonicity increasing, but about 0.04 $'A^0$ expansion of Fe-O bond length in CTAB-coated hematite. The interface/surface atomic configuration were compared and discussed.

The phase distribution and magnetic properties of nanoparticulate Fe/SiO_2 samples was analysed by Julian. De. C., et al [68] by high-energy ball milling. From our data, suggest that the elevated coercivities measured in the samples are linked to the coupling of the core of the particles (α-Fe) with a highly disordered phase present in their surface region and whose behavior exhibits sonic similarities with it spin-glass phase.

Nanosized indium oxide (InO_3) particles, dispersed within pores of mesopoious silca were synthesized by Huijuan. Zhou., et al [69] soaking and thermal decomposition of indium sulfate. The particles were characterized by transmission electron microscopy (TEM) and nitrogen sorption isotherms. Photoluminescence spectra of the samples annealed at different temperatures were measured. It was shown that the In_2O_3 nanoparticles were isolated from each other and highly uniformly dispersed inside the pores of silica hostwhich were less than 8 nm in diameter. New photoluminescences were observed for- the samples annealed at different temperatures.

The fabrication and structural observation of in nanoparticles deposited on Si (110) substrate were investigated by Tanaka. M., et al [70] in an ultrahigh vacuum field emission transmission electron microscope. High-resolution electron microscopy of deposited in shows the formation of nanoparticles with various sizes. Nanoparticles more than 7 nm in diameter have tetragonal structure similar to the bulk, whereas nanoparticles of about 3 nm sizes seem to have FCC structure. Their shapes fluctuate fluently, sometimes showing: coexistence of solid and liquid. Nanoparticles more than 10 nm in diameter show transitions between single crystal, single twin and decahedral multiply twinned particles.

Guo. Lin., et al [71] aimed to prepare PbS nanoparticles modified by manoxol OT (AOT) and determine its transient nonlinear optical properties. The PbS nanoparticles were prepared by using rnicroemulsion method and the, transient nonlinear optical properties' were investigated with standard time resolved pump-probe techniques. A very rapid' induced absorption was investigated. The decay time of the PbS nanoparticles modified is about 100 fs. The transient induced absorption in PbS

nanoparticles modified by AOT arises from the biexciton effect and the trapped carrier induced Stark effect. The surface chemical modification environment has significant effects on the transient nonlinear optical properties.

Sengupta. A., et al [72] was reported the first direct measurements of ultrafast electronuic relaxation dynamics in PbI_2 colloidal, natiopartices using femtosecond transient absorption spectroscopy. The PbI_2 nanoparticles were prepared using colloidal chemistry methods in different solvents. including ethanol. 2-propanol. 1-butanol. water. and acetonitrile. as well as in poly (vinyl alcohol) (PVA) matrix. The particle sizes were determined using low aed high-resolution transmission electron microscopy and atomic force microscopy. Whitch provided direct evidence of photodegradation of the nanoparticles. The ground state electronic absorption spectra of aged PdI_2 particles in acetonitrile and alcohol solvents showed two major peaks near 360 and 292 nm, which slightly blue shift with decreasing size. In aqueous solution containing PVA a new sharp excitonic peak appeared 414 nm. indicative of nanoparticle formation. With excitation at 390 nm and probing in the visible to nearinfrared region. the electronic relaxation dynamics a PbI_2 nanoparticles were directly monitored. The electronic relaxation is found to be sensitive to solvent and insensitive to particle size. In acetonitrile the relaxation was dominated by a 75 ps decay. In alcohol solvents. in addition to a 75 ps decay, fast decay was observed. The relaxation in aqueous PVA solution featured double exponential decay with time constants of 1 and 40 ps. There appeared to be ,oscillations at early times with a period changing with solvent but not with particle size. The dynamics observed were somewhat dependent the probe

wavelength and independent of the excitation intensity. The results suggest that the surface plays a major role in the electronic relaxation process of PbI_2, nanoparticles. The influence of particle size is relatively minor in the size range studied (3-100 nm). probably becise the relaxation is dominated by surface characteristics that do not vary significantly with size and/or the size is larger than the exciton Bohr radius (1.9 nm) ard thereby spatial confinement is not significant in affecting the relaxation process.

The growth and characterization of iron oxide nanoparticles by polyionic multilayers assembled by electrostatic layer-by-layer adsorption were reported by Dante. S., et al [73] the polyions poly (diallyldimethylammonium) chloride (PDDA) and polystyrenesulfonate (PSS) were used for the layer-by-layer assembly of the polyions. Nanoparticle nucleation was achieved by a cyclic repetition of Fe oxidative hydrolysis under an inert atmosphere. We employed U V- vis analysis for both monitoring the multilayer assembly process and ascertaining the influence of the Fe oxidative hydrolysis pro-cess on the integrity of the polymer film. No degradation of the multilayers due to the particle growth procedure was observed. The nucleation and growth of needle-shaped nanoparticles with a length of about 100 nm and a width of about 10 nm were detected by transmission electron microscopy (TEM). The void volume of the poly-mer matrix provided an upper limit to the particle size. As shown by selective area electron diffraction (SAED), the polycrystalline particles were identified as β-FeOOH (akaganeite). a result confirmed by reflection-absorption IR spectroscopy.

The thermal behaviour of CdS nanoparticles and especially of their surfaces had been investigated by Winkler. U., et al [74] using high

resolution photoelectron spectroscopy. Different annealing char-acteristics were observed for particles of different sizes. From the changes of surface corelevel shifts in the S 2p and $Cd3d_{5/2}$ spectra we derive that the nanoparticle surface, which is S-terminated at room temperature. changes after annealing by removal of S atoms and segregation of Cd atoms. Furthermore. It observes that the tempera-ture at which this process takes place depends on the particle size.

The formation of an amorphous phase in nanosized Bi particles embedded in an Al-based glassy alloy matrix. High-resolution electron microscopy (HREM) has been used to show that the particles contain crystalline and amorphous portions were reported by Goswami. R., et al. [75] A depression of the melting point by more than 100 K of the crystalline portion of the Bi particles was found by differential scanning calorimetric studies and by in-situ electron microscopy using a heating stage. The same techniques established the absence of an amorphous phase in the particles when the matrix is crystallized. It is shown that the formation of the amorphous phase and the depression of the melting point cannot be explained by the pressure developed by the volume change during solidification in this constrained system.

The observed lattice contraction of nanoparticles is attributed to: both the surface bond that contracts with coordination number reduction of surface atoms, and the surface-to-volume ratio that increases with decreasing particle size. Surface bond contraction varies with materials and crystalline orientations while the surface-to-volume ratio depends on particle shape

and size.The lattice contraction of nanometer – sized Sn and Bi particles produced by Sun. C. O., [76]

In this contribution, Buschmann. V., et al [77] reported on the influence of the growth conditions on the final crystalline quality of 3C-SiC nanoparticles with dimensions around 3-10 nm. The nanoparticles are grown by chemical vapour synthesis in a hot wall reactor using tetramethylsilane [$(CH_3)_4Si$] as precursor. By altering the decomposition temperature and reactor pressure, the clusters may be amorphous at low temperatures or crystal-line at elevated temperatures. Crystalline nanoparticles show a one-dimensional stacking disorder with slip planes lying on different families of (111) planes when prepared at high reactor pressure. By lowering the pressure, only one-dimensional disordered particles along single (1 l 1) planes are observed.

The conversion of an amorphous carbon film under Al nanoparticles to giant onionlike fullerenes (GOLFs): This was induced by electron irradiation in a transmission electron microscope, was investigated by Xu. B. S., and Tanaka. S.I., [78] it has become clear that the nucleation and growth processes forming GOLFs from an amorphous carbon film consist of three steps: first, the flakes of GOLFs are induced under Al nanoparticles; second, the flakes grow into a few ellipsoidal graphitic shells; and third, a gradual reorganization occurs into structures comprising the quasispheroidal graphitic shells that are GOLFs. Fullerenes containing Al nanoparticles and Al atoms have been generated, through these processes. It is suggested that the mechanism involves collisions with highenergy electrons and a catalytic effect of Al, while any temperature rise due to electron irradiation seems to be negligibly small.

A new approach for the structural and morphological characterization of powders was characterized by Jimenez. V. M., et al. [79] It has been applied to characterize a nanostructured SnO_2 material prepared by the gas phase condensation method. Transmission electron microscopy, X-ray diffraction, X-ray absorption spectroscopy and infrared spectroscopy have been used for the characterization of the samples. Besides the conventional fitting procedure of the EXAFS spectra, the mathematical method of factor analysis applied to the XANES spectra has been used to determine the percentage of amorphous phase existing in the samples after annealing at increasing temperatures up to 773 K. The results are confirmed by a FEFF simulation of the EXAFS spectra. The original powder was partially amorphous and was formed by very fine particles (d ≈ 8-10 nm) linked in a fractal-like structure. No significant sintering occurs at T=573 K, although the powder becomes more crystalline. At 773 K, sintering (d ≈ 20-30 nm) and further crystallization takes place. Factor analysis has been also applied for the study of the FT-IR spectra of SnO_2 nanaparticles and the results confirm semiquantitatively the degree of crystallization calculated from the analysis of the XANES spectra. The effective medium theory permits a description of the particle shapes that constitutes the crystalline component of the FT-IR spectra determined by factor analysis.

Capped copper nanoclusters were successfully synthesized by Joshi. S. S., et al [80] a gamma radiolysis method by optimizing various conditions like metal ion concentration, polymer or surfactant concentration and pH. The increasing amount of capping agent was responsible for decrease in size as small as 17 nm of the metal clusters. The radiolytic method provides

copper nanoparticles in fully reduced and highly pure state compared to other synthetic routes. Formation of copper nanoclusters (FCC) was confirmed by X-ray diffraction technique. UV-vis spectrophotometry was employed to examine changes in plasmon resonance absorption peaks of copper metal. The purity of copper particles was further confirmed by electron spin resonance studies. Transmission electron microscopy results revealed the particle size distribution from 17 to 80 nm. An electron diffraction pattern confirms a FCC copper phase. The.role of various parameters in the formation of stable copper clusters is discussed.

Highly-oriented Si nanoparticles (SNP) were precipitated in amorphous SiO_2 using separation by implanted oxygen (SIMOX) method and showed visible luminescence at room temperature that were characterized by Okui. M., et al. **[81]** In order to investigate the microstructure of the SNPs, we observed the Si/SiO_2 interface by cross-sectional high-resolution transmission elec-tron microscopy (HRTEM). The three-dimensional shape of the SNPs observed from different directions is an (1 1 1) -surrounded octahedral structure, each apex of which has an (100) facet. The upper (surface-side) interface of SiO_2/Si(100) contains miss-ing atomic rows, while the lower (substrate-side) interface of $Si(100)/SiO_2$ is atomi-cally flat except for the steps at the intersection with '(111) plane. Similar atomically sharp structures were observed at the $Si(111)/SiO_2$ interfaces. Image-simulation of the interfaces well reproduced the microstructures observed by HRTEM and proved that the interfaces are those of amorphous SiO_2 and singlecrystal Si without any intermediate layer.

Aqueous and nonaqueous colloids of a series of ternary semiconductor compounds: $CuInS_2$, $CuInSe_2$, $CuGaS_2$, $CuFeS_2$ and $AgInS_2$ were prepared by Gurin. V. S., [82] the disperse phase was identified by X-ray diffraction analysis of solid precipitates. The optical proper-ties of colloids, and polymer films with ultrasmall particles fabricated from the col-loids, were studied. Features of the absorption in the UV, visible and near IR regions are interpreted as quantum-size effects and the result of partial oxidation of copper compounds.

Small-angle X-ray scattering is used to study size distributions of noble metal nanoparticles embedded in polyelectrolyte hydrogels with oppositely charged surfactants was reported by Svergun. D. I., et al. [83] A procedure is proposed to subtract matrix scattering and to extract pure scattering due to the nanoparticles allowing,to evaluate their size distribution functions by means of a regularization technique. Two kinds of collapsed gel-surfactant complexes were studied: a complex of a cationic gel of poly (diallyldimethylammonium chloride) with an anionic surfactant sodium dodecyl sulfate (PDADMACl/SDS), and that of an anionic gel of poly(methacrylic acid) with a cationic surfactant cetylpyridinium chloride (PMA/CPC). Addition of a gold com-pound ($HAuCl_4.3H_2O$) to the PDADMACl/SDS system forms the metal compound clusters and leads to a partial distortion of the gel structure. After subsequent reduction of the gold compound with sodium borohydride ($NaBH_4$) ordering in the gel disappears and gold nanoparticles are formed. Their size distribution includes a fraction of small particles with approximately the same size as the compound clusters before reduction and a fraction of larger particles with the radii up to 40 nm. For the collapsed PDADMACl/SDS gels, aging

does not change the size distribution profile; for the noncollapsed PDADMACl gels without surfactant, metal particles are found to grow with time. This suggests that the aggregation of metal colloids is prevented by the ordering in the collapsed gel-surfactant complex. The addition of $HAuCl_4.3H_2O$ and the subsequent reduction of the metal ions in the PMA/CPC system does not distort the gel structure as the degree of incorporation of $AuCl_4$ ions is very low. Particle sizes in the PMA/CPC system are found to be somewhat larger than those in the PDADMACl/SDS system. The PDADMACl/SDS gels loaded with the $PtCl_4$ compound were also studied to analyze the influence of the reducing agent type on the particle size distributions. Fast reduction with $NaBH_4$ yielded mostly small particles with the radii around 2 nm grown from the compound clusters similar to those observed for the gold-loaded gels. In contrast, slow reduction with $N_2H_4.H_2O$ was found to produce larger nanoparticles and the size distribution func-tion shows a major fraction of the particles with the radii up to 30 nm.

An amphiphilic poly (acrylic acid)/polystyrene graft copolymer (PAA-g-PS) has been used to form "nanoreactors" for the synthesed by Plummer. C. J. G., et al **[84]** of gold clusters. Such'copolymers tends to form stable micelles in non-polar organic solvents where the poly (acrylic acid) chains constitute the core, and the polystyrene chains, the shell. In the present study, the micellar structure of PAA-g-PS in toluene has been demonstrated by dynamic light scattering and transmission electron microscopy (TEM). The subsequent prepa-ration of goldgraft copolymer composites involved the introduction of gold chloride ($AuCl_3$), either in powder form or previously dissolved in ether, into the micellar cores of the

PAA-g-PS in toluene. The gold salt was then reduced by ultraviolet (UV) irradiation of the emulsion, or of dried cast films. TEM and ultraviolet-visible (UV/Vis) spectroscopy were used to characterize the resulting composites. Gold particles of less than 5 nm in diameter were observed in all cases, but the size distribution and the spatial arrangement of the clusters in the cast films were modified when diethyl ether was used to introduce $AuCl_3$ into the PAA-g-PS micellar cores. This was thought to be due to enhanced nucleation of the gold particles and partial disrup-tion of the micellar cores in the presence of diethyl ether.

Andersson. O. E., et al [85] were investigated the structure and electronic properties of graphite nanoparticles prepared by heat treating diamond nanoparticles. The prepared nanographite forms polyhedron with a hollow in its inside, whose faces comprise a stacking of 3-6 planar graphene sheets with an in-plane size of 7-8 nm and an intersheet distance of 0.353 nm. The large intersheet distance suggests a considerably large reduction in interlayer interaction compared to the case of bulk regular graphite. Electron-spinresonance and magnetic-susceptibility measurements show that there is a considera-ble enhancement in the density of states at the Fermi energy, indicating the presence of an additional band superimposed upon the bonding π and the antibonding π^* hands around the Fermi energy. Taking into consideration the discontinuous shape at an edge line formed by crossing adjacent graphene sheets, graphene sheets in a nanographite particle are considered to have open rcbond edges. On the basis of the theoretical suggestion that nonbonding π orbitals give edgeinherited surface states depending on the shape of the graphene edge, this is

suggestive of the contribution of the edge states to,the electronic structure of nanosized graphene having open π-bond edges.

Using the aqueous cores of reverse miecelles as nanoreactors. Nanoparticles (d ≈ 10 nm) of the mixed ferrite $MnFe_2O$, were produced by Carpenter. E. F., et al [86] seven processing trials were performed where the concentration of ammonium hydroxide. reaction temperature, and the oxidizing agent were varied. All trials rekilt in Mn-ferrite particles with varying chemistry and structure. The Mn concentration in the resulting ferrite is strongly enhanced by both the presence of H_2O_2 as an oxidizing agent and a surplus of ammo-nium hydroxide. The increased Mn concentration correlates with a higher fraction of octahedrally coordinated Mn cations. When nearstoic amounts of ammonium hydroxide are used. The resulting ferrites are nearly stoichiometric with a more equi-table distribution of Mn cations on the octahedral and tetrahedral sublattices. In all ferrite nanoparticles. the Mn cations have a preference for octahedral site occupancy that is larger than the 20% measured in bulk Mn-ferrite. We attribute the cation fill-ing trends to the stabilization of excess trivalent Mn during processing.

Neutron powder diffraction is used to study the order-disorder transformation in carbon-coated .$FexCo_{1-x}$ nanoparticles produced using a radio frequency plasma torch. The nanoparticles. nominally $Fe_{50}Co_{50}$), are produced from alloy powder and acetylene precursors by gasphase nucleation from the plasma was reported by Scott. J. H., et al. [87] The resulting nanoparticles undergo an orderdisorder transformation near 730^0C, passing from an ordered B_2(CsCl) structure to .a disordered Al (body-centered-cubic) structure upon heating, similar to the transformation

seen in bulk equiatomic FeCo. Although it is very difficult to quench the disordered state in bulk samples. the extreme cooling rates present in the plasma reactor produce metastable disordered nanoparticles. Neutron powder diffractograms acquired during a heating-cooling cycle at 27, 500, 710, 800, 710, and 400°C indicate the particles relax to their equilibrium ordered state upon heating first, disorders as they pass through the transformation temperature, and reorder upon cooling.

Chain of cubes iron nanoparticles borohydride reduction of acicular akaganeite particle was prepared by Chen. Min., and Nikles. D. E., [88] Ellipsoid shaped akaganeite (β-FeOOH) particles. 70 nm long and 10 nm in diameter. were prepared by forced hydrolysis of ferric chloride. The β-FeOOH particles. were suspended in a lamellar liquid crystal phase at 0˚C and reduced with: dilute. sodium borohydride solution to iron particles. These conditions allowed its to slow the reduction reaction and isolate partially reduced iron particles. Transmission elec-tron microscopy images showed that the particles were being reduced from the outside and there were nanometer-sized spherical iron clusters on the surface. Fully reduced iron particles were chains of cubes, with the cubes about 20 to 25 nm in size. The cubes were connected either corner to corner. edge to edge. or face to face. The face to face chains of cubes had the desired acicular shape, with aspect ratios exceeding five. This face to face chain of cubes microstructure was also observed in com-mercial iron particles.

Terbium oxide napoparticles were produced by Wakefied. G., et al [89] a colloidal chemical technique. High resolution transmission electron microscopy has identified particles with a mean size of 4.2 nm crystallised in the cubic phase. Optical absorption spectroscopy has ruled out the presence of any Tb^{+} ions in the nanoparticies. There by confirming the chemi-cal composition as Tb_2O_3,. A strong absorption peak at 225 nm corresponds to the $4f^8 - 4f^7$ transition. Under excitation at 254 nm the nanoparticles exhibit strong green luminescence corresponding to $^4D_4 - {}^7F_{n-3}$ transitions of Tb^{3+} ions. No blue transitions from the $^5D_3$ state were observed. The quantum efficiency of the nanopar-ticle luminescence is 37%.

Characteristic differences are observed for the dielectric response and microstructures of $BaTiO_3$ nanoscale fine powders reported by Jiang. B., et al [90] using sol gel (SG) and steric acid gel (SAG) methods. The former exhibit a critical size below which there is no paraelectric/ferroelectric phase transition whereas $BaTiO_3$ prepared via the SAG route remained cubic for all conditions of preparation. The SAG preparations always showed chemical intergrowth defects and (111) multiple twinning. The density of such defects tended to increase as the particle size decreased. The SG preparations were single phase and became tetragonal above some critical size (>130 nm). Some SG $BaTiO_3$ showed (111) twinning. The electron optical image analysis of nanocrys-talline $BaTiO_3$ particles by computer simulation and image-matching techniques has identified the intergrowth phase as polytypic variants of the perovskite structure of $BaTiO_3$ i.e., mixtures of cubic and hexagonal $BaTiO_3$. These defects are

stoichiomet-ric and were found for SAG $BaTiO_3$ particles of all sizes. Image analysis was used to determine that the nanoscale multiple twins involve a pure mirror symmetry operation with BaO atoms forming the twin composition plane. The relationship between the observed nanostructures and defects and the dielectric properties is discussed.

Lattice constants in monosize CeO_{2-x} nanocrystalline particles increase with decreasing particle size. This phenomenon called lattice relaxation is well explained by the model that the number of surface oxygen is reduced to half and its nominal valence is not -2 or -0.5 but -1. This suggests that all the surface oxygen form O_2^{2-} species in the nanocrystallites that was investigated by Tsunekawa. S., et al. **[91]**

The formation process of CuCl crystals has been studied in (3 MeV $6x10^{16}$ Cl^{2+} ions/cm^2+3 MeV $6x10^{16}$ Cu^{2+} ions/cm^2) -implanted silica glass by X-ray absorption spectroscopy and secondary ion mass spectroscopy. It was synthesized by Fukumi. K., et al **[92]** found from X-ray absorption spectroscopy that Cu atoms were mainly coordinated by oxygen atoms in as-implanted glass. Heat-treatment at 600°C caused the formation of Cu-Cl bonds and heat-treatment at 1000°C caused the formation of CuCl crystals in silica. It was deduced that the migration of Cl atoms is a rate-determining step for the formation of CuCl crystal. on the basis of the conventional precipitation model.

Starting with ferric alcoxide, α –Fe_2O_3 (hematite) nanoparticles were synthesized by Zysler. R. D., et al **[93]** using XRD, TG, TEM and magnetization measurements were employed for characterizing the samples. The results show nanoparticles of 55A° and 73A° mean diameter

for the diverse series with a narrow size distribution. We present correlations between the synthesis parameters and the final particle size.

The groth of manometer scale Cu metal particles in an amorphous SiO_2 film was derived under a finely focused. intense electron beam in a dedicated scanning transmission electron microscope. Annular dark-field images show that the particle illuminated by the beam grows at the expense of surrounding Cu particles. Electron energy-loss spectroscopy was used for identifying the oxidation states of particles scanning Cu atoms. An electric-field induced diffusion model explains the growth of metal particles in a dielectric medium that was examined and compared by Ito. Y., et al. [94]

An aluminosilicate with the MCM-41 structure (AlMCM-41) was used as a host for the synthesized by Jung. Jin – Seung., et al [95] of nickel metal nanoparticles. Initially, ion exchange in aqueous solu-tions allows the introduction of nickel cations into AlMCM-41, and then reduction with sodium borohydride produces nanometer-sized nickel metal particles. Products (Ni-AlMCM-41) were characterized by elemental analysis. transmission electron microscopy (TEM), X-ray powder diffraction (XRD), and magnetic susceptibility. Ni-AlMCM-41 was found to have a Ni:Al:Si ratio of ca. 1:4:28. The nickel metal particles were 1-2 nm in diameter and showed superparamagnetic behavior with a blocking temperature (Tb) of 5 K.

Dialkyldithiophosphate - modified copper nanoparticles (DDP-nano Cu) were reported by Zhou. Jingfang., et al [96] means of a redox surface modification technique. The structure of DDP-nano Cu was investigated

with an ultraviolet-visible light spectrometer and a trans-mission electron microscope. The elemental composition of DDP-nano Cu was determined with an elemental analyzer. The dispersing behavior of DDP-nano Cu in vari-ous organic solvents was compared with nonmodified copper nanoparticles. The antiwear ability of DDP-nano Cu as additive in liquid paraffin was examined with a four-ball machine. It was found that DDP-nano Cu could well disperse in some organic solvents and had good antioxidation stability in air. The modified copper nanoparticles used as additives in liquid paraffin showed different antiwear ability depending on their particle size. The difference in the antiwear behaviors of nonmodified and DDP-modified copper nanoparticles is explained by their different interactions with the surface of the friction pairs during the friction process.

Microemulsion techniques have been used to prepare Co nanoparticles subsequently covered with an Ag coating.The resulting particle were characterized by Garcia – Bastida. A. J., et al [97] neutron activation analysis to determine the actual Co/Ag ratio and the organic proportion in asprepared samples. XRD and TEM were used to characterize the degree of crystal-lization and size of the particles. TEM results show grain sizes of. ≈ 10.nm and a small size variation among the nanoparticles. As prepared samples show a small degree of crystallization which improves with the annealing temperature in a H_2 reducing atmosphere. Magnetization versus temperature measurements showed the same blocking temperature, T_B = 4.0 ± 0,5 K, in all the as-prepared samples independently of the Co/Ag ratios. Upon annealing at low temperatures ($T_A \leq 200°C$), TB shows a modcrate increase and a saturation magnetization (M,) enhancement of near 40% over the Co bulk value. We propose that in this range of

annealing temperatures, the reduction of the Co cores, initially partially oxidized. is the main process. When $T_A \geq 250$'C. the separation between zero field cooled (ZFC) and field cooled (FC) magnetization data begins at temperatures over the maximum in ZFC and M, decreases with T_A These results can be interpreted as the formation of larger particles,

Synthesis and optical properties of europium oxide nanoparticles immobilized by Ramesh. S., et al [98] europium oxide nanoparticles with an average size of ≈ 5 nm were deposited on the surface of preformed silica submicrospheres with the aid of power ultrasound. The morphology and optical properties of the final product were examined by electron microscopy and spectroscopic techniques. Amorphous europium oxide nanoparticles immobilized on the spherical silica surface exhibited the characteristic $5D_0 - {}^7F_0$, ${}^5D_0 —{}^7F_1$, ${}^5D_0$ - ${}^7F_2$ transitions with increasing wavelength, arising from the 4f states of the Eu^{3+} ion.

Nano-size $Bi_{1.8}Y_{1.2}Fe_5O_{12}$ particles were prepared by Hirano. T., and Namikawa. T., [99] with a coprecipitation and heat treatment method. The coating films of the particles were prepared with coating tech-niques. The crystalline sizes of the $Bi_{1.8}Y_{1.2}Fe_5O_{12}$ particles were calculated using the Scherrer equation with the X-ray diffraction data. The calculated size of the 0 h milling particle is about 400 nm that is almost the same as the measured size with a transmission electron microscope. The calculated particle size after 100 h milling is about 50 nm that is almost the same as the measured size with an atomic force micro-scope. The size of the prepared particles is

changed $Bi_{1.8}Y_{1.2}Fe_5O_{12}$ with the milling process. The crystalline size calculation using the Scherrer equation with the X-ray diffraction data is a method of a size estimation of nano-size $Bi_{1.8}Y_{1.2}Fe_5O_{12}$ fine par-ticles.

The interaction of iron oxide with the silica matrix in a Fe_2O_3 –SiO_2 nanocomposite prepared by a sol-gel method has been investigated by Bruni. S., et al **[100]** using Near-, Mid-, and Far-IR, and 29SiMAS-. and ^1H NMR techniques. Samples of nanocomposites and of pure silica obtained by the same preparation procedure and subjected to the same thermal treatments have been examined. Spectroscopic data indicate that the Fe_2O_3 nanoparticles interact with the silica or silanol groups at the surface of'the cavities in which they form. This result allowed us to propose a model for the nanoparticle/silica interface.

The particle size effect on the formation of palladium hybrid and on surface hydrogen adsorption was reported by Min. Wei. Tew., et al **[101]** using in situ X-ray absorption spectroscopy at the Pd K and L_3 edges. Hydride formation was indirectly obsd. By lattice expansion in Pd K edge XANES spectra and by EXAFS anal. Hydride formation was directly detected in the L_3 edge spectra. A characteristic spectral feature caused by the formation of Pd-H antibonding state showed strong particle size dependence. The L_3 as spectra were reproduced using full multiple scattering anal. and d. of state calcns., and the contributions of bulk absorbed and surface hydrogen to the XANES spectra could be distinguished. The ratio of hydrogen on the surface vs. that

in the bulk increased with decreasing particle size, and smaller particles dissolved less hydrogen.

Water mediated ordering of nanoparticle in electric field was investigated by Dusan. Bratko., et al [102] interfacial polar mols. feature. A strongly anisotropic response to applied elec. field, favoring dipole orientations parallel to the interface. In water, in particular, this effect combines with generic orientational preferences induced by spatial asymmetry of water H bonding under confined geometry, which may give rise to a Janus interface. The 2 effects manifest themselves in considerable dependence of water polarization on both the field direction relative to the interface, and the polarity (sign) of the field. Using mol. simulations, demonstrate strong field – induced orientational forces acting on a polar surfaces through water mediation. At a field strength comparable to elec. fields around a DNA polyion, the torques prodict to act on an adjacent nanoparticle are sufficient to overcome thermal fluctuations. This torques can align a particle with surface as small as $1nm^2$. The mechanism can support elec. controlled ordering of suspended nanoparticles as a means of tuning their properties, and can find application in electronanomech devices.

Dongbei Daxue Xuebeo Bianjibu PAAS (polyacrylic acid sodium salt) was selected as dispersant to evaluate the despersionstabilization of SiO_2 nanoparticles by a diffraction-based laser granulometric analyzer and identify the state of absorption of the dispersant on the surface of nanoparticles was characterized by Yong – xiao. Niu., et al [103] an IR

spectrometer. The results indicate that adding PAAS can remarkably improve the dispersion stabilization of SiO_2 nanoparticles in aq . soln. but degrade it if the added amt.of PAAS is over – satd.if the maas fraction of PAAS remains unchanged, the low pH value of suspension will increase the probability to form the hydrogen bond between SiO_2 nanoparticles and PAAS, thus stimulating the absorption effect of PAAS on the surface of SiO_2 nanoparticles so as to improve their dispersion stabilization.

Millions of people worldwide are exposed to chronic levels of arsenic poisoning due to drinking water with elevated concns. of arsenic. To decrease these concns., various metal based compds. have been explored as arsenic adsorbents. Martinson. Carol. A., and Reddy. K. J., **[104]** was synthesized CuO nanoparticles and evaluated them as an adsorbent to remove As(III) and As(V) from groundwater. The CuO nanoparticles had a surface area of 85 m^2/g and were 12-18 nm in diam. Adsorption occurred within minutes and CuO nanoparticles effectively removed As-(III) and As(V) between pH 6 and 10. The max. adsorption capacity was 26.9 mg/g for As(III) and 22.6 mg/g for As(V). The presence of sulfate and silicate in water did not inhibit adsorption of As(V) but only slightly inhibited adsorption of As(III). High concns. of phosphate (>0.2 mM) reduced the adsorption of arsenic onto CuO nanoparticles. XPS indicated that As(III) was oxidized and adsorbed in the form of As(V) on the surface of CuO. The CuO nanoparticles were also able to remove arsenic (to less than 3 µg/L) from groundwater samples. These results suggest that CuO nanoparticles are an effective material for arsenic adsorption and may be used to develop a simple and efficient arsenic removal method.

The performance of nanoparticles for biomedical application is often. Assessed by their narrow size distribution, suitable magnetic satn. and low toxicity effects.That work was disscaribed by Mahmoudi. M., et al [105] super paramagnetic iron oxide nanoparticles (SPIONs) with different size, shape and satn. magnetization levels were synthesized via a co—pptn. technique using ferrous salts with a Fe^{3+}/Fe^{2+} mole ratio equal to 2. A parametric study is conducted, based on a uniform design—of—expts. methodol. and a crit. polymer/iron mass ratio (r—ratio) for obtaining SPION with narrow size distribution, suitable magnetic satn., and optimum biocompatibility is identified. Polyvinyl alc. (PVA) has been used as the nanoparticle coating material, owing to its low toxicity. A 3 —(4,5 —dimethylthiazol —2—yl) — 2,5 —diphenyltetrazolium bromide (MTT) assay is used to investigate the cell biocompatibility/toxicity effects of the samples. From the MTT assay results, it is obsd. that the biocompatibility of the nanoparticles, based on cell viabilities, can be enhanced by increasing the r—ratio, regardless of the stirring rate. This effect is mainly due to the growth of the particle hydrodynamic size, causing lower cell toxicity effects.

Langmuir—Blodgett films were prepd. at the air/water interface from dispersions of hydrophilic and partially, hydrophobically modified industrially manufd. silica nanoparticles were prepared by Blute. Irena., et al. [106] The hydrophilic particles featured expanded, fairly easily compressible, surface pressure (r)—area (A) isotherms with well defined collapse pressures which appeared to be caused by the formation of loosely structured agglomerates which exhibited elastic behavior at low surface pressure and inelastic behavior at high surface pressure. Lateral electrostatic inter particle interactions seemingly played an important role in this

hydrophilic system. This contrasted with the hydrophobically modified particles which were more difficult to disperse in the ethanol/chloroform spreading solvent and appeared to be in the semiagglomerated state at low surface pressures and exhibited a more difficult to compress compacted film. Both types of particulate films were shown to be sensitive to the spreading environment and changes in pH were found to increase particle agglomeration which drastically reduced the particulate area for the hydrophilic sol but less so, in the case of the moderately hydrophobically modified sol. In general, the LB technique proved to be a useful method to monitor changes in the state of aggregation of nanosized silica particles at the air/water interface. These results also appear to give some support of our ideas, presented in earlier publications in which it was suggested that the major role of the hydrophobically modified hydrophilic particles in foaming was to produce an aggregated particulate film surrounding the air/water interface which provides a phys. barrier preventing coalescence of bubbles.

The platinum nanoparticles were prepared by Haiyang. Cheng., et al **[107]** in situ redn. with polyethylene glycols (PEGs). The catalytic performance of Pt nanoparticles immobilized in PEGs (Pt—PEGs) is discussed for the hydrogenation of o—chloronitrobenzene (o—CNB). A high selectivity to o—chloroaniline (o—CAN) of about 99.7% was obtained with the Pt—PEGs catalysts at the complete conversion of o—CNB, which is much higher than that (83.4%) obtained over the conventional catalyst of Pt/C. The Pt nanoparticles could be immobilized in PEGs stably and recycled for four times with the same activity and selectivity. It presents a promising perfomance in the hydrogenation and its wide application in catalytic reactions is expected.

The concept of constitutional dynamic chem. (CDC) based on the control of noncovalent interactions in supramol. structure are promising for having a large impact on nanoscience and nanotechnology was reported by Alencar. Wagner. S., et al. [108] The layer- by—layer (LbL) technique may be used to produce electroactive electrodes with ITO coated by tetrasulfonated nickel phthalocyanine (NiTsPc) alternated with poly(allylamine hydrochloride) (PAH) incorporating gold nanoparticles (AuNP), in which synergy was achieved in the interaction between the nanoparticles and NiTsPc. The catalytic activity toward hydrogen peroxide (H_2O_2) in multilayer films was studied using cyclic voltammetry, where oxidn. of H_2O_2 led to increased currents in the PAH—AuNP/NiTsPc films for the electrochem. processes assocd. with the ph-thalocyanine ring and nickel at 0.52 and 0.81 V vs. SCE, resp., while for PAH/NiTsPc films (without AuNP) only the 1st redox process was affected. In control expts. the catalytic activity was not solely due to the presence of AuNP, but rather to the nanoparticles inducing NiTsPc supramol. structures that favored access to their redox sites, thus yielding strong charge transfer. The combined effects of NiTsPc and AuNP, which could only be obsd. in nanostructured LbL films, point to another avenue to pursue within the CDC paradigm.

Nanoscale zerovalent iron (NZVI) particles have recently become subject of great interest in the field of groundwater remediation for their ability to treat a wide variety of org. and inorg. contaminants. However, the field application of this technol. Is strongly hindered by the lack of stability of NZVI water suspensions. This study demonstrates that highly concd. NZVI slurries (15 g/L) can be stabilized for >10 days adding 6g/L of xanthan gum biopolymer Stability against aggregation and sedimentation was achieved in

the range of ionic strength $6x10^{-3}$ – 12mM and is mainly due to the formation of a viscous gel characterized by shear- thinning behavior that work were stabilized by Comba. Silvia., and Sethi. Rajandrea., **[109]**

A very facile synthesis of nanometer—sized germania—coated nanotubules and germania crystals was studied through hydrolysis of germanium tetraalkoxide (TEOG) and subsequent condensation of germania in aq. synthetic diacetylene phospholipid [1,2—bis(tricosa-10,12—diynoy1)—sn—glycero-3—phosphocho-line ($DC_{8,9}$—PC)] solns that work synthesized by Haiqing. Kim. Il. Li., et al. **[110]** In the presence of the $DC_{8,9}$—PC, TEOG rapidly hydrolyzes in aq. ethanol soil., leading to solvated germinatet species at lower germania concns. yielding germania/lipid composite nanotubules and the onset of nanometer—sized germania crystals at room temp. with increasing germania content. Phospholipid and germania concn. both influence crystallite size and morphol. (i.e., polyhedral, cubic). Germania mols. hydrolyzed on the surface of lipid bilayer bring up to the secondary tubular structure by the self—assembling driving force of the lipid mols. The fact that the germania crystal morphol. formed at higher TEOG concns. shows no signs of nanoparticle aggregative assembly in the absence of $DC_{8,9}$—PC suggests that the crystal growth should take place by addn. of dissolved species like weakly acidic $DC_{8,9}$—PC rather than nanoparticles.

Scanning Probe Microscopy (SPM) was a powerful tool for detecting surface properties of nanomaterials. Prepg. sample was the key process for SPM imaging. Detecting nanoparticles with SPM often faced the problem

that the nanoparticles were usually repolymd. by the mol. force and form nanoparticle—reunions in the process of prepg. SPM specimens. To conquer this difficulty, a new method for prepg. SPM nanoparticle specimens by soft microprinting combined with enhanced diffusing was proposed, in which proper nanoparticle dispersal system could be formed on the substrate surface sepd. in the liquor nano—film after soft—lithographed. Expts. validated that it was an available artifice for prepg. nanoparticle sample in SPM detecting that was prepared by Dongxiao. Niu., et al. [111]

By choosing appropriate microemulsion systems, hexagonal cobalt (Co) and cobalt—nickel (1:1) alloy nanoparticles wasn obtained by Ahmed. Jahangeer., et al [112] with cetyltrimethylammonium bromide as a cationic surfactant at 500°C. This method thus stabilizes the hcp cobalt even at sizes (<10 nm) at which normally fcc cobalt is predicted to be stable. On annealing the hcp cobalt nanoparticles in H_2 at 700°C it transforms them to fcc cobalt nanoparticles. Microscopy studies show the formation of spherical nanoparticles of hexagonal and cubic forms of cobalt and Co—Ni (1:1) alloy nanoparticles with the ay. size of 4, 8 and 20 nm, resp. Electrochem. studies show that the catalytic property towards oxygen evolution is dependent on the applied voltage. At low voltage (less than 0.65 V) the Co (hexagonal) nanoparticles are superior to the alloy (Co—Ni) nanoparticles while above this voltage the alloy nanoparticles are more efficient catalysts. The nanoparticles of cobalt (hcp and fcc) and alloy (Co—Ni) nanoparticles show ferromagnetism. The satn. magnetization of Co—Ni nanoparticles is reduced compared to the bulk possibly due to surface oxidn.

FePt alloy in a balk state is well known as a magnetic material FePt nanoparticles, which are protected by poly(N—vinyl-2— pyrrolidone) (PVP) and have a face—centered tetragonal (fct) structure at a size of a few nanometers in diam., were directly synthesized by Iwamoto. Takashi., et al [113] a polyol process in high—b.p. tetraethylene glycol used as a reducing reagent for the redn. of Fe(III) acetylacetonate and Pt(II) acetylacetonate. Their magnetic properties (coercivity and satn. magnetization) were dependent on the size and made progress as their diams. increased. The size in diam. was easily controlled by altering the content of PVP, the time for refluxing, and reaction temp. FePt nanoparticles showed diam.—dependent coercivities at room temp. and they abruptly increased at over 4 nm in diam. Ferromagnetic FePt nanoparticles with an fct structure were also synthesized at relatively low reaction temp. without refluxing. Likewise, as—synthesized FePt nanoparticles prepd. by refluxing at 251°C for 3h displayed the fct structure and clearly indicated the ferromagnetism at room temp. reaction kinetics such as long refluxing time and slow temp. elevation rate were found to be important key factors to synthesize the ferromagnetic FePt nanoparticles although the reaction temp. was very crit. as well.

H_2O – sol., exceptionally stable, naked Ag nanoparticles were obtained in a single step by simple decompn. of a com. Ag complex at room temp. without the need of external reducing agents and conventional stabilizing ligands. The green synthesis of ‘naked’ aqueous silver nanoparticles was investigated by Giuffrida. Salvatore., et al. [114]

Al- Ghoul. Mazen., et al [115] was studied the spatiotemporal dynamics of a new system consisting of sulfide ions (outer electrolyte) diffusing into an org. gel (gelatin) contg. Mercaptoethanol- capped Cd ions (inner electrolyte). The product, Cd sulfide, exhibits a faint yellow transparent propagating front starting at the gel-outer electrolyte interface. When subjected to UV light, this system reveals fluorescing CdS nuclei localized spatially in a narrow region, called pulse, that leads the front and propagates down the tube. The pulse consists of CdS nanoclusters of an av: size of -4 nm, whereas the trailing front consists of 6-8 nm cubic-phase CdS crystallites. The width of the pulse remains const. in time, t, at -2 mm and independent of the outer concn. SD. The speed of the pulse fluctuates as the concn. of the capping agent is varied, with fastest pulses attained at a concn. of 40 mM for 2 different outer concns. of sulfide ions. The origin of the yellow fluorescence of the pulse originates from emission from surface states. This dynamical system was then theor. studied using a competitive particle growth model. The resulting evolution equations were solved numerically, and the results were compared to the exptl. findings. The model agrees in many aspects with the expt. The densities of small particles Q and large particles Q evolved like a pulse and a front, resp. The front was shown to extend diffusively as $t^{1/2}$, as found exptl. The distance traveled by the pulse X_{peak} increases with outer concn. S and obeys a concn. power law X_{peak} approx. $S^{1/4}$ 0. The with w of the pulse also obeys a time power law w approx. t^{a} with a crossover between early times (a = 1/3) and intermediate times (a = 0). This system would enable one to study the early time dynamics of Liesegang systems.

Metal nanoparticles embedded into porous oxides was stabilized by Loredana. De. Rogatis., et al [116] a review; catalysis is considered the central field of nanoscience and nanotechnol. The majority of the industrial catalysts are made of small metal particles 1-100 nm in size, carried by a solid support. The extremely small size of the L- particles maximizes surface area exposed to the reactant, allowing more reactions to occur. Moreover, the higher the no. of metal atoms in contact E with the support better are the catalyst performance. However, thermal stability of these nanomaterials is limited by their crit. sizes; the smaller the crystallite size, the lower thermal stability. The ability to fabricate and control the structure of nanoparticles allows to influence the resulting properties and, ultimately, design stable catalysts with desired properties. The control of metal particle nanosize is of the utmost importance for the performance of any industrial catalyst based on supported metals. Tuning particle sizes provides the possibility to modulate the catalytic activity. A typical example is gold, which was historically considered catalytically inert. However, in the nanosize regime and in it combination with appropriate support materials, gold has been found to be more active than Pt and Pd catalysts for many reactions such as CO oxidn. at room temp. Synthesis and processing of nanoparticles pose a no. of difficulties, esp. in terms of aggregation and monodispersity of the y particle size. Nacked metal nanoparticles have a tendency to form aggregates during the prepn. process and the control of particle—particle interaction is crit. for obtaining stable and homogeneous dispersion of nanoparticles in the catalyst. Moreover, aggregation may occur also f during the catalyst use promoted for example by high temps. Several strategies to overcome these problems have been proposed in the last years and will be discussed in this chapter. The attention will be focused on the recent strategies to produce

metal nanoparticles embedded into iporous oxides. Examples of characterization and catalytic performances of Au, Rh, Pt, Pd, Ag, Ni, Fe and some bimetallic particles will be presented. Most of the attention will be dedicated to silica as inorg. stabilizer / porous matrix which surround the nanoparticles, due to its larger use in the prepn. methods used nowadays. Notably, while there is a relatively remarkable literature on noble metals, much less reports are present on non noble metals, more likely due to the easier reoxidn. / partial dissoln. of those metal nanoparticles in the usual reaction media.

Langmuir—Blodgett technique was used for the deposition of ordered 2D arrays of Fe oxides (Fe_3O_4/Fe_2O_3) nano-particles onto the photovoltaic hydrogenated amorphous Si (a—Si:H) thin film. Elec. field at the a—Si:H/Fe oxides nanoparticles interface was directly in the electrochem. cell modified by light soaking and bias volt-age (neg. or pos.) pretreatment resulting in the change of the dominant type of charged deep states in the a—Si:H layer this work was reported by Gmucova. Katarina., et al. **[117]** Induced reversible changes in the nanoparticle redox behavior were obsd. We suggest 2 possible explanations of the data obtained, both of them are needed to describe measured electrochem. signals. The first one consists in the electrocatalytical effect caused by the defect states (neg. or pos. charged) in the a—Si:H layer. The second one consists in the possibility tomanipulate the nanoparticle cores in the prepd. structure immersed in aq. soln. via the laser irradn. under specific bias voltage. In this case, the nanoparticle cores are assumed to be covered with surface clusters of heterovalent complexes created onto the surface regions with prevail-ing ferrous or ferric valency.

Immersed in the high viscosity surround-ing composed of the wet org. nanoparticle envelope these cores are able to perform a field—assisted pivotal motion. The local elec. field induced by the deep states in the a—Si:H layer stabilizes their "orientation order-ing" in an energetically favorable position.

The structural characteristics of α — Fe_2O_3 nanoparticles prepd. by a mech. milling were explored. The structure and morphol. of samples were characterized by x—ray powder diffraction, field—emission scan-ning electron microscope (FE—SEM) and FT—IR measurements. The crystallite size and internal strain were evaluated by XRD patterns us-ing Williamson—Hall and Scherrer methods. The results did not reveal any phase change during the milling. The ay. particle size decreases with a prolongation of milling times, while the lattice parameters and internal strain increase. Using this method allowed the formation of hematite nanoparticles. Microstructural of α – Fe_2O_3 nanoparticles using ,XRD line profiles analysis, FE – SEM and FT – IR was characterized by Lemine. O. M., [118]

Freely suspended Si nanowires and nanobridges were fabricated on silicon—on— insulator substrates by patterned FIB Ga^{+-} implantation and subsequent wet chem. etching. This technol. is combined with classical microelectronic processing steps of photolithog. patterning and broad beam ion t implantation to position and integrate the nanostructures into current a technol this work was reported by Bischoff. L., et al [119] therefore to increase the fabrication efficiency. Design, performance, and fabrication considerations to achieve free— r standing Si nanostructures are discussed

and some typical examples are v shown. Static and dynamic elec. measurements are presented, including t I—V characteristics and displacement excitation by applying an a.c. volt- c age. The temp.—dependence of the elec. resistance of Si nanostructures i is demonstrated, which reveal, for example, the applications as nanowire thermal sensors.

Rizza. G., et al [120] show that the high—energy ion irradn. of embedded metallic spherical nanoparticles (NPs) is not limited to their transformation into prolate nanorods or nanowires. Depending on their pristine size, the three following morphologies can be obtained: (i) nanorods, (ii) facettedlike, and (iii) almost spherical nanostructures. Planar silica films contg. nearly monodisperse gold NPs (8-100 nm) were irradiated with swift heavy ions (5 GeV Pb) at room temp. for fluences up to 5 x 1013 cm-2. The exptl. results are accounted for by considering a liq.—solid transformation of the premelted NP surface driven by the in—plane stress within the ion—deformed host matrix. This work demonstrates the interest of using ion—engineering techniques to shape embedded nanostructures into nonconventional configurations. (c) 2009 American Institute of Physics.

The three—dimensional nanoparticle ;, morphol. and the nanoparticle—substrate relationship during the submonolayer growth of three metals (gold, tantalum, and palladium) on p the alkali halide KBr (001) surface is investigated by Mativetsky. Jeffrey. M., et al [121] combining in situ high—resoln. noncontact at. force microscopy and ex situ transmission n electron microscopy approaches. Highly varied growth behavior between Ls the

metals is revealed. Gold produces nearly spherical multiply twinned h nanoparticles at room temp. and an increasing no. of epitaxial particles at elevated temps. In contrast, the tantalum grows as relatively flat fractal particles, despite the square symmetry of the substrate lattice, a condition which normally precludes fractal growth. The tantalum also [a exhibits a strong affinity for KBr surface steps, leading to one—t- dimensional chains of nanoparticles. The deposition of palladium results i- in the creation of protruding substrate distortions and monolayer—high al rectangular KBr islands in addn. to the growth of palladium nanopar-• tides. It is hypothesized that the unusual growth obsd. in the palladium—:). KBr system is caused by the interdiffusion of palladium under the KBr surface. The range of growth behavior in the three systems is described • in terms of the surface and interface energies, yielding bounds on the Lg metal/KBr interface energies.

The formation of carbonaceous deposits on Pt (111) surfaces and Pt nanoparticles was investigated by Vines. Francesc., et al [122] using suitable models and d.—functional calcns: The Study addresses a broad range of processes, from the very first stage of carbon deposition up to a final building of graphene monolayers (ML) defined as a 1:1 ratio of the no. of C atoms to surface Pt atoms. A carbidic phase is formed below a coverage of —0.3 ML, when neg. charged carbon atoms are strongly adsorbed preferentially on fcc hollow sites. On Pt nanoparticles, the adsorption of carbon atoms seems to be enhanced near particle edges due to the special flexibility of defect sites. Above a coverage of —0.3 ML, the formation of small C,, aggregates becomes pos-sible. Interestingly, thermodn. favors the

formation of C3 trimers at a coverage of 0.33 ML, whereas the formation of C2 dimers requires a higher coverage of 0.5 ML. The covalently bonded C2 species is sup-posed to be the key fragment for the formation of benzene—like rings at coverages above 0.6 ML. These rings are expected to be the building blocks for the graphene monolayer. However, the typical electronic structure of graphene is not obsd. until a coverage above —1.8 ML is reached. We corroborated the exptl. suggested C double—layer to be stable. It is proposed to consist of a monolayer of carbidic atoms C adsorbed on Pt with a graphene layer adsorbed on the carbidic layer. Some of the carbidic atoms serve as anchors for the graphene layer, with noticeably strong covalent bonds formed. This double—layer model would imply a much higher adhesion of the graphene layer than in the single—layer model.

Well characterized Au nanoparticles were deposited on com. TiO_2(P25, Degussa) and analyzed by mean of STEM and thermo gravimetry coupled with mass spectrometry (TG—MS). That were characterized by Veten. Van . Niels., et al **[123]** the adsorption was studied on Au/TiO_2 samples with Au loadings in the range of 1.1-9.9 wt.% by injecting pulses of CH_3SH po Me mercaptan, MM) until no further mass increase could be obsd. A B3 prerequisite for detn. of the surface area of the deposited Au nanoparticles is the proper discrimination of species adsorbing on the Au nanoparticles and the TiO_2 support. The adsorption of Me mercaptan on the gb TiO_2 support strongly depended on the pretreatment temp. (30-400°), fal whereas the adsorption on Au nanoparticles was virtually unaffected by I this parameter. A very mild thermal pretreatment was identified as a se requirement for avoiding the adsorption of the MM on the TiO_2 support. 13/ CH_3SH

adsorbed on the support desorbed at lower temps. (maximal rate Bi of desorption was centered at ca. 150°) compared to species desorbing 2C from Au nanoparticles (max. at ca. 200-220°). Moreover, CH_3SH ad- se sorbed on Au nanoparticles desorbed in the form of di—Me sulfide efl $(CH_3)_2$ S. Part of MM adsorbed on the Au surface was not desorbed even on at high temps. (above 500°) and stayed on the surface in the form of w] relatively stable $C_xH_yS_z$ fragments. This residue could be removed by ar 0 pulses resulting in the formation of CO_2, SO_2, and H_2O. The good m: discrimination of MM chemisorption on Au .nanoparticles and on TiO_2 co renders the detn. of the Au surface area viable. Potential and limita- er tions of the CH3SH chemisorption for the surface area detn. of Au nano- cr particles are discussed.

The results of silirface-enhanced resonance Raman scattering (SERRS) spectral probing of citrate- and/or citric acid-modified Ag nanoparticles by selected free-base porphyrins, a tetracationic 5,10,15,20-tetrakis(1-methyl-4-pyridiniumyl) porphine and neutral 5,10,15,20-tetra(pyridyl)porphine (H_2TP_yP) and 5,10,15,20-tetrakis (4- aminophenyl) porphine (H_2TAPP) were reported by Siskova. K., et al **[124]** along with a novel proce-dure of the functionalized Ag nanoparticle hydrosols prepn. by laser ablation of a Ag target in aq. sodium citrate and/or citric acid solns. of various concns. SERRS spectra obtained from the Ag nanoparticle hydro-sol/porphyrin system were analyzed using the spectral marker bands of free-base, Ag metalated and diacid forms. In freshly prepd. SERRS-active systems, adsorbed citrate was found to function as an efficient mol. spacer for pos. charged porphyrin species both in the pH-neutral and in the acidic media,

allowing for SERRS spectral detection of not only cationic, but also addnl. protonized neutral porphyrins in the native free-base (and/or, at low pH, in the diacid) form without denaturation by Ag incorporation. Also, a substantial increase of the SERRS signal obsd. for H2TPyP and H2TAPP in systems with Ag nanoparticles prepd. by laser ablation in 1 x 10-2 M citric acid solns. is attributed to both the electromagnetic enhancement increase stemming from the presence of hot spots in compact aggregates of touching and intergrown Ag nano-particles (visualized by /HR/-TEM), and from the mol. resonance en-hancement increase originating from a close match between the Soret band of the diacid form (440 nm) and the 457.9 nm excitation. For 112- , TAPP, the large SERRS enhancement manifests itself in the 1 x 10-10 SERRS spectral detection limit.

Self—assembled monolayers contg. disulfide—functionalized diacetylenes are of particular interest for applications in photonics and sensor devices was investigated by Alloisio. M., et al. **[125]** To this purpose a diacetylene deriv., the henicosa-10,12—diyn-1—y1 (DS9) disulfide, was synthe-, sized and employed to prep. gold nanoclusters capped with this monomer. The nanohybrids were obtained through a direct synthesis in toluene. f The preparative conditions were varied to modulate the nanoparticle a size and shape. The resulting org.—protected gold nanoassemblies were y spectroscopically studied as colloidal suspensions. TEM anal. allowed s the detn. of the ay. dimensions at 1.6-7.5 nm. DS9 monomer chemi-e sorbed onto the gold nanoclusters was photopolymd. in colloidal suspen-a sion by exposure to UV radiation for variable time intervals. The polymn. s process was monitored step by step through UV—visible, Raman and FTIR

spectroscopies. The polymn. occurs with the dominant polydiacety-lene phase critically depending on the nanoparticle diam.

A thermodn. colloid—chem. model about the interactions with participation of nano-sized phases in silicate—carbonate and silicate—slag dispersions was considered accounting for the thickness and structure of the contact zone, for the chem. mineralogical compn. of the contact structures as well as for the presence of NaC1 and CO2 in the disperse medium. Exptl. verification of the model by rheol., x—ray phase, thermog. and electron—microscopy methods confirmed the generalizations made and gave an opportunity to define more precisely these generalizations for systems based on dispersions of solidifying natural silicates and acid metallurgi-cal slags, as well as for carbonate—silicate compns. contg. ultradispersed particles that work oblized by Kovzun. I. G., et al. **[126]**

A kinetic equation describing the formation of inorg. nanoparticles from solns. contg. well adsorbing org. compd. Simplified anal. solns. of this equation were found and different limiting cases were considered. In solving the problem, the dimensional dependences of the reaction kinetic parameters were taken into account, as well as the surface tension dependence on the nanopar-tide size and the extent of surface coverage by the well adsorbing org. molecules were examined and compared by Rekhviashvili. S. Sh., et al. **[127]**

Silicas with deposited hybridepolysiloxane layers were used for the in situ were prepared by Tertykh. V. A., et al [128] of Au nano particles by the redn. of metal ions from a soln. of chloroauric acid. The metal – contg. SiO_2 obtained were characterized by x-ray powder diffraction, transmission electron microscopy, and UV, IR, and laser correlation septroscopy.

This work was reported by Tan. Say – Hwa., et al [129] studies on the droplet formation of deionized water and a nanofluid in a heat—induced microfluidic flow focusing device. Besides the effect of temp., the effects of nanoparticle suspension (nanofluid) and the flow rate of aq. fluid on the droplet formation and size manipulation were studied. At const. flow rates of the two liqs., three different droplet breakup regimes were obsd. and their transition capillary nos. as well I as temps. were identified. The heat generated by an integrated micro-heater changes the droplet formation process. Increasing the temp. enlarges the size of the droplets significantly. Also the titanium oxide (15 nm)/deionized water—based nanofluid exhibits similar characteristics in droplet formation at different temps. and any small change in the flow rate of this nanofluid has little impact on the size of the droplets formed in a flow focusing geometry.

Packing patterns of silica nanoparticles on surfaces of armored polystyrene latex particles was reported by Sara. Fortuna., et al [130] fascinating packing patterns of identical spherical and discotic objects on curved surfaces occur readily in nature and science. Examples include C_{60} fullerences, 13-atom cuboctahedral metal clusters, and S-layer proteins on outer cell membrane

.Numerous situations with surface- arranged objects of variable size also exist, such as the lenses on insect eyes, biomineralized shells on coccolithophorids, and solid—stabilized emulsion droplets and bubbles. The influence of size variations on these tl packing patterns, however, is studied sparsely. Here we investigate the 11- packing of nanosized silica particles on the surface of polystyrene latex R particles fabricated by Pickering miniemulsion polymn. of submicrome- D ter—sized armored monomer droplets.That rationalize the exptl. morphol. and the nearest—neighbor distribution with the help of el Monte Carlo simulations, that broadening of the nanoparticle size distribution has pronounced effects on the self—assembled equil. packing structures, with original 12—point dislocations or grain—bound- tc 'ary scars gradually fading out.

In an effort to maximize the liq. slip on superhydro-phobic surfaces, Choongyeop. Lee., et al [131] was investigated the role of the nanoscale roughness on microscale structures by developing well—defined micro—nano hierarchi-cal structures. The nonwettifig stability and slip length on the dual—scale micro—nano structures are measured and compared with those on single—scale micro—smooth structures. A force balance between a liq. pressure and a surface tension indicates that hydrophobic nanostruc-tures on the sidewall of microposts or micrograte would expand the range of the nonwetted state. When a higher gas fraction or a larger pitch can be tested without wetting, a larger slip length is expected on the microstructures. An ideal dual—scale structure is described that isolates the role of the nanostructures, and a fabrication technique is developed to achieve such a microstructure—smooth tops and nanostructured sidewalls. The tests

confirm such micro—nano structures allow a nonwetted state at a higher gas fraction or a larger pitch than the previous micro—smooth structures. As a result, we achieve the max. slip length of —400 gm on the dual—scale structures, an increase of —100% over the previous max. reported on the single—scale (i.e., micro—smooth) structures. The study ameliorates our understanding of the role of each scale on hierarchical structures for a wetting transition and a liq. slip. The resulting giant slip is large enough to influence many fluidic applications, even in macroscale.

33. **[132]** Ogawa. Atsushi., and Maeda. Mizuo., were developed an easy method for constructing based logic gates using nanocrosslinking gold nanoparticle aggregation.

The measurement of induction time in pptn. of Ag nanoparticles at different temps. and supersaturations, and models it with Smoluchowski's coagulation theory. Ag nanoparticles are synthesized by reaction of $AgNO_3$ with hydrazine in the presence of sodium citrate as stabilizer. The rate of assocn. between clusters is found to depend on temp. and their sizes. The activation energy for the assocn. between two clusters and interfacial tension of Ag nanoparticles were also estd. Induction time decreases with increasing supersatn. This Ag nanoparticles synthesized by Hatami. N., and Ghader. S., **[133]**

Pd nanoparticles with uniform, self—assembled pompon—like nanostructure were prepared by Tong. Xia., et al [134] thermal decomposiyion of palladium acetate under microwave irradn. with Me iso—Bu ketone (MIBK) as a solvent in the presence of a little amt. of ethylene glycol (EG) and KOH without using any special stabilizers. The as—prepd. Pd nano—pompons were characterized by TEM, XPS, and x—ray powder diffraction. The as—prepd. Pd nano—pompons with the ay. di-ams. in the range of 28-81 nm were self—assemblies organized by hundreds of smaller primary nanoparticles with an ay. dimension of nm. The sizes of Pd nano—pompons can be well controlled by adjusting the concn. of palladium acetate. A little amt. of EG and KOH also plays an important role in controlling the size, uniformity and dispersion of Pd nano—pompons. The Pd nano—pompons can be easily supported on γ-Al_20_3 and their catalytic activity was examd. preliminarily.

With the development of nanotechnologies, a large no. of nano—materials with novel properties are being released into the environment was investigated by Jiajuan. Lu., et al [135] however, little ie is known about their fate, transport, toxicity, and interactions with org. ,Te matters in aq. environment. In this study, nano—SiO_2 or kaolinite, coated with soil humic acid (SHA) and peat humic acid (PHA), were used as m sorbents. The original and HA—coated nanoparticles were characterized. .s. for particle size, TEM, and electrophoretic mobility. Sequential ultrafil-le (UF) was used to characterize the mol. size fractionations of A dissolved HAs. Sorption data of atrazine (AT) under various soln. concn., se ionic strength, and pH were well fitted with Freundlich model. Sorption id amt. of AT on HA—

coated nanoparticles was significantly lower than ,e, that on original particles. The sorption max. appeared at I = 0.001 mol/L ($NaNO_3$), pH 3. Size of nanoparticle aggregates, conformation of HA and sp. surface area were factors affecting the sorption process. The compressed conformation of HA was more favorable for HA sorption to than expanded one. Size of aggregation was not a determinant factor n, for the sorption process, while the sp. surface areas of nano—sorbent was 0. an important one. HA plays an important role in the transport and), toxicity of nanoparticles and AT in aq. environment.

An improved, exact anal. of surface Ostwald ripening of a collection of nanoparticles is presented in an effort to redefine the crit. radius involved in the kinetic models of ripening. In a collection of supported particles of different s sizes, the crit. radius is the size of the particle that is in equil. with the r. surrounding adatom concn. Such a particle neither grows nor shrinks due to Ostwald ripening, whereas larger particles grow and smaller s particles shrink, that previous definitions of crit. radius are c applicable only for limiting regimes where the Kelvin equation has been linearized. Houk. Levi. R., et al **[136]** proposed a more universally applicable definition of crit. radius that satisfies the constraints of mass balance.

Synchrotron radiation expts. were carried out during the in situ growth of ZnO nanoparticles by the aq. chem. growth technique. The first results of this exploratory in situ is; grazing—incidence diffraction (GID) expt. were reported by Fall. S., et al **[137]** with emphasis on the difficulties encountered.

In particular, it is shown that, when in)e, situ GID expts. are carried out in a 25 mm—long cell, scattering by the it solvent dominates. This impedes the observation of the formation of or ZnO nanoparticles during the early stages of the growth process. Nev-)r- ertheless, it is clearly shown that the wurtzite hexagonal structure is tly present in the soln. At a specific concn., it is shown how the peak .ch intensities and widths of the Bragg peaks evolve as a function of time.

The role opf hydrogen bonding in nanocolloidal morphous silica particles in electrolyte solutions were oblyzed by Jenkins. S., et al **[138]** explicit solvent (water) mol. dynamics simulations were undertaken contg. 3 pairs of amorphous SiO_2 nanoparticles, having dims. of 2.0 nm, 2.4 nm and 2.8 nm, resp. Mean forces acting between the SiO_2 nanoparticles were calcd. in a background electrolyte, i.e., NaCl salt 4 different concns. Dependence of the inter—particle potential of mean force on the center of mass sepn., Si to Na ratio ($Si:Na^+$), background. ectrolyte concn., no. of H bonds directly linking pairs of SiO2 nanoparticles and the d. of charged surface sites, are calcd. The pH was indirectly accounted for via the ratio of Si to Na used in the simulations. The close relationship between the variation of the no. of H bonds between the airs of SiO2 nanoparticles and the interparticle potential of mean force indicates that the degree of interparticle H bonding quantifies, for a geven size of nanoparticle, the degree of nanoparticle stickiness'. Simulations also show that the no. of H bonds between the charged surface (OH^-) sites and the surrounding water mols. increases with increase in charged sites, in agreement with the interaction behavior of SiO2 nanoparticles usually seen in exnts.

Biological synthesis of silver nanoparticles using Glycine max (soybean) leaf ext. as reducing agent was investigated by Vivekanandhan. Singaravelu., et al [139] the effect of different soybean varieties on the formation of silver nanoparticles was investigated. The micro-structure of silver nanoparticles was identified from TEM and the particle size of silver nanoparticles were from 25 to 100 nm. x—Ray diffraction anal. showed that the silver nanoparticles crystd. in fcc. symmetry. The purity and the agglomerations of silver nanoparticles were resp. investi-gated through particle size and FTIR anal. Soybean leaf ext. shows rapid redn. of silver ions and yields org.—free silver nanoparticles.

Swift heavy ions (SHI) induce high densities of electronic excitations in narrow cylindrical vols. around their path. These excitations were used to manipulate the size and shape of noble metal nanoparticles embedded in silica matrix. Films contg. noble metal nanoparticles were prepared by Singh. Fouran., et al [140] by magnetron co—sputtering techniques. SHI irradn. of films resulted in the formation of prolate Ag nanoparticles with major axis along the ion beam direction. The nanoparticles smaller than the track size dissolve and other grow at their expense, while the nanopar-ticles larger than track size show deformation with major axis along the ion beam direction. The aspect ratio of elongated nanoparticles is found to be the function of electronic energy loss and ion fluence. Present report will focus on the role of size and vol. fraction on the shape deformation of noble metal nanoparticles by electronic excitation induced by SHI irradn. The detailed results concerning irradn. effects in silica—metal composites for dissoln.,

growth and shape deformation is discussed in the framework of thermal spike model.

Thiele. U., et al [141] compatibilizing the colloidal nanoparticle suspensions (nanofluids) and discuss several theor. approaches to describe the ongoing processes including coupled transport and phase changes. These approaches range from microscopic discrete stochastic theories to c aesoscopic continuous deterministic descriptions. In particular, we t lescribe (i) a microscopic kinetic Monte Carlo model, (ii) a dynamical d. 1: unctional theory and (iii) a hydrodynamic thin film model. Models (i) and (ii) are employed to discuss the formation of polygonal networks, 1] pinodal and branched structures resulting from the dewetting of an a ltrathin 'postcursor film' that remains behind a mesoscopic dewetting g ront. We highlight, in particular, the presence of a transverse instability in the evaporative dewetting front, which results in highly branched.

Castez . Marcos. F., and Albano. Ezequiel. V., [142] were revied some recent research on the surface diffusion—mediated decay of two—dimensional nanostructures. These results include both a continuous, vectorial model and a discrete kinetic Monte Carlo approach. Predictions from the std. linear continuous theory of surface—diffusion—driven interface decay are contrasted with simulational results both from kinetic and morphol. points of view. In particular, we focused our attention on high—aspect—ratio nanostructures, where strong deviations from linear theory take place, including nonexponential amplitude decay and the emergence of several

interesting nanostructures such as overhangs developing, nanois-lands and nanovoids formation, loss of convexity, nanostructures—pinch off and nanostructures—break off, etc.

Mixts. of oppositely charged nanoparticles (NPs) ppt. sharply only at point of NP electroneutrality. This behavior – reminiscent of the threshold pptn. of inorg. Ions – is specific to the nanoscale and can be attributed to the formation of like – charged NP clusters stabilized in soln. by mutual electrostatic repulsions. NP titrns. Based on this phenomenon provide a uniquely accurate tool for measuring charges tethered onto nanoscopic objects and for studying the thermodn. of suface reactions at the nanoscale that was reported by Bishop. Kyle J. M., and Grzybowski. Bartosz A., [143]

Reinforcement of elastomers by colloidal nanoparticles is an important application where microstructure needs to be understood – and if possible controlled – if one wishes to tune macroscopic mech. Properties was investigated by Oberdisse. Julian., et al [144] here the 3 – dimensional structure of big aggregates of nanometric SiO_2 particles embedded in a soft polymeric matrix is detd. by Small Angle Neutron Scattering. Exptl., the crowded environment leading to strong reinforcement induces a strong interaction between aggregates, which generates a propose to anayze the total signal by a decompn. In a classical colloidal structure factor describing aggregate interaction and an aggregate form factor detd. by a Reverse Monte Carlo technique. The result gives new insights in the shape of aggregates and

their complex interaction in elastomers. For comparison , fractal models for aggregate scattering ate also discussed.

The growth and the magnetic behavior of cobalt on porous silicon are studied as a function of substrate prepn. Rinsing the porous silicon (PS) substrate with ethanol leads to and oxidn. of the layer that offers a 3D growth. The magnetic behavior of Co particles grown on PS substrates is rather different than the conventional one and may exhibit a superparamegnatic effect was examinend and compared by Belkacem. W., et al. **[145]**

The decomp. of the organometallic ruthenium precursor [Ru(COD)(COT)] (COD: 1,5 – cyclooctadiene; COT: 1,3,5 – Cyclooctatriene) in mild conditions (20^0, 3bar H_2) in n- pentane leads in the presence of octylsilane ($H_3SiC_8H_{17}$) to the formation of stable Ru nanoprticles with narrow size distribution was stabilized by Pelzer. K., et al **[146]** the solids obtained after washing and drying were fully characterized by elemental anal. TEM with EDX , IR measurements as well as solid state C^{13} CP- MAS NMR studies. The influence of the initial octylsilane /Ru(COD)(COT) ratio ranging from 0.2 to 2.0 was studied. The nanoparticles decreases with the initial Si/Ru ratio. The thermal stability of these nanoprticles (Si/Ru = 1) was also studied and as expected the size of the particles drastically increases after treatment under H_2 at 500^0, while surprisingly under neutral atm, there is only a slight increase.

FT – Raman spactra were obtained for thiophenol (TP) and TP on gold nanoprticles were oblized by Shujin. Li., et al [147] all vibrational fundamentals for the TP mol. were assinged on the basis of the scaled quantum force field procedure. Three moden system are studied and compared for the interactions of TP with the Au atom,(i) TP with Au atom, $C_6H_5SH^-$ - Au; (ii) TP anion with a Au atom, $C_6H_5S^-$ - Au; and (iii) TP with a Au atom and subsequent formation of thiophenolate, C_6H_5SAu. The equil. Structures and Raman spectra were calcd. For the model systems using d. functional theory (DFT) with the B3LYP functional and the mixed basis set 6 – 311+G^{**} (for C, S, H) and LANL2DZ (for Au), and theo. Raman wave numbers of C_6H_5SAu and $C_6H_5SH^-$ - Au; were assigned according to potential energy distributions. The third model system is shown to be preferred over the other two. The calcd. binding energies are also shown to support the third model system. A simple model, such as the one used in the present study, is reasonable to describe surface –enhanced Raman spectroscopy of thiophenol adsorbed on gold nanoparticles.

The exptl. Control of silver nano particle shape in citric acid soln. is rationalized by Kilin. Dmitri S., et al [148] ab initio calcns. The apporx. three – fold symmetry of the acid matches that of ag (111) and results in four silver- oxygen bonds. In contrast, citric acid forms only tow bonds with Ag (100) because of the geometry mismatch. Migration of a hydrogen atom within citric acid activates the electrons of the carboxyl oxygens and provides addnl. Binding affinity towards Ag (111). The preferential binding energy of citric acid to Ag (111) promotes crystal growth the Ag (100) surface.

The propose of this paper was to investigated by Aubry. Nadine., and Singh. Pushpendra., [149] the physics underlying the controlled self – assembly of microporticles and nanoparticles at under certain conditions an elec. Field can cause particles floating at a two – fluid interface to assemble into a virtually defect free monolayer whose lattice apacing can be adjusted by varying particles are a perfect dielecs. and for this case analyze the (capillary and elec.) forces acting on the particles, deduce an expression for the lattice spacing under equil. condition , and study the dependence of the latter upon the various paramaters of the system , including the particles radius , the dielec. Properties of the fluids and particles the particle's position within the interface, the particles buoyant wt. and the applied voltage. While for relatively large sized particles whose buoyant wt. is much larger than the vertical electrostatic force , the equil. distance increases with increasing elec. Field, for submicron sized particles whose buoyant wt. is negligible, it decreases with increasing elec. field. For intermediate sized particles, the distance first increases and then decreases and then decreases with increasing elec.field strength.

Branched polyethylenimine (PEI) – capped Au nanoparticles were prepared by Kim. Kwan., et al [150] the size of Au nanoparticles, ranging from 10 to 70 nm, is readily controlled by varying the relative amt. of PEI used initially vs. $HAuCl_4$. The PEI- capped Au nanoarticles are further demonstrated to be assembled into a large area of 2- D aggregates at a toluene – water interface either by heating the mist. Or by adding benzenethiol to the toluene phase at room temp. Both film are homogeneous, but Au nanoparticles appear to be more closely packed in the film assembled via the mediation o fcontrolled

by the amt. of benzenethiol added to the toluene phase. The obtained large area of PEI – capped Au film exhibits strong SERS activity of benzenethiol and also exhibits a very intense SERS spectrum of 4 – nitrobenzenethiol via a place – exchange reaction that takes place between benzenethiol and 4-nitrobenzenethiol. Because the roposed method is cost – effective and is suitable for the mass prodn. of diverse Au fils irresp. Of the shapes of the underlying sunstrstes, it is exected to play a significant role in the development of optical nanotechnol. esp . for surface Plasmon – based anal. Devices.

Aggregation behavior of colloidal cilvernanoparticles for surface- enhanced Raman scattering (SERS) on a hydrophobic surface was investigated by Culha. Mustafa., et al. [151] A regular glass slide is used to deposit dicholoromethylsilane in order to inactivate the free hydrozyl groups and increase the hydrophobicity of the glass surface. A submicron vol. of colloidal suspension is spotted on the hydrophobic surface. During the evapn. of water from the droplet, the nanoparticles start to form aggregates with a definite size and shape. Increasing colloidal suspension concn. By more than 4 times helped to complete the size of silver nanoparticles aggregates to about a μm diameter. The SERS activity of aggregates was investigated using Rhodamine 6G as a probe. The aggregates formed from higher colloidal suspension concns. show a significant improvement in SERS activity. The SERS enhancement factor for the aggregates and the limit of detection (LOD) for Rhodamine 6G are ested. as about $3x10^5$ and $1.0x10^{-5}$, respectively . the percent coeff. of variance (CV) improved about 300% by increasing the colloidal suspension concn. 8- fold on the prepd.

aggregates. A min. 2- fold ncrease in SERS enhancement on the aggregates. prepd. from silver colloidal suspension contg. NaCl and SDS is also obsd.

Ultrafine monodisperse gold nanoparticles (AuNPs) were synthesized by Hhatri. Om P., et al [152] an elegant suttering of gold onto 1-n-butyl-3-methylimidazclium hexaflourophosphate (BMI – PF_6) ionic liq. It was found that the BMI-PF_6 supramol. aggregates were loosely coordinated to the ogld nanoparticles and were replaceable with thiol mols. The self – assembly of BMI- PF_6 stabilized AuNPs onto a (3- mercaptoropyl) trimethoxysilane (MPS) – functionalized silcon surface in 2D arrays, followed by dedecanethiol (DDT) treatment have been demonstrated using ZPS, field emission SEM, and contact amgle measurements. DDT treatment of tethered AuNPs revealed two types of interactiosn between AuNPs and the MPS-funtionalized surface: (a) AuNPs anchor through Au- S chemisorptions linkage resulting in strong immobilization and (b) some of the AuNPs are supported by physisorption, driven by BMI- PF_6 . the attachment of these particles remains unchanged with sonication. The replacement of BMI-PF_6 agtgregates from physisorbed AuNPs with DDT mols. Advances the diln. of their interaction with the MOS-functionalized surface, and they subsequently detach from the silicon surface. The present finding is promising forn the immobilization of inonic liq. – stabilized nanoparticles, which is very desirable for electronic and catalytic device fabrication. Addnl., these environmentally friendly expected to replace conventional citrate – stabilized AuNPs.

Increasingly growing application of nanoparticles in biotechnol. requires fast and accessible tools for their manipulation and for characterization of their colloidal properties was characterized by Chang. Moon – Hwan., et al. [153] The ζ- potentials for polystyrene nanoparticles using micro- elec. field flow fractionation (μ-EFFF) which is an efficient method for sorting particles by size. The data obtained by μ-EFFF were compared to ζ-potentials detd. by std. capillary electrophoresis. For proof of concept, the authors used plystyrene nanoparticles of 2 different sizes , impregnated with 2 different fluorescent dyes. Fluorescent emission spectra were used to evaluate the particle sepn. in both systems. Using the theory of electrophoresis , the authors estd. the ζ-potentials as a function of size, dielec. Permittivity, viscosity and electrophoretic mobility. The results obtained by the μ & EFFF technique were confirmed by the conventional capillary clectrophoresis measurements. These results demonstrate the applicability of the μ & EFFF method not only for particle size sepn. But also as a simple and inexpensive tool for measurements of nanoparticle ζ & potentials.

Fahmi. Amir., et al [154] was reported a simple method of forming Au nanostructure arrays over large areas. A thin film of oligothiodendrimer-stabilized Au nanoparticles was prepd. via spin-coating on a solid substrate. The morphol. of the adsorbed thin films is markedly sensitive to the hydrophobicity of the underlying substrate. Adsorption on hydro-philic surfaces (native oxide-terminated Si (111) and mica) gave spatially correlated droplet aggregates with an ay. diam. of -300 nm, an ay. height of -30 nm, and an ay. areal d. of -3 x 108 cm-2. On a highly hydro-phobic

surface (H:Si (111)), however, the dendrimer-coated particles aggregate so that the ay. height and diam. of the clusters are much lower (-5 nm and -100 nm, resp.) whereas the areal d. is significantly higher (-5 x 109 cm-2). Also, and importantly, there are key differences in the topog. of the aggregates on the hydrophobic and hydrophilic surfaces. While for the hydrophilic surfaces the aggregates form droplets with an approx. hemispherical shape, on H:Si (111) the dendrimer-coated nanoparticles aggregate to form mesalike or 'doughnut' features.

Nucleation, growth, and thermal stability of Pd particles vapor—deposited on an ultra—thin cryst. silica film grown on Mo(112) was reported by Lu. J. – L., et al [155] using STM, XPS, IR reflection absorption spectroscopy, and temp.—programmed desorption of CO. No preferential nucleation of Pd on the silica film was found at room temp. deposition: the hemispherical Pd nanoparticles were homogeneously dispersed on the support at all coverages studied (0.01 — 1 ML (monolayer)). The Pd particles are resistant toward sintering .≤ 700 K as judged by STM; however, CO adsorption studies have revealed surface chem. modification at temps. as low as 550 K. Strong morphol. changes were obsd. above 800 K (ultimately resulting in elongated rectangular islands at 4000 K), which is accompanied by strong alterations of CO adsorption properties. The results are rationalized in terms of Pd and Mo substrate interdiffusion at elevated temps., while the silica film basically preserves its structure.

A new class of SERRS – active macromal. designed to protect silver nanoparticle surface against salt corrosion while retaining colloidal stability of the particles was reported by Cormack. Peter. A. G., et al. [156]

Polymeric films contg. TiO_2 nanoparticles have potential as dielec. Films for flexible electronic applications were synthesized by Song. Lixin., et al [157] for this porpose, the nanoparticles must be homogeneously distributed. Self assembly is emerging as a neat, elegant method for fabricating such nanostructured hybrid materials with well—distributed nanoparticles. The author report a micellar soln. approach for the assembly of copolymer- Ti precursor nanostructures in which TiO_2 nanoparticles were synthesized. The ratio of the amt. of Ti precursor, Ti isopropoxide, to the blocks forming the micellar core, poly (4—vinylpyridine), was found to play a key role in controlling film morphol. A sphere—to—ribbon transition was obsd.when the amt. of Ti isopropoxide was increased.The thin film morphol. can be tuned using the precursor—copolymer interaction rather than just the polymer—polymer interaction or the polymer soln. interaction. This method provides yet another way to control the morphol. of nanostructures.

The development of surface—modification technologies has greatly expanded the application areas of nanomaterials. It was established by Zhang. Wanzhong., et al [158] steady foundation to prep. high qualities nanometer materials. The research survey of surface—modification was reviewed. The surface characteristics of nanoparticles, the purpose and the methods of surface—modification were introduced. The applications in

prepg. nano—semiconductors, rare earth compd. nanomaterials, oxide nanoparticles and metal—nanoparticles were also represented. At last, the development trends of surface—modification technologies were predicted.

Lin. Ming – Nung., et al [159] was provided a useful technol. to fabricate a long—range ordered nanoparticle array with a feature size under 30 nm. By adjusting the incident angle of Ar^+ beam milling on a U—shaped barrier layer of anodic Al_2O_3, they were able to create a long—range ordered nanoaperture array with samples prepd. by a focused—ion—beam (FIB)—guided process. Compared to the naturally self—organized Al_2O_3 nanochannels, the FIB—guided process has increased long—range ordering and uniformity of aperture size, and the aperture size can be varied by changing the grazing angle. The nanoaperture membrane can be used as a contact mask and its undercut structure has another advantage for nanolithog. This technique could be extensively applied to the manufg. of advanced nanodevices in large areas and as a catalyst to fabricate 1D nanosized materials.

Creating hybrid nanostructures consisting of disparate nanoscale blocks is of interest for exploring new types of quantum device architectures. Here, Pan. Bifeng., et al [160] was demonstrated the novel anchoring of Au nanoparticles of -13 nm diam. to side-walls and ends of C nanotubes (CNTs) via covalent interactions between Me mercaptoacetate capping the nanoparticles and amine -terminated CNT surfaces. Ethylenediamine was grafted onto the surface of the nanotubes by covalent interaction between amine groups and

the chlorocarbonyl groups on the C nanotube surface to give amine-functionalized CNTs. Mercaptoacetate capped 13 nm Au nanoparticles were subsequently anchored to the surface of the nanotubes through the covalent interaction between nanotubes and the nanoparticles. Novel nanoassemblies of C nanotubes (CNT) and Au nanoparticles were obtained. These assemblies were confirmed by UV-visible, transmission electron microscopy, FTIR, and X-ray powder diffraction methods. This approach provides an efficient method to attach other nanostructures to C nanotubes and can be used as an illustrative detection of the functional groups on carbon nanotube surfaces. Such molecularly interlinked hybrid nanoblocks are attractive for building biocompatible nanodevices.

Nearly monodispersed CdS nanoparticles with cubic phase have been synthesized via a thermally triggered liposomes—mediated mineralization. The results showed that the cadmium—loaded liposomes mixed with Na_2S did not mineralize immediately at 20°C. However, shallow yellow—colored CdS colloids rapidly formed when the mixed suspensions were heated to above the lipid chain melting transition. The CdS obtained was characterized by transmission electron microscopy, X—ray powder diffraction, UV—Vis absorption, and photoluminescence spectroscopies. That thermally triggered CdS nanoparticles formation from cadmium – loaded liposomes were reported by Chu. Maoquan., and Liu. Guojie., **[161]**

Polymer—stabilized Au colloidal nanoparticles were prepared by Yang. Li – Ping., and Tu. Wei – Xia **[162]** using microwave irradn. Size of the Au

colloidal nanoparticles in the relative system with adding of NaOH was obviously faster and particles varied from 5 nm to 120 nm along with different reactive conditions. Effects of the alc. reducing agent and NaOH on particle size and shape were studied. The prepd. Au nanoparticles were characterized by transmission electron microscope (TEM) and UV—visible- (UV—visible) spectrophotometer. The Au nanoparticles prepd. by micro-wave irradn, have small particle size and good size distribution. The nanoparticle size and shape are highly dependent on the nature of the reducing agent and concn. of NaOH. Using UV—visible spectra, the velocity of the formation of the Au nanoparticles in the reactive system with adding of NaOH was obviously faster and easier to form spherical particles than that without NaOH.

A water – sol. gold nanoparticle was synthesized by Yin. Hong – Zong., et al **[163]** with trisodium citrate by redn. method, and using cystine as a selfassembled mol., three dimensional net structure of gold nanoparticle with cystine was obtained. Various techniques, such as UV—visible spectrophotometry, TEM, Religh light—scattering spectrum, were used to characterize gold nanoparticle and the 3-dimensional net structure. The av. diam. of gold nanoparticle assembled by cystine in this 3-dimensional net structure was -5.1 nm, bigger than that of gold nanoparticle of 4.5 nm. To form 3-dimensional net structure, the optimal molar ratio of gold to cystine was 1:1, and a pH 5.1buffer solution of sodium citrate- citric acid was required only 14% of cystine mols. was assembled to surface of gold nanoparticle, while excessive cystine played an important role in the 3-dimensional net structure, where cystine mol. was a bridge among gold

nanoparticles and ion band was a dominating factor. Compared with gold nanoparticle (518 nm), its UV-visible absorption peak was red shifted to 670 nm and such 3-dimensional net structure had a nonlinear light-scattering characteristics.

Deposition of pos. charged nanosized latex particles onto planar silica and cellulose substrates was investigated by Kleimann. Joerg., et al [164] in monovalent electrolyte solns. at pH 9.5. The deposition was probed in situ with optical reflectometry in a stagnation point flow cell. The surface coverage can be estd. reliably with island film theory as well as with a homogeneous film model, as confirmed with at. force microscopy (AFM). The deposition kinetics on the bare surface was of first order with respect to the particle concn., whereby the deposition rate was close to the value expected for a perfect collector. The efficiency coeff., which was defined as the ratio of the exptl. and theor. deposition rate consts., was in the range from 0.3 to 0.7. Subsequently, the surface satd. and a limiting max. coverage was attained (i.e., blocking). These trends were in qual. agreement with predictions of the random sequential absorption (RSA) model, where electrostatic interactions between the particles were included. It was obsd., however, that the substrate strongly influenced the max. coverage, which was substantially higher for silica than for cellulose. The major conclusion of this work was that the nature of the substrate played an important role in a satd. layer of deposited colloidal particles.

This article was reported by Laaksonen. Timo., et al [165] on the ion permeability of self—assembled monolayers (SAMs) formed on the surface of charged al.- kanethiol—protected Au nanoparticles, so called monolayer protected clusters (MPCs). The capacitance and thus the charging energy required to add/remove an electron from the metal core are extremely sensitive to ions entering the monolayer, and the extent of ion penetration can be tuned by the charge and size of the ions and the permittivity of the solvent. Exptl., this effect is comparable to ion assocn. with conventional redox mols., indicating that MPCs despite their large size and the fundamentally differing nature of the electron transfer process can be treated analogously to redox mols.

Tanaka. Akinori., et al [166] were carried out the photoemission study of various alkanethiolate— (AT—) passivated Au nanoparticles. From the detailed line—shape analyses of Au 4f core—level photoemission spectra, the interface chem. states are independent on the surface passivants of AT mols. among the AT—passivated Au nanoparticles with the same size. Also, the interface electronic structures of AT—passivated Au nanoparticles with the same size also, the interface electronic structurs of AT- passivated Au nano particlecls were characterized. The surface—potential shifts due to the interface dipoles accompanying the adsorption of AT mols. are —0.36 eV and are independent on the surface passivants of AT mols. The detailed interface electronic state of AT—passivated Au nanoparticle is discussed.

Cd sulfide nanoparticles (6-12 nm) were characterized by Sathish. M., et al [167] a pptn. process using different zeolite matrixes as templates. The nanoparticles were characterized by UV—visible, XRD, SEM, TEM and sorptometric techniques. XRD study shows hexagonal and cubic phases for the nanoparticles whereas in case of the bulk samples only the hexagonal phase is obsd. These nanomaterials were used as catalysts for the photocatalytic decompn. of H_2O. The nanoparticles show a higher hydrogen evolution rate compared to the bulk samples which correlates well with the particle size and surface area. Noble metal (Pt, Pd, Rh, Ru)—loaded samples were subsequently prepd. and tested for hydrogen evolution reaction. The presence of Pt metal is found to enhance the hydrogen prodn. rate whereas the hydrogen prodn. rate is retarded in the presence of Ru metal. This was explained from metal hydrogen bond, redox potential and work function of the noble metal. AP. 0 Ani rlynsimit, in tryincitnnrt—limited tthacelln.

Vibrational sum frequency generation (VSFG) spectroscopy was used to study the nanoscale geometric effects on mol. conformation of dodecanethiol ligand on Au nanoparticles of of varying size between 1.8 and 23 nm. By analyzing the Me and CH_2 stretch transitions of dodecanethiol using the spectroscopic propensity rules for the SFG process, Weeraman. Champika., et al [168] were observed the increase of the gauche defects in the alkyl chain of the ligand on the nanoparticle surface when the curvature approaches the size of the mol. (-1.6 nm). But linear IR absorption and Raman spectra, governed by different selection rules, do not allow observation of the sizedependent conformational changes. The results are understood in terms of the geometric packing effect, where the curvature of

the nanoparticle surface results in the increased conical vol. available for the alkyl chain.

Sun. Yuan., et al [169] was compared the characteristics of dodecanethiolate Pd nanoparticles synthesized by 2 different techniques, a 1—phase method and 2—phase method. From TEM, the particle sizes were 46 ± 10 A° and 20 ± 5 A° for the 1— and 2—phase particles, resp. Electron diffraction confirmed that their structure was fcc, The lattice const. a_0 was 3.90 ± 0.01 A° and 3.90 ± 0.01 A° for the 1— and 2—phase particles, resp. High—resoln. TEM (HRTEM) showed that the 1—phase particles had an ordered core surrounded by a disordered shell structure, while the 2—phase a particles appeared to be crystal throughout. The particles were also analyzed with extended x—ray absorption fine structure (EXAFS). A cuboctahedral fcc. model was used to fit the data, which implied particle sizes of <10 A° for both the 1— and 2—phase particles. The discrepancy between the 2 techniques was attributed to the presence of a disordered of phase, which the authors presumed was composed of Pd—S compds. Compared with the bulk Pd, lattice expansion was obsd. in both 1— and 2—phase particles by electron diffraction, HRTEM, and EXAFS. At the air/H_2O interface, a uniform film that produced surface pressure/area isotherms could only be obtained from the 2—phase particles. The 1—phase particles did not wet the H_2O surface. X—ray reflectivity data indicated that the Langmuir monolayer of the 2—phase particles was only 13 A° thick. TEM revealed the diam. of the particles in this layer of to be 23 A°., hence the particles

assumed an oblate structure after spreading. EXAFS examn. of a stack of 750 Langmuir monolayers indicated far fewer Pd—S compds., which may have dissolved in the H_2O. The 01 data were consistent with a model of a monolayer of truncated cuboctahedron Pd particles that were 7 A° thick and 19 A in diam.

CO monolayer oxidn. on Pt nanoparticles with different shapes (semi—spherical, cubic, and tetrahedral—hexagonal nanoparticles) was studied by Solla – Gullon. J., et al. [170] A very clear dependence was found between bidimensional (111) and (100) ordered domains present on the surface of the nanoparticles and their CO electrocatalytic activity. The results work demonstrate the importance of controlling the intrinsic structural properties of the Pt nanoparticles, in terms of no. and nature of the surface active sites, to understand their electrocatalytic properties. Thus, adsorbed CO oxidn. was revealed as an extremely structure sensitive reaction useful to establish correlations with the surface properties of Pt nanoparticles.

Nucleation and growth mechanisms of Ni nanoparticles synthesized by Li. P., et al [171] an incipient wetness technique on a high—surface area TiO_2 support (i.e., a mixt. of anatase and rutile) are studied using environmental transmission electron microscope (ETEM). Most Ni nanoparticles are found to nucleate from the Ni precursor coated on the surface of the TiO_2 support. Even though both anatase and rutile supports are the nucleation sites for Ni nanoparticles, it was obsd. that the particles have different morphologies on the supports, i.e., a none—wetting morphol. on the anatase support vs. a

wetting morphol. on the rutile (101). This is because the interfacial energy of Ni/rutile is lower than that of Ni/anatase. TiO_2 clusters are found to nucleate on the surface of the Ni particles during in situ ETEM redn., indicating that the presence of partial TiO_2 overlayers is directly related to the synthesis of the Ni/TiO_2 catalysts. The growth mode of the Ni nanoparticles on the TiO_2 support is 3D, while that of the rutile cluster on the surface of the Ni is 2D layer—by—layer.

Mercapto—terminated linear polymers, which were prepd. by a reversible addn.—fragmentation chain transfer (RAFT) technique, were used to modify metal nanoparticles surfaces. Au and Ag nanoparticles which are approx. 3-6 nm were used. This modification resulted in easy dispersion of the nanoparticles in polymer resins by simple mixing. The quality of the dispersion was confirmed by UV—Vis spectroscopy and transmission electron microscopy that were synthesized by Matsumoto. Kazuaki., et al. **[172]**

Zhang. Dan., et al **[173]** was reported a simple route for the effective synthesis of Ag/TiO_2 nanoparticles in H_2O —in—oil (w/o) emulsions and provide detailed characterization of the materials with TEM, TG—DTA, IR, XRD, and SPS measurements. Such core—shell hybrid nanoparticles can be fabricated in two simple steps: the formation of the Ag core by the redn. of a Tollens reagent with glucose in the H_2O phase, and the hydrolysis of $Ti(OBu)_4$ at the H_2O /oil interface for the formation of the amorphous TiO_2 shell. The procedure gave nanocomposites with a cryst. core in a size range

from 5 to 15 nm in diam. and an amorphous shell of 6-10 nm thickness in a typical synthesis. The shell was converted to cryst. oxide upon thermal treatment. Surface photovoltaic spectroscopy (SPS) measurements indicate that the materials have potential for application in photoinduced electron storage and photocatalysis.

Correa – Duarte. Miguel A., and Liz – Marzan. Luis M. [174] was presented a simple, generally applicable procedure for the assembly of nanoparticles on carbon nanotubes in aq. soln. The method makes use of polyelectrolytes for wrapping carbon nanotubes and providing them with adsorption sites for electrostatically driven nanoparticle deposition. The method is exemplified by the assembly of gold nanoparticles which results in single, optically labeled carbon nanotubes.

The influence of nanoscale out—of—plane roughness on the ordering of submicron spheres during evaporative deposition from colloidal suspension was examd. using shallow corrugated substrates possessing optical wavelengths and nanoscale amplitude was investigated by Mathur. Anant., et al [175] under conditions in which spheres were embedded in a liq. layer with thickness on the order of the sphere diam., it was obsd. that the spheres overwhelmingly deposited in the valleys of the surface corrugations rather than on their peaks. This behavior persisted to surprisingly shallow corrugation amplitudes, sometimes 100 times smaller than the sphere diam. An anal. of the capillary forces on the spheres explains this behavior and also yields a crit. corrugation amplitude below which a substrate will appear

"flat" to depositing spheres. The observation that substrate features significantly smaller than the sphere diam. can influence deposition morphol. may lead to simple methods to create large domains of order in colloidal crystals.

This study deals with the synthesis of cysteine capped gold nanoparticles with an av. Size of 12nm by borohydride redn. and spectroscopic identification of S- Au interaction was Aryal. Santosh., et al [176] studied the interaction of thiol with gold nanoparticles in aq. medium by employing UV – vis, Raman, NMR, and FT- IR spectroscopy. The shifting of goldplasmon resonance in the UV—vis spectra shows the stabilization of gold nanoparticles by cysteine. The disappearance of S—H stretching in both the IR and Raman spectra and the shifting of the NMR, signals of the protons in close proximity to the metal center supported the existence of the S—Au interaction in cysteine capped gold nanoparticles. The TEM images shows cysteine capped gold nanoparticles as distinct and spherical entities as compared to free colloidal gold nanoparticles.

High—angle annular dark—field (HAADF) imaging technique in the scanning transmission electron microscope was exploited to study self—assembled multilayer structures of Au/Ag nanoparticles. The HAADF image intensity depends monotonically on the mass and thickness of the sample. Various film thicknesses between one to four monolayers can be easily distinguished by evaluating the contrast this work was reported by Ziyuo. Li., et al. [177]

Zhou. Yong., et al [178] were illustrated that the dense helical arrays of CdS nanoparticles, which are aligned one — by — one and side—by—side, form on the self —assembled nanotube template from the binary components, glycolipid, N —(11 — cis — octadecenoy1) — β — D — glucopyranosy – lamine (1) and aminophenyl—β—D—glucopyranoside (2) as an additive. The present formation mechanism greatly differs from preceding examples that utilize residual helical marks on the surfaces of lipid nanotubes and nanoribbons or org. templates with a helical morphol. In this work, it functionalized the glycolipid nanotube of 1 by incorporation of 2 through self assembly. This functionalization process enabled us to create active binding sites, which trace the chiral mol. packing of the nanotube. Consequently, the helical nucleation and growth of the CdS nanoparticles took place on the template surfaces. The helical arrangement of the CdS nanoparticles was characterized by field—emission SEM (FE—SEM) and scanning transmission electron microscopy (STEM). The phase anal. and optical properties of the helical CdS nanoparticle were also discussed.

Curve fitting of extended x—ray absorption fine structure (EXAFS) spectra, transmission electron microscopy (TEM) imaging, and Scherrer anal. of x—ray diffraction (XRD) are compared as methods for detg. the mean crystallite size in polydisperse samples of platinum nanoparticles. By applying the techniques to mixts. of pure samples, it is found that EXAFS correctly dets. the relative mean sizes of these poly-disperse samples, while XRD tends to be weighted more toward the largest crystallites in the sample. Results for TEM are not clear cut, due to polycrystallinity and aggregation,

but are consistent with the other results were characterized by Calvin. S., et al. [179]

This route was presented by Mallick. Kaushik., et al [180] for the prepn. of a Ag film in presence of UV—radiation. Methoxy polyethylene glycol, a water—sol. polymer, was used as the reducing agent of the Ag^+ in the presence of an UV source to produce Ag nanoparticles. During soln. stirring, a centrifugal force was generated at the center of the soln. At this point on the surface of the soln., the nanoparticles coalesced to form a self—assembly of small subunits that ultimately develops into a film—like network.

Nanocermet trilayered thin films consisting of Ag nanoclusters sandwiched between 2 dielec. layers (the buffer and the cap) were synthesized by Toudert. J., et al [181] ion—beams sputtering with an alternate deposition of the metal and the dielec. species. The influence of the amt. of Ag, the nature of the buffer and the cap (BN or Si_3N_4), and a time delay before the cap deposition on e clusters morphol. and repartitions were investigated by transmission electron microscopy. The clusters display truncated ellipsoidal shapes in which the height to diam. ratio H/D decreases as the amt. of deposited). Ag increases. For a given amt. of Ag, this ratio is lower in the case of a Si_3N_4 cap, whatever the nature of the buffer. 2 Explanations are proposed to account for this "cap effect" on clusters morphol.: the first one is based on a calcn. of the H/D minimizing the surface free energy of the clusters embedded between the buffer and the cap; the second one holds on the shape relaxation of the coalesced nonequil. clusters towards their equil.

shape with the buffer, this process occurring until clusters. are fully covered with the cap. Because of the higher deposition rate of Si_3N_4 compared to BN, a Si_3N_4 cap would allow a less efficient reshaping and consequently lead to flatter clusters. This explanation is supported by the temporal evolution of clusters morphol. and repartition obsd. during the time delay before deposition of the cap. The evolution of the spectral position of the surface—plasmon resonance (SPR) of the trilayers as a function of their structure was also investigated by optical transmittance measurements. The influences of cluster morphol., as well as the nature of the buffer and the cap on the SPR spectral position are discussed.

This article was reported by Yang. Hanmin., et al **[182]** the lubrication of the mixed system of CdS nanoparticles and Triton X-100/C_{10} H_{21} OH/H_2O lamellar liq. crystals. CdS nanoparticles 'could be synthesized in the lamellar liq. crystal's solvent layer, limited by its amphiphile bilayer. The CdS nanoparticles were spherical and the size was —5 nm. The lubrication properties of the mixed system of the lamellar liq. crystal and CdS nanoparticles were detd. The presence of CdS nanoparticles could improve the antiwear ability and extreme pressure property of Triton X-100/C_{10} H_{21} OH/H_2O lamellar liq. crystals.

A mono—layer of nano—sized metal particles was prepared by Lim. Sung. K., et al **[183]** on the surface of a polyimide film by simply depositing a thin film of $Ni_{80}Fe_{20}$ on top of the polyamic acid that was spin coated onto a Si wafer. During thermal imidization of the polyamic acid film, Fe was

selectively etched by reacting with the corbonyl group of the polyamic acid to leave behind uniformly distributed Ni—rich metallic particles. The av. diam. of the particles was 4 nm and particles were confined into a single layer on top of the polymer film. Also, the morphol. of the nanoparticles can be substantially altered any curing the precursor film in a hydrogen atm., without significantly amaging the polymer film. Thus produced nanoparticles lay exposed top of the elec. insulating and chew. stable polymer film so that it is possible that the nanoparticles can be directly used for fabricating a nonvolatile flash memory device or as a template for building functional nano—structures.

Colloidal aq . soln. of zerovalent copper (Cu(0)) nanoparticles were synthesized by Kuo. Ping – Liang. Wuu – Jyh., and Wang. Fu – Yu., **[184]** from the Cu^{2+} ions coordinated with polyethyleniminated polyoxypropylenediamines ($D400(EI)_x$) followed by chem. redn. of $NaBH_4$. Aq. soln. of copper clusters formed in the presence of $D400\text{-}(EI)_8$ with a loading ratio of $[EI]/[Cu^{2+}] = 3$ were stable without pptn. for standing more than 1 mo. The protective effects of D400(EI)x and the particle size of the resulted Cu nanoparticle are regulated by the attachments of ethylenimine (EI) groups per polymer backbone and the normality ratio of $[EI]/[Cu^{2+}]$ used. It is found that the more EI—content per polymer backbone results in the smaller particle size and the narrower size dispersity of the colloidal Cu(0) particles, and the av. particle size of 5.07 nm with std. deviation of 0.86 nm was obtained in the presence of $D400(EI)_8$ with the ratio of $[[EI]/[Cu^{2+}] = 3$. As the polymer concn. of $D400(EI)_8$ increases (the increase of $[EI]/[Cu^{2+}]$, the av. particle size of the prepd. Cu(0) nanoparticle slightly

changes, but interestingly, the size dispersity gradually decreases, where the std. deviation for the concn. at $[EI]/[Cu^{2+}] = 5$ is 0.82 nm approaching that for monodispersed nanoparticles (0.5 nm).

Reversible interparticle self- organization was reported by Van Herrikhuyzen. Jeroen., et al [185] for gold nanoparticles functionalized with and oligo (p-phenylene vinylene) moiety in butanol. The aggregates show a clear melting temp. at 80^0C, and force microscopy and transmission electronmicroscopy indicate a fractal –like organization of the particles.

Conclusion

Nanoparticles were synthesized successfully by chemical reduction and green synthesis methods respectively.

The detail characterization of the nanoparticles was carried out using UV-Vis spectroscopy, Dynamic Light Scattering (DLS) particle size analysis, Scanning Electron Microscopy (SEM), X-Ray Diffraction (XRD) analysis. From Dynamic Light Scattering (DLS) particle size and SEM image analysis, the average particle size was found to be 90 nm and 50 nm, The XRD of These sample reveals that the required phase is present with a little amount of impurities. The particle size which was done by particle analyzer was supported by the XRD Scherer's formula.

The test was performed by both Disc diffusion assay and colony forming unit (CFU) estimation method. From the study of nanoparticles were observed to have strong antimicrobial potential. When the result was compared with the effect by antibiotics like Vencomycin, Tobramycin and Erythromycin, nanoparticles were found more potent than antibiotics.

In vivo biological activity of expressed β-glucosidase enzyme in *Escherichia coli* was measured in the presence of various concentrations of nanoparticles. It was found that the incubation of *Escherichia coli* in the presence of nanoparticles caused the substantial enhancement of the biological activity of β-glucosidase *in vivo*.

In vitro interaction between α-lactalbumin, nanoparticles were also investigated. When the binding experiments were monitored in DLS particle size analyzer, the stable protein-NP conjugate formation was confirmed. The result also helped to develop a model where multiple numbers of proteins bind to a single or multiple NP molecules.

Anti-fungal and anti-cancerous activity of the nanoparticles may be investigated in details. Various plants and fruit extract can be used to synthesize nanoparticles to find a more non-toxic and economical method of synthesis. Detail mechanistic study of antibacterial function of nanoparticle may be elucidated. Nanoparticles may be used to examine the effect on other industrially and clinically important gene expression *in vivo*. α-lactalbumin and nanoparticles conjugate may be applied in various cancer cell to observe any anti-cancerous potential of the protein-NP conjugate.

Reference of Introduction.

Reference of Synthesis,

Refrence of Methods:-

[70] Cao, G., E. Wolf., and VCH- Wiley. Weinheim., Nanostructures and Nanomaterials, Synthesis, Properties and Applications.,. *Imperial College Press, London., Nanophysics and Nanotechnology,.* **2004.**

[71] Lin, S. T., Franklin, M. T., Klabunde, K. J., *Langmuir*, *2*, 259, **1986.**

[72] Becker, M. F., F. Kohno., J. Takeda., and Y.Kondow., *Nanostruct. Mater*, *10*, 853, **1998**.

[73] Gachard. E., *New J. Chemistry* 1257, **1998.**

[74] Lal.Ashwin., Synthesis of Metal nanoparticles by electrolytical stm and electrochemical discharges. *Indian Institute of Technology Kanpur, India*, **2007.**

[75] VJ. Mohanraj., and Y. Chen., Nanoparticles , *A Review Tropical Journal of Pharmaceutical Research*, June **2006.**

[80]

[81]

[82] C.Burda., X.Chen., R.Narayanan., M.A. El-Sayed., *Chemistry Review*. 105, 1025, **2005.**

[83]W.Schulz., Crafting a National Nanotechnology Effort. *Chemical & Engineering News (C&E News)*. 78. **2000.**

[85]C. Burda., X. Chen., R. Narayanan. And M.A. El-Sayed., *Chemistry Review*. 105, 1025, **2005.**

[86] Chair. Mark. Anderson., Karen Brewer., John Morris., and Yee. Gordon. Blacksburg., Optical Properties and Interaction with Chemical Warfare Agent Simulants, *Virginia, Metal Oxide Nanoparticles*, p.03. Nov. **2006.**

[84]Roy. Rajneeta., Synthesis and Characterisation of different Nanoparticles of potential use utilising cheap resources p.25, **2008.**

References of Characterization

[100] L.Reimer., Scanning electron microscopy: physics of image formation and microanalysis. *Springer*,**1998.**

[101] Omkar Behera., Synthesis and Characterization of ZnO nanoparticles of various sizes and Applications in Biological systems, *Orissa India (INT)*, p.31.

[102]P.J. Goodhew., and F.J.Humphreys., Electron Microscopy and Analysis,
Second Edition, *Taylor and Francis Inc. London, UK* , **1988.**

[103]M.Roco., and R.Tomelini., , Revolutionary Oppurtunities and Soceital Iplications, *Nanotechnology***, 2002.**

[104] K.M.Lang., D. A. Hite., R. W. Simmonds., R. McDermott., D. P. Pappas., John M. Martinis "Conducting atomic force microscopy for nanoscale tunnel barrier characterization". *Review of Scientific Instruments* **75**(8): 27262731.Bibcode:2004RScI...75.2726L. doi:10.1063/1.1777388, **2004.**

[105]C.Julian.Chen., Introduction to Scanning Tunneling Microscopy (PDF). *Oxford University Press*. ISBN 0-19-507150-6, **1993.**

[106] "STM References - Annotated Links for Scanning Tunneling Microscope Amateurs". *Retrieved July* 13, **2012.**
[=]
[107] D.R.G.Mitchell., *J. Nucleus Chemistry*, **33**, 69, **1996.**

[108] Jayanta Kumar Behera., Synthesis and Characterization of Zno nano-particles, *Rourkela-769008, Orissa, India* p. 21-22.

[109] Jayanta Kumar Behera., Synthesis and Characterization of Zno nano-particles, *Rourkela-769008, Orissa, India* .

[110] H.C. Van de Hulst., Light scattering by small particles. *New York* Dover. ISBN 0-486-64228-3, **1981.**

[111] Paula Cole., Nanoparticles in aqueous environments, A physicochemical and ecotoxicological study of cerium dioxide, *The University of Birmingham, UK* p.56. July **2011.**

Refference of Properties

[A] M.Ramani., S.Ponnusamy., C. Muthamizhchelvan., Zinc oxide nanoparticles, A study of defect level blue–green emission. *Optical Materials* 34, pp. 817–820, **2012.**

[B] P.M.Aneesh., K.A. Vanaja., M.K.Jayaraj., Synthesis of ZnO nanoparticles by hydrothermal method.Proc. of SPIE 6639, pp. 66390J-1, **2007.**

[C] J. F. Nye., Physical Properties of Crystals,. *Clarendon, Oxford,* **1975.**

[D] http://www.aadet.com/article/nanoparticle, Nanoparticle Data.

[E] J.I. Mrtin., J. Nogues., K. Liu., J.L. Vicent., I.K. Schuller., and J. Magn., *Mater*. 256. 449, **3003.**

Refference of Limitations;

[1] Omkar Behera National Institute of Technology Rourkela,Synthesis and Characterization of ZnO nanoparticles of various sizes and Applications in Biological systems Rourkela-769 008, *Orissa, India* p.19.

References;

Reff. of IIT Kanpur

[1] Xu Bing She, Tanaka. S., (ERATO, JRDC, Yokohama, Japan) *Nanostructure. Mater (USA)* vol.6, no.5-8, p. 727-30, **1995.**

[2] Saito. Y. (Dept.of Electr. &Electron .Eng., Mie Univ., Tsu, Japan) *Carbon (UK),*vol.33, no.7, p.979-88, **1995.**

[3]Reznik. D., Olk. C., H., Neumann. D., A., & Copley. J., R., D., (Mater. Sci. & Eng. Lab., Nat. Inst. of Stand. & Technol., Gaithersburg M USA), *Phys. Rev. B, Condens. Matter (USA)* vol.52, no,1, p.116-24, **1995**.

[4] Boulanger. L., Andriot. B., Cauchetier M., and Willaime. F., (Section de Recherches de Metallurgie Physiques, Centre d'Etudes de Saclay, Gif-sur-Yvette, France) *Chem. Phys. Lett. Netherlands*, vol. 234, no. 1-3, p. 227-32, **1995.**

[5] Tognini. T, Geddo. M, Stella. T, Cheyssac. P, and Kofman. R, (Dipartimento di Fisica A. Volta, Pavia Univ., Italy), *J. Appl. Phys. 9USA*) vol.79, no.2, p. 1032-9,**1996.**

[6] Weber. A. P., Thorn. J. D., and Friedlander. S. K., (Dept. of Chem., Eng., California Univ., Los Angeles, CA, USA), *Material Fabrication and Patterning at the Nanoscle. Symposium, San Francisco, CA, USA*, P. 87-92, **1995.**

[7] Pileni. M. P., and Tanori. J., (Lab. S. R. S. I., Univ. P. et Curie. M., Paris, France). *Adv. Matter. Germany*, vol. 7, no. 10, p. 862-4, **1995.**

[8] Li. Ping., and Sattler. K., (Dept. of phys. & Astron., Hawaii Univ., Honolulu, HI, USA)., *Microcrystalline and Nanocrystalline Semiconducter. Symposium, Boston, MA, USA*, 29 Nov – 2 Dec.**1994.**

[9] Borsella. E., Botti. S., Cesile. M. C., Di Nunzio. P. E., Martelli. S., and Nessterenko. A., (Div. INN-FIS-SPET, ENEA, Frascati, Italy), *Matter. Sci. Forum Switzerland*, vol. 195, p. 37-42,**1995.**

[10] Van der Putten D., Olevano. D., Zanoni. R., Krautscheid. H., and Fenske. D., (Dipartmento di Chimica, Rome Univ., Italy), *Matter Sci. Forum Switzerland*, vol, 195, p. 123-6 , **1995.**

[11] Allard L. F., Volkl. E., Carim. A., Datye. A. K., and Ruoff R., (Osk Ridge Nat. Lab ., TN, USA), *Nanostruct. Mater. USA*, vol. 7, no. 1-2, p. 137-46, **1996.**

[12] Groza. J. R., and Dowding. J. R., (Dept. of Chem. Eng & Mater. Sci., California Univ., Davis, CA, USA), *Nanostruct. Mater.USA*, vol.7, no.7, p. 749-68. Sept - Oct., **1996.**

[13] Arcoleo. V., and Liveri. V. T., (Dipartmento di Chimica Fisica, Palermo Univ. Italy), *Chem. Phys. Lett, Netherland*, vol. 258, no. 1-2, p.223-7, Aug. **1996.**

[14] Fei G. T., Lu. R., Zhang. Z. J., Cheng. G. S., Zhang. L. D., and Cui. P., (Inst. of Solid State Phys., Acade. Sinica, Hefei, China), *Mater. Res. Bull. USA*. vol. 32, no.5, p.603-8, May **1997.**

[15] Averitt. D., Sarkar. D., and Hals. N. J., (Dept. Electr. & Comput. Eng., Rice Univ., Houstron, TX, USA), *Phys. Rev. Lett. USA*, vol.787, no.22, p. 4217-20 June **1997.**

[16] Zhang. L., and Manthirama A., (Centre for Mater. Sci. Eng. Texas Univ., Austin, TX, USA), *Appl. Phys. Lett. USA*, vol.70, no. 18, p. 2469-71, May **1997.**

[17] Raina. G., and Sen. R., (Jawahrlal Nehru Centre for Adv. Sci. Res., Banglore, India), *Bull. Mater. Sci. India*, vol. 20, no. 1, p.1-7 Feb., **1997.**

[18] Muramoto. J., Nakata. Y., Okada. T., and Maeda M., (Graduate Sch. Of Inf. Sci. & Electr. Eng., Kyushu Univ., Fukuoka, Japan), *Jpn. J. Appl. Phys. 2, Lett. Japan* vol. 36, no. 5A, p. L.563-5, **1997.**

[19] Gorla. C. R., Liang. S., Tompa,. G. S., Mayo. W. E. M., and Lu.Y., (Dept. of Ceramics, Rutgers Univ., Piscatassy, NJ, USA), *J. Vec. Sci. Technol. A, Vac. Surf. Films USA,* vol.15, no.3, pt.1, p.860-4, june **1997.**

[20] Maser. W, K., Bernier. P., Luk'Yanchuk. I., Molinie, P., Lefrant. S., Redich. P., and Ajayan P. M., (Groupe de Dynamique des phases Condensees, Montpellier - 2 Univ., France), *Adv. Mater. Germany*, vol. 9, no.6, p. 503-6, May **1997.**

[21] Newbury. D. E., (Nat. Inst. of Stand. & Techol., Gaithersburg, MD, USA), *Nanostruct. Mater.,USA.* vol.9., no.1-8, p.251-60, **1997.**

[22] Ishikawa. Y., Shibata. N., and Fukatsu. S., (Japan fine Ceramics Center, Nagoya, Japan), *Thin Solid Films Switzerland*, vol.294, no.1-2, p. 227-30 Feb.**1997.**

[23] Schiffmann. K. I., Fryda. M., Goerigk. G., Lauer. R., and Hinze.P., (Fraunhofer Inst. Schicht und Oberflachentech., Braunschweig, Germany), *Ultramicroscopy Netherland* vol.66, no.3-4, p. 183-92, Dec. **1996.**

[24] Gao. H. Y., Zhang. Z., Liao. L. S., and Bao. X. M., (Lab. of Electron Microscopy, Acad. Sinica, Beijing, China), *J. Res. USA*, vol.12, no.6, p. 1640-5, June **1997.**

[25] Mei. Li., Jiang Ming and Chi. Wu., (Dept. of Macromolecular Sci., Fudan Univ., Shanghai, China), *J. Polym. Sci. B, Polym. Phys. USA*, vol. 35, no.10, p.1593-9, July **1997.**

[26] Dutta. J., Houriet. R., Hofmann. H., and Hofmeister. H., (Dept. des Mater., Ecole Polytech. Federal de Lausanne, Switzerland), *Nanostruct. Mater. USA*, vol.9, no.1-8, p. 359-62, **1997.**

[27] Shek. C. H., Lai. J. K. L., Lin. G. M., Zheng. Y. H., and Lui. W. H., (Dept. of phys. & Mater. Sci., City Univ.of Hong Kong, Kowloon, Hong Kong), *J.Phys. Chem. Solids UK*, vol.58, no.1, p.13-17,Jan **1997.**

[28] Wang. Wendong., Zhu. Fengwa., Weng. Jun., Xiao. AJimei., and Lai. Wuyan., (Dept. of, Mater. Phys., Univ. of, Sci. & Technol. of China, Beijing, China), *Appl. Phys. Lett. USA*, vol.72, no.9, p.1118-20, March **1998.**

[29] Martino. D. M., Willigen. H. Van., and Spitler. T. M., (Dept. of Chem., Massachusetts Univ., Boston, MA, USA), *J. Phys. Chem. B, USA*, vol.101, no. 44, p.8914-19, Oct.**1997.**

[30] Jim. J., and Seraphin. S., (Dept. of Mater. Sci. & Eng., Arizona Univ., Tucson, AZ, USA), *J. Appl. Phys. USA*, vol.83, no.5, p.44-8, March **1998.**

[31] Pant. D., and Levinger. N. E., (Dept. of Chem., Colorado State Univ. Fort Collins, CO, USA), *Chem. Phys. Lett. Netherlands* ,vol.292, no.1-2, p.200-6, July **1998.**

[32] Harris. P. J. F., and Tsang. S. C., (Dept. of Chem., Reading. Univ., UK), Chem. Phys. Lett. Netherlands vol.293, no.1-2, p.53-8, Aug. **1998.**

[33] Wautelet. W., (Mons Univ., Belgium), *Phys. Lett. A Netherlands* ,vol. 246, no.3-4, p.341-2, Sept. **1998.**

[33] Oshima. Y., Hirayama. H., and Takayanagi. K., (Dept. of Mater. & Eng., Tokyo Inst. of Technol., Yokohama, Japan), *Electron Microscopy and Analysis* **1997.**

[35] Yeadon. M., Yang. J. C., Averback. R. S., Bullard. J. W., and Gibson. J. M., (Mater. Res. Lab., Illinois Univ., Urban, IL, USA), *Electron Microscopy and Analysis,* **1997.**

[36] Nakanishi. T., Ohtani. B., Shimazu. K., and Uosaki. K., (Lab. of Phys. Chem., Hokkaido Univ., Sapporo, Japan), *Chem. Phys. Lett. Netherlands,* vol.278, no.4-6, p.233-7, Oct.**1997.**

[37] Li. S., Silvers. S. J., and El-Shall. M. S., (Dept. of Chem., Virginia Commonwealth Univ., Richmond, VA, USA), *Advances in Microcrystalline and Nanocrystalline Semiconductor*, **1996.**

[38] Kezuka. H., and Zhang Qiang. Z. Xi., (Tokyo Eng. Univ., Tokyo, Japan), *Phys. C Netherlands* ,vol. 282-287, p.523-4, pt.2, Aug. **1997.**

[39] Pinizzotto. R. F., Rho. Y. G., Chen. Yandong., Pirtle. R. M., Pirtle. I. L., Coffer. J. L., and Li. Xin., (Dept. of Mater. Sci., North Texas Univ., Denton, TX, USA), *Advances in Microcrystalline and Nanocrystalline Semiconductors* – **1996.**

[40] Hongyou. Fan., Yuqing. Zhou., and Lopez. G. P., (Center for Micro-Engineered Ceramics, New Mexico Univ., Albuquerque, NM, USA), *Adv. Mater. Germany*, vol.9, no.9, p. 728-31, July **1997.**

[41] Majetich. S. A., Scott. J. H. J., McHenry. M. E., and Turgut. Z., (Dept. of Phys., Carnegie Mellon Univ., Pittsburgh, PA, USA), *Proceeding of the Symposium on Recent Advances in the Chemistry and Physics of Fullerenes and Related Materials.vol.3, Los Angeles, CA, USA*, May **1996.**

[42] Lee. C. L., Radojevic, B., Chen. F. R., and Perng. T. P., (Dept.of Eng. & Syst. Sci., Nat Tsing Hua Univ., Hsinchu, Taiwan), *Metall. Mater. Trans. A, Phys. Metall. Mater. Sci. USA*, vol.29A, no.1, p.131-7, Jan. **1998.**

[43] Uan. D. N., and Heilmann. A., (Inst. of Phys., Tech. Univ. Chemnitz, Germany), *Vacuum UK*, vol.49, no.1, p.51-7, Jan **1998.**

[44] Viera. G., Sharma. S. N., Costa. J., Zhang. R. Q., Andujar. J. L., and Bertran. E., (Dept. Fisica Aplicada Electron., Barcelona Univ., Spain), *Vacuum UK*, vol.48, no.7-9, p.665-8, Sept. **1997.**

[45] Iron. S. H., Nemchuk. N. I., Rohrs. H. W., Kowalewski. T., Faircloth. B. O., Krchnavek. R. R., and Ruoff. R. S., (Dept. of Phys., Washington Univ., St. Louis, MO, USA), *Proceeding of the Symposium on Recent Advances in the Chemistry and Physics of Fullerenes and Related Materials.vol.4, Montreal, Que., Canada,* 4-9 May **1997.**

[46] Jose- Yacaman. M., and Mehl. R. F., (Inst. de Fisica, Univ. Nacional Autonoma de Mexico, Mexico City, Mexico), *Metall. Mater. Trans. A, Phys. Metall. Mater. Sci, USA*, vol. 29A, no.3, p.713-25, March **1998.**

[47] Petroski. J. M., Wang. Z. L., Green. T. C., and El- Sayed. (Laser Dynamics Lab., Georgia. Inst. of Technol., Atlama, GA, USA), *J. Phys. Chem. B, USA*, vol.102, no.18, p.3316-20, April **1998.**

[48] Fukunaga. A. F., Chu. Shaoyan., and Mc Henry. M. E., (Dept. of Mater. Sci. & Eng., Carnegie Mellon Univ. Pittsburgh, PA. USA), *Proceeding of the Fourth Symposium on Low Temperature Electronics and High Temperature Superconductivity, Montreat, Que., Canada*, May **1997.**

[49] Setlur. A. A., Dai. J. Y., Lauerhaas. J. M., and Chang. R. P. H., (Dept. of Mater. Sci. & Eng., Northwesterm Univ., Evanston, IL, USA), *Carbon UK*, vol.36, no.5-6, p.721-3, **1998.**

[50] Hunt. E. M., Hampikian. J. M., Poker. D. B., and Evans. N. D. (Sch. of Mater. Sci. & Eng., Georgia Inst. of Technol., Atlanta, GA, USA), *Surf. Coot. Technol. Switzerland*, vol.103-104, p.409-14, May **1998.**

[51] Lauter - Pasyuk. V., Lauter. H. J., Ausserre, D., Gallot. Y., Cabuil. V., Kornilov. E. I., and Hamdoun. B., (Fakultat fur Phys., Konstanz Univ., Germany), *Phys. B, Netherlands*, vol.241-243, p.1092-4, Dec. **1997.**

[52] Babonneau. B. D., Bobonneau. D., Cabioch. T., Naudon. A., Girard. J. C., and Denanot. M., (Lab. de, Metall. Phys., Poitiers Univ., France) *Surf. Sci. Netherlands,*vol.409, no.2.p.358-71, July **1998.**

[53] Arunachalam.V., Marlow. W. H., and Lu. X. J., (Dept. of Nucl. Eng., Texas A & M Univ., College Station, TX, USA), *Phys. Rev. E. Stat. Phys. Plasmas Fluids Relat. Interdiscip.Top.USA*, vol.58, no.3, p.3451-7, Sept. **1998.**

[54] Mori. H., and Yasuda. H., (Res. Center for Ultra –High Voltage Electron Microscopy, Osaka Univ., Japan), *Bull. Mater. Sci. India*, vol.22, no.3, p.181-7, May **1999.**

[55] Moscovici. J., Michalowicz. A., Decker. S., Lagadic. I., Latreche. K., and Klabunde. K., (Groupe, de. Phys. Des Milieux, Uenses, Paris-12 Univ. Creteil, France), *Synchrotron Radiat.Denmark*, vol.6, no.3, p.604-6, May **1999.**

[56] Lyer. R., and Sastry. S. M. L., (Dept. of Mech. Eng.,Washington Univ., St. Louis, MO, USA), *Acta Mater.UK*, vol.47, no.10, p.3079-98, Aug. **1999.**

[57] Perez - Rodringuez. A., Garrido. B., Bonafos. C., Lopez. M., Gonzalez-Varona. O., Monrante. J. R., Montserrat. J., and Rodriguez. R., (Dept. d'Electron., Barcelona Univ., Spain), *J. Mater. Sci., Mater. Electron. USA*, vol.10, no.5-6, p.385-91, July **1999.**

[58] Liu. T., Guo. L., Tao. Y., Wang. Y. B., and Wang. W. D., (Inst. of High Energy Phys., Acad. Sinica, Beijing, China), *Nanostruct. Mater.USA*, vol.11, no.4, p. 487-92, **1999.**

[59] Hofmeister. H., (Max - Planck - Inst for Mikrostrukturphysik, Halle, Germany), *Mater. Sci. Forum Switzerland*, vol.312-314, p.325-32, **1999.**

[60] Dzhardimalieva. G. I., and Pomogailo. A. D., (Inst. of Chem. Phys., Acad. of Chemogolovka. Russia), *Phys. Adv. Technol.UK*, vol.9, no.8, p.527-35, Aug, **1998.**

[61] Cezar. J, C., Alves. M. C. M., Cruz. D. Z., Silva - da. F. C. S., Knobel. M., and Tolentino. H., (Nat. Synchrotron, Light. Lab., Campinas, Brazil), *Mater. Sci. Forum Switzerland*, vol.302-303, p. 38-42, **1999.**

[62] Oshima. R., Yamamoto. T. A., Mizukoshi. Y., Nagata. Y., and Maeda. Y., (Res. Inst. for Adv. Sci. & Technol., Osaka Prefecture Univ., Japan), *Nanostruct. Mater. USA.* vol.12, no.1-4, p.111-14, **1999.**

[63] Hofmeister. H., and Kodderitzsch. P., (Max – Planck - Inst. of Microstruct. Phys. Halle, Germany), *Nanostruct. Mater.USA*, vol.12, no. 1-4, p. 203-6, **1999.**

[64] Heilmann. A., Kiesow. A., Gruner. M., and Kreibig. U., (Phys. Inst., Tech. Hochschule Aachen, Germany), *Thin Solid Films Switzerland*, vol.343-344, p. 175-8, April **1999.**

[65] Gurinovich. J., Gurin. V. S., Lvanov. V. A., and Bodnar. I. V., (Inst. of Molecular & Atomic Phys., Acad. of Sci. Minsk, Byelorussia), *Proc. SPIE., Int. Soc. Opt. Eng. USA*, vol.3573, p. 268-71, **1999.**

[66] Lutzenkirchen - Hecth. D., Buchner. P., Uhlenbusch. J., Strehblow. H., and Frahm. R., (Inst. fuer Angewandte Phys., Duesseldorf Univ., Germany), *J. Synchrotron Radiat. Denmark*, vol.6, no.3, p.722-4, May **1999.**

[67] Zhonghua.Wu., Lin. Guo., Xin. Ju., Qianshu. Li., Hesun. Zhu., (Inst. of High Energy Phys., Acad. Sinica, Beijing, China), *J. Synchrotron Radiat. Denmark*, vol.6.no. 3, p. 749-51, May **1999.**

[68] Julian. C. De., Alcazar. G. A. P., Cebollada. F., Montero. M. I., Gonzalez. J. M., and Marco. J. F., (Inst. de Ciencia de Mater ., CSIC, Madrid, Spain), *J. Magn. Mater. Netherland*, vol.203, no. 1-3, p. 175-7, Aug. **1999.**

[69] Huijuan. Zhou., Weiping. Cat., and Zhang. Lide., (Inst. of Solid State Phys., Acad. Sinica, Hefei, China), *Mater. Res.Bull. USA*, vol.34, no.6, p.845-9, April **1999.**

[70] Tanaka. M., Takeguchi. M., and Furuya. K., (Nat. Rest. for Metals, Tsukuba, Japan*), Surf. Sci. Netherland*, vol.433-435, p. 491-5 Aug. **1999.**

[71] Lin. Guo., Hao. Wang., Xicheng. Ai., Qinglin. Yang., Yinghua. Zou., Qianshu. Li., and Hesun. Zhu., (Center for Res. on Mater. Sci., Beijing Inst. of Technol., China), *J. Beijing Inst. of Technol., China* , vol.8, no.1, p. 48 54, March **1999.**

[72] Sengupta. A., Jiang. B., Mandal. K. C., and Zhang. I, Z., (Dept. of Chem. California Univ. Santa Cruz. CA, USA, J. Phys. Chem. B,USA, vol.103, no. 16, p. 3128-37, April **1999.**

[73] Dante. S., Zhizhong. Hou., Subhash Risbud., and Stroeve. P., 9 Dept. of Chem, Eng. & Mater. Sci., California Univ., Davis. CA, USA), *Langmuir USA*, vol.15, no.6, p. 2176-82 March **1999.**

[74] Winkler. U., Eich. D., Chen. Z. H., Fink. R., Kulkarni. S. K., and Umbach. E., (Lehrstuhl fur Experimentelle Phys.2, Wurzburg Univ., Germany), *Phys. Status Solid A, Germany* , vol.173, no.1, p. 253-9, May **1999.**

[75] Goswami. R., Ryder. P., and Chattopadhyay. K., (Fachbereich Phys., Bremen Univ. Germany *), Philos. Mag. Lett. UK*., vol.79, no. 7, p. 481-9 July **1999.**

[76] Sun. C. O., (Sch. of Appl. Sci. Nanyang Technol. Univ., Singapore)., *J. Phys., Condens. Mater. UK*, vol. 11, no. 24, p. 4801-2, June **1999.**

[77] Buschmann. V., Klein. S., Fuess. H., and Hahn. H., (Fachbereich Materialwissenshaft, Tech. Univ. Darmstadt, Germany), *J. Cryst. Growth Netherlands,* vol.193, no.3, p.335-41, Qct.**1999.**

[78] Xu. B. S., and Tanaka. S. I., (Tanaka Solid Juction Project, Japan Sci. & Technol. Corp., Yokohama, Japan), *Acta Mater.UK*., vol.46, no.15, p.5249-57, Sept.**1998.**

[79] Jimenez. V. M., Caballero. A., Fernandez. A., Espinos. J. P., Ocana. M., and Gonzalez - Ellpe. A. R., (Inst. de Ciencia de Mater., CSIC, Sevilla, Spain.), *Solid State Ion, Diffus. React. Netherland*, vol.116, no.1-2, p.117-27, Jan. **1999.**

[80] Joshi. S. S., Patil. S. F., Lyer. V., and Mahumuni. S., (Dept. of Chem. Univ. of Pune, India), *Nanostruct. Mater. USA*, vol. 10, no.7, p. 1135-44. **1998.**

[81] Okui. M., Saitou. T., Ishikawa, Y., Shibata. N., and Ikuhara.Y., (Japan Fine Ceramics Center, Nagoya, Japan), *J. Ceram. Soc. Jap. Japan*, vol.106, no.12, p. 1255-8, Dec. **1998.**

[82] Gurin. V. S.,(Physico - Chem. Res. Inst., Minsk, Byelorussia), *Colloids. Surf. A, Physicochem. Eng. Aspects, Netherland*, vol. 142, no.1, p.35-40, Nov. **1998.**

[83] Svergun. D. I., Shtykova. V., E., Dembo. A. T., Bronstein. L. M., Platonova. O. A., Yakunin. A. N., Valetsky. P. M., and Khokhlov. A. R., (Inst. of Crystallogr., Acad. of Sci., Moscow. Russia), *J. Chem. Phys. USA*, vol.109, no.14, p.11109-16, Des. **1998.**

[84] Carrot. G., Plummer. C. J. G., Hilbord. J. G., Valmalette. JC., Scholz. S. M., Dutta. J., and Hofmann. H., (Polymer Lab., Swiss Federral Inst. of Tech., Lausanne, Switzerland), *Colloid Polym. Sci. Germany*, vol.276, no.10, p.853-9, Oct. **1998.**

[85] Andersson. O. E., Prasad. B. L. V., Sato. H., Enoki. T., Hishiyama,Y., Kaburagi. Y., Yoshikavwa. M., and Bandow. S., (Dept. of Chem.,Tokyo Inst. of Technol., Japan*), Phys. Rev. B., Condens. Mater USA*, vol.58, no.24, p.1638-95.Dec. **1998.**

[86]Carpenter. E. E., Connor. C. J. O., and Harris V. G., (Adv. Mater. Res. Inst., New Orleans Univ., LA, USA), *J. Appl. Phys. USA*.vol.85, no.8, p.5175-7, April **1999.**

[87] Scott. J. H. J., Chowdary. K., Turgut. Z., Majetich. S. A., and McHenry. M. E. (Microanal. Res. Group, Nat. Inst. of Stand. & Technol.), *Gaithersburg, MD, USA*, vol.85, no.8, p. 4409-11, April **1999.**

[88] Chem. Min., and Nikles. D. E., (Centre for Mater. for Int. Technol., Alabama Univ. Tuscaloosa. AL., USA), *J. Appl. Phys. USA*., vol.85, no.8, p.5504-6, April **1999.**

[89] Wakefied. G., Keron. H. A., Dobson. P. J., and Hutchison. J. L., (Dept. of Eng. Sci. Oxford Univ.UK), *J. Phys. Chem. Solids UK*., vol.60, no.4, p. 503-8. April **1999.**

[90] Jiang. B., Peng. J. L., and Bursill. L. A., (Sch. Of Phys., Melbourne Univ., Parkville, Vic., Australia), *Ferroelectrics Switzerland* ,vol. 207, no.3-4, p. 587-710, **1998.**

[91] Tsunekawa. S., Sahara. R., Kawazoe. Y., Ishikawa. K., (Inst. for Mater. Res., Tohoku Univ., Sendai. Japan), *Appl. Surf. Sci. Netherland*, vol.152, no.1-2, p.53-6, Nov.**1999.**

[92] Fukumi. K., Chayahara. A., Kageyama. H., Kadono, K., Akai, T., Kitamura. N., Mizoguchoi. H., Horino. Y., Makihara. M., Fujii. K., and Hayakawa.J., (Osaka Nat. Res. Inst., Japan), *J.Non – Cryst. Solids , Nitherland*, vol.259, p.93-9, Nov. **1999.**

[93] Zysler. R. D., Arciprete. C. P., and Dimitrijewits. M. I., (Inst. Balseiro, Centro Atomico Bariloche, Rio Negro, Argentina), *Proceedings of the fith Internationl Workshop on Non – Crystalline Solids. Non. Crystalline and Nanoscale Materials, Santiago de Compostela, Spain*, July **1997.**

[94] Ito.Y., Jain. H., and Williams. D. B., (Lehigh Univ., Bethlehem, PA, USA), *Phys. Lett. USA*, vol.75, no.24, p.3793-5, Dec. **1999.**

[95] Seung Jung. Jin., Won - Sil. Chae., McIntyre. R. A., Seip. C. T., Wiley. J. B., Connor. C. J. O., (Dept. of Chem., Kangnung Nat. Univ., South Korea). *Mater. Res. Bull.USA*, vol.34, no.9, p.1353-60, July **1999.**

[96] Jingfang. Zhou., Jianjun.Yang., Zhang. Zhijun., Liu. Weimin., and Xue. Qunji., (Inst. of Chem. Phys., Acad. Sinica, Lanzhou, China), *Mater.Res. Bull. USA*. vol.34, no.9, p.1361-7 July **1999.**

[97] Garcia – Bastida. A. G., Sanchez. R. D., Penedo. Gonzalez. A., Solla. J., Lopez- Quintela. M. A., Rivas. J., Ramos. C. A, and Zysler. R. D.,(Dept. de Fisica Aplicada y Quimica- Fisica, Santiago de Compostela Univ., Spain), *Proceeding of the Fifth International Workshop on Non-Crystalline Solid.Non-Crystalline and Nanoscale Materials, Santiago de Compostela, Spain*, July **1997.**

[98] Ramesh. S., Minti. H., Reisteld. R., and Gedanken. A., (Dept. of Chem., Barllan Univ. Ramat - Gan, Israel), *Opt. Mater. Netherland,* vol.13, no.1, p.67-70, Oct. **1999.**

[99] Hirano. T., and Namikawa.T., (Toppan Printing Co. Ltd., Saitama, Japan), *IEEE Trans. Magn. USA*, vol.35,no.5, pt.2, p.3487-9, Sept.**1999.**

[100] Bruni. S., Cariati. F., Casu. M., Lai. A., Musinu. A., Piccaluga. G., and Solinas. S., (Dipt. Di Chimica Inorg. Metallorg. Analitica, Milan Univ., Italy), *Nanostruct. Mater.USA*, vol.11, no.5, p. 573-86, **1999.**

Reff.Of CDRI. Lucvknow.

[101] Tew. Min. Wen, Miller, T. Jeffey., Bokhoven.Van., A., and Jeroen., (Institute for chemical and Bioengineering, ETH Zurich, 8093 Zurich, Switz.). *Journal of physical Chemistry* C, 113(34), 15140-15147, **2009.**

[102] Bratko., Dusan., Daub., D. Christopher., Luzzar., and Alenka., (Department of Chemistry, Virginia Commonwealth University, Richmond, VA 23284 - 2006 USA). *Xiv. org, e - Print Archive, Condensed Matter* Jun, **2008**

[103] Niu., Yong - xiao., Yi. Wang., En - de.Wang., and Jiafei. Fu., (School of Resources and Civel Engineering, Northeastern University, Shenyang, Peop. Rep. China 110004). *Dongbei Daxue Xuebao, Ziran Kexueban*, 29 (11), 1641- 1644 (Ch), **2008.**

[104] Martinson., A. Carol., and K. J., Reddy,. (Dupartment of Renewable Resources, College of Agriculture, University of Wyoming, Laramie, WY

82071 USA). *Journal of colloid and Interface Science*, 336 (2), 406- 411, **2009.**

[105] M. Mahmoudi., A.Simchi., A.S.Milani., A.Stroeve., (Institute for Nanoscience and Nanotechnology, Sharif University of Technology, Tehran, Iran). *Journal of colloid and Interface Science*, 332(2), 510-518, **2009.**

[106] Irena. Blute., Robert. Pugh., J. Robert., John.Van de Pas., Ian. Callaghan., (Inst. for Surface Chemistry,YKI, SE-114 86 Stockhoim, Swed.) *J. of Colloid and Interface Sci.*, 336(2), 584-591, **2009.**

[107]Haiyang. Cheng., Chunyu. Xi., Xiangchun. Meng., Yufern. Hao., Yu. Yanchun., and Fengyu. Zhao., (State Key Laboratory of Electroanalytical Chemistry, Changchun Institute of Applied Chemistry, Chinese Academy of Sci. Changchun, Peop. Rep. China 130022). *J. of Colloid and Interface Science*, 336(2) 675- 678, **2009**.

[108] S. Alencar, Wagner., Crespilho, N. Frank., Martins., V.A., Marccus., Zucolotto., Valtencir., Oliveira., N., Osvaldo., Jr.Silva., C.Welter., (Dept. de Quimica,C CN, Universidade Federal do Piaui, 64049-550 Brazil), *Phys. Chem. Chemical Physico*, 11 (25), 5086 5091, **2009.**

[109] Comba., Silvia., Sethi., and Rajandrea., (DITAG, Pept. di, Ingegneria del Territorio., Politechnico di Torino, Italy), *Water Res*.43(15), 3717-3726, **2009.**

[110] Il. Kim., Li. Haiqing., Nam Ho. Shin., Ha. Chang - Sik., Suh. Hongsuk., and Carl A.Batt., (Dept. of Polymer Science and Eng. Pusan National Univ. Pusan, 609-735 S.Korea). *Chem. Materials* 21(16) 3782-3787, **2009.**

[111] Niu. Dongxiao., Feng. Xiaolu., Cai. Xiangzhou., and Shen. Wernqing., (Shanghai Inst. of Applied Physics, Chiness Academy of Sci. Shanghai, Peop. Rep. China 201800). *He - jishu* 31(4), 307-311, **2008.**

[112]Ahmed. Jahangeer., Sharma. Shudhanshu., V. Ramanujachary. Kandalam., E. Lofland .Samuel., and K. Ashok. Ganguli., (Dept. of Chem. India Inst. of Tech. Hauz Khas, New Delhi, 110 016 India), *J. of Colloid and Interface Science*, 336 (2) 814-819, **2009.**

[113] Iwamoto., Takashi., Matsumoto., Kinya., Matsushita.,Toru., Inokuchi., Makoto., Toshima., and Naoki., (Dept. of Innovative and Eng. Materials.,Tokyo Inst. of Tech., 4259 Nagatsuta, Midori –ku, Yokohama., Kanagawa, Japan 226-8502) *J. of Colloid and Interface Science* 336(2), 879-888, **2009.**

[114] Giuffrida., Salvatore., Ventimiglia., Gioergio.,Sortino., and Salvatore. (Dept. di Scienz Chimiche, Univversita di Catania, I -95125 Catania, Italy), *Chem.Communications Cambridge, United Kingdom*, (27), 4055-4057, **2009.**

[115] Ghoul. Al., Mazen., Ghaddar., Tarek., Moukalled., and Tharwat.(Dept. of Chem. and Center for Advanced Mathematical Sci. American Univ. of Beirut, Beirut, Lebanon), *J. of Phys. Chem.*113(34), 11594-11603, **2009.**

[116] De. RogatiS., Loredana., Montini., Tiziano., Gombac., Valentina., Cargnello., Matteo. Fornasiero., and Paolo., (Chem. Dept. ICCOM - CNR Trieste Res. Unit, Center of Excellence for Nanostructured Materials and INSTM, Univ. of Trieste, 34127 Trieste, Italy), *Nanorods,Nanotubes and Nanomaterials Res.Progress* 71-123, **2008.**

[117] Gmucova. Katarina., Weis. Martin., Nadazdy.Vojtech., Capek. Ignac., Satka. Alexander., Chitu. Livia., Cirak. Julius., and Eva. Majkova., (Inst.of Phys., Slovak Acadmey of Sci., Bratislava, Slovakia SK - 845 110), *Applied Surface Science*, 254 (21) 7008-7013, **2008.**

[118] O. M. Lemine. (College of Sci. Phys. Dept., Al –imam Mohmmed Bib Saoud Islamic Univ. Riradh, Saudi ARABIA), *Superlattices and Microstructures* 45(6), 576-582, **2009.**

[119] L. Bischoff., B. Schimidt., H. Lange., and D. Donzev., (Inst. of Ion Beam Phys., and Materials Res. Foeschungszentrum Dresden Rossendorf, 01314 Dresden, Germany), *Nuclear Inst. & Methods in Phys.Res., Section B.Beam Interactions with Materials and Atoms* 267(8-9) 1372-1375, **2009.**

[120] G. Rizza., E. A., Dawi., A. M.,Vredenberg., I. Monnet., (Laboratoire des Solides Irradies, CEAIRAMIS - CNRS, Ecole Polytechnique, 91128 Palaiseau,Fr.*), Applied Phys. Letter* 95(4), 043105/1 -043105/3, **2009.**

[121] Mativetsky., M., Jeffrery., Fostner., Shawn., Burke., A. Sarah., and Grutter. Peter., (Dept. of Phys. McGill. Univ. Montreal, Can. H3A 2T8), *Phys. Review B,Condensed Matter and Materials Phys*. 80(4), 04530/1-04530/9, **2009.**

[122] Francesc. Neyman., M. Goerling., Andress. (Lehrstuhi fur Theoretische Chemie and Interdisciplinary Center for Interface Controlled Processes,Friedrich- Alexander- Univ. Erlangen - Nuernberg, D-91058 Eelangen, Germany). *J. of Pys. Chem. A* 133(43), 11963- 11973, **2009.**

[123] Van. Vegten., Niels., Haider. Peter., Maciejewski., Marek., Krumeich., Frank., Baiker. Alfons. (Inst.for Chem.and Bioengineering., Dept.of Chem.

and Applied Biosciences, ETH Zurich. CH- 8093 Zurich, Switz.), *J. of Colloid and Interface Science* 339(2), 310-316, **2009.**

[124] K. Siskova., B. Vlckova., P.- Y.Turpin., A. Thorel., A.Grosjean, (Dept. of Phys. and Macromolecular Chem. Charles University in Prague, Prague. Czech Rep. 128 40). *vibrational Spectroscopy* 48(1), 44-52, **2008.**

[125] M. Alloision., A. Demartini., C. Cuniberti., G. Dellepiane., M. Muniz-Miranda., and E.Giorgetti.,(INSTM and Dept. di Chimica E. Chimica Industriale, Univ.di Genova,16146 Genova, Italy). *Vibrational Spectroscopy* 48(1), 53-57, **2008.**

[126] I. G. Kovzun., I. M. Kovalenko., I. T., Protsenko., and Z. R. Uiberg., (Inst. Biokolloidnoi khim. im. F. D. Ovcharenko, NAN Ukr., Kiev, Ukraine 03680), *Nano sistemi, Nanomateriali, Nanotechnologii* 5(2) 445- 465, **2007.**

[127]S. Sh., Rekhviashvili., E. V., Kishtikov., and B. A. Rozenberg., (Kabardino - Balkarian State Uni. Nalchik, Russia), *Nano-I Mikrosistemnaya Tekhnika* (6), 4-9, **2008.**

[128] V. A., Tertykh., K. V. Katok., and V. V. Yanishpolskii., (Chuiko Inst. of Surface Chemistry .National Academy of Sci. of Ukraina, Kiev, Ukraine), *Russion, J. of Physical Chem*. 82(9), 1438-1441, **2008.**

[129] Say - Hwa. Tan., S. M. Murshed., Sohel., Nguyen, Nam - Trung., Wong., Neng. Teck., and Yobas. Levent., (School of Mechanical and Aesospace Eng. Nanyang Technological Univ., Singapore, 639798). *J. of Phys. D. Applied Physics* 41 (16), 165501/1-165501/7, **2008.**

[130] Sara. Fortuna., Colard., A. L. Catheline., Troisi., Alessandro., and A. F. Bon. Stefan. (Dept. of Chem. Univ. of Warwick, Coventry, UK CV4 7AL), *Langmuir* 25(21), 12399-12403, **2009.**

[131] Lee. Choongyeop., and Kim. Chang - Jan. (Mech. and Aeroscape Eng. Dept. Univ. of California, Los Angles (UCLA), Los Angeles, CA 90034 USA.) *Langmuir* 25(21) 12812 - 12818, **2009.**

[132] Ogawa. Atsushi., and Mizuo. Maeda., (Senior Res. Fellow Center, Ehime Univ.3 Bunkyo cho, Mastsuyama, Ehime, Japan 790-8577), *Chem. Communications (Cambridge,United Kingdom)* (31)4666-4668, **2009.**

[133] N. Hatami., and S. Ghader., (Dept. of Chem. Eng. College of Eng., Shahid Bahonar Univ. of Kerman, Iran 76175). *Crystal Res. and Technology* 44(9) 953-960, **2009**.

[134] Xia. Zhao. Yanxi., Tao. Huang., Liu. Hafnfan., and Liew. Kong.Yong., (Key Lab. of Catalysis and Material Sci. of the State Ethnic Affairs Commission & Ministry of Education , Hubei Provinvce, College of Chem. and Material Sci. South – Centeral Univ. for Nationalities, Wuhan, Peop. Rep. China 430074), *Applied Surface Sci*. 255(23), 9463- 9468, **2009.**

[135] Lu. Jiajuan., Li. Ying., Yan. Xiaomin., Shi. Baoyou., Wang. Dongsheng., and Tang. Hongxiao. (State Key Lab of Env. Aquate Chem. RCEES, Chinese Academy of Sci. Beijing, Peop. Rep. China 100085). *Colloids and Surface, a, Physicochemical and Eng. Aspect* 347(1-3), 90-96, **2009.**

[136] R. Houk. Levi., R. Challa. Sivakumar., Grayson., Benjamin., Paul. Fanson., and K. Abhaya. Datye., (Center for Microeng. Material, Univ. of

Nev Mexico, Albuquerque, NM 87131 – 0001 USA). *Langmuir* 25(19), 11225 – 11227, **2009.**

[137] S. Fall., O. Konovalov., M. Maaza., A. C. Beye., and A. Gibaud., (Lab. De Physque de I'Etat Condense, UMR CNRS 6087, Univ. du Maine, 72085 Le Mans, Fr.), *J. of Applied Crystallography* 42(2), 815 – 819, **2009.**

[138] S. Jenkins., S. R. Xirk., M. Persson., J. Carlen., and Z. Abbas (Dept. of Tech. Mathematics, CS Univ. West, SE 461 86 Trollhaettan Swed), *J. of Colloid and Interface Sci.* 339(2), 351- 361, **2009.**

[139] Singaravelu.Vivekanandhan., Misra. Manjusri., Mohanty., Amar Kumar (School of Eng. Univ. of Guelph, ON Can.N1G 2W1), *J. of Nanoscience and Nanotech*. 9(12), 6828 – 6833, **2009.**

[140] Singh. Fouran., S. Mohaptra., J. P. Stoquert., D. K. Avasthi., and J. C. Pivin., (Materials Sci. Group, Inter Univ. Accelerator Center , New Delhi, 110067 India), Nuclear *Instruments & Methods in Phys. Res. Section B. Beam Interactions with Materials and Atoms* 267(6), 936 – 940, **2009.**

[141] U. Thiele., I. Vancea., J. A. Archer., M. J. Robbins., L. Frastia., A. Stannard., E. Pauliac - Vaujour., C. P. Martin., M. O. Blunt., and P. J. Moriarty., (Dept. of Mathematical Sci., Loughorough Univ., Leicestershire, UK LE11 3TU). *J. of Phys. Condensed Matter* 21(26), 264016/1-264016/13, **2009.**

[142] F. Castez. Marcos., and V. Albano. Ezequiel., (Inst. de Investigaciones Fisicoquimics Teoricas y Aplicadas INIFTA, CCT La Plata, 1900 La Plata, Argent.). *J. of Phys. Condensed Matter*, 21 (26), 263001/1-263001/12, **2009.**

[143] J. M. Kyle. Bishop., Grzybowski., and A, Bartosz., (Dept. of Chemical Univ., Evanston, 60208 USA), *Chem. Phys. Chem*. 8(15), 2171- 2176, **2007.**

[144] Oberdisse., Julian., Hine. Peter., Pyckhout - Hintzen., Wim., (Mac Diarmid Inst. for Advanced Materials and Nanotechnology, School of Chemical and Phys. Sci., Victoria Univ. Wellington, N. Z.*)*, *Chem. in New Zealand* 71(1), 15-19, **2007.**

[145] W. Belkacem., N. Mliki.,. L.Bessais., S. Aouida.,W. Saikaly., and B. Yangui., (Lab. Materiaux, Organisation et Properietes, Faculte des Sci. de Tunis, Univ. El Manar II, Tunisia 2092), *AIP Conference Proceeding* , 935, **2007.**

[146] K. Pelzer., J. P. Candy., G. Bergeret., and J. M. Basset., (Dept.for Inorganic Chem., Fritz - Haber – Inst. of the Max – Planck - Socity, 14195 Berlin, Germany). *European Physical J. D. Atomic, Molecular, Optical and Plasma Phys*. 43(1-3)197-200, **2007.**

[147] Li. Shujin., Wu, Deyin., Xu. Xiaoyan., Gu. Renao (Dept. of Chem, Suzhou Univ. Suzhou, Peop. Rep. China 215006), *J. of Raman Spectroscopy*, 38(11), 1436 – 1443, **2007.**

[148] S. Kilin. Dmitri., V. Oleg. Prezhdo., Xia. Younan., (Dept. of Chem. Univ. of Florida, Gainesville, FL 32611 USA). *Chem. Phys. Letters* 458 (1-3), 113 -116, **2008.**

[149] Aubry. Nadine., and Singh. Pushpendra (Dept. of Mech. Eng., Carnegie Mellon Univ., Pittsburgh., PA 15213USA). *Phys. Rev. E, Statistical, Nonlinear, and Soft Matter Phys.* 77(5-2),056302/1- 056302/11, **2008.**

[150] Kim. Kwan., Lee. Hyang Bong., Lee. Ji Won., Kun. Park. Hyoung., and Soo. Shin. Kuan., (Dept. of Chem. Seoul National Univ. Seoul., 151-742 S.Korea). *Langmuir* 24(14), 7178- 7183 , **2008.**

[151] Culha. Mustafa., Kahraman. Mehmet., Tokman. Nilgun., and Guler. Turkoglu., (Faculty of Eng. and Architecture, Dept. of Genetics and Bioeng. Yeditepe Univ., Kayisdagi – Istanbul, Turk. 34755). *J. of Physical Chem*.C., 112(280, 10338 – 10343, **2008.**

[152] P. Om. Khatri., Kosaku. Adachi., Kuniki. Murase., Ken - ichi. Okazaki., Tsukasa. Torimoto., Nobuo. Tanaka., Kuwabata. Susumu., and Hiroyuki. Sugimura., (Dept. of Materials Sci. and Eng., Kyoto Univ. Sakyo – ku, Japan 606 - 8501), *Langmuir*,. 24(15), 7785 – 7792, **2008.**

[153] Chang. Moon - Hwan., Dosev. Dosi., M. Ian. Kennedy., (Dept. of Mechanical and Aeronautical Eng.,Univ. of Californiya Davis, CA 95616 USA). *Sensors and Actuators, B.Chem.* B124(1), 172- 178, **2008.**

[154] Fahmi. Amir., Barragan. Susana Prieto., D' Aleoa. Anthony., M. Rene. Williams., van Heyst. Jeroen., De. Cola. Luisa., and Fritz.Vogtle., (School of Phys. and Astronomy, The Univ. of Nottingham, UK NG72RD). *Materials Chemistry and Phys*. 103(2-3), 361 – 361, **2007.**

[155] J. L. Lu., J. Weissenrieder., S. Kaya., H. J.Gao., S. Shaikhutdinov., and H, -J. Freund., (Beijing National Lab. of Condensed Matter Phys., Inst. of Phys., Chem. Chinese Academy of Scinces, Beijing, Peop. Rep. China 100080). *Surface Rev. and Letters* 14(5), 927-934, **2007.**

[156]A. G. Cormack. Peter., Hernandez – Santana. Aaron., R. Arun. Prasath., McKenzie. Fiona., Graham. Duncan., and W. Ewen. Smith., (West

Chem. Dept. of pure and Applied Chem. Univ. of Strathclyde, Glasgow, UK G1 1XL). Chem. *Communications Cambridge, United Kingdom*) (22), 2517-2519, **2008.**

[157] Song. Lixin., Yeng. Lam. Ming., Boothroyd, Chris, Teo. Puat. Wen., (School. of Material Science and Eng. Nanyang Technological Univ. Singapore, 639798). *Nanotechnology* 18(13), 13565/1- 135605/6, **2007.**

[158] Zhang. Wanzhong., Qiao. Xueliang., Chen. Jianguo., and Wang. Hongshui (State key Lab. of Die and Mould Technique, Huazhong Univ. of Sci. and Tech., Wuhan, Peop. Rep. China 430074*). Huagong Jinzhan* 23(10), 1067 – 1071, **2004.**

[159] Lin. Ming - Nung., C. Y. Liu., W. N. Liu., M. Y. Lai., C. Y. Peng., H. H. Wang., Y. L. Wang., Lin. Minn - Tsong (Dept. of Phys., National Taiwan Univ.,Taipei, Taiwan 106), *Nanotechnology*. 17(1), 315 – 319, **2006.**

[160] Pan. Bifeng., Cui. Daxiang., Gao. Feng., He. Rong., (Dept. of Bio Nano Sci. and Eng. National Key Lab. of Nano/Micro Fabrication Technology, Key Lab. For Thin Film and Microfabrication of Ministry of Education, Inst. of Micro and Nano Rep. China 200030). *Nanoscience*, 11(2), 95 -101, **2006.**

[161] Chu. Maoquan., Liu, Guojie. (Inst. of Life Sci. and Technology, Tongji Univ.Shanghai, Peop. Rep. China 200092), *J. of Metastable and Nanocrystalline Materials* 26, 22-28, **2005.**

[162] Li - Ping. Yang, and Tu. Wei – Xia (Key Lab. Nanomater. Ministry of Education, Div. Mol.and Mater. Simulation, Dep. Chem. Eng. Beijing Univ.

Chem. Technol., Beijing, Peop. Rep. China 100029). *Wuli Huaxue Xuebao* 22(4), 513 – 516, **2006.**

[163] Yin. Hong – Zong., Chem. Lang – Xing., Li. Wen – You., He. Xi-Wen., (Dept. of Chemistry, Nankai Univ.Tianjin, Peop. Rep. China 300071). *Huaxue Xuebao,* 64 (70, 617 – 622 (Ch), **2006.**

[164] Kle - Imann, Joerg., Leocoultre. Guy., Papastavrou. Georg., Jeannenert. Stephane., Galletto. Paolo., Kaolo., J. M. Koper. Ger. and Borkvec. Michal, (Dept. of Inorganic, Analytical, and Appied Chem. Univ. of Geneva, CH - 1211 Geneva 4, Switz). *J. of Colloid and Interface Sci*. 303 (2), 460 471, **2006.**

[165] Laaksonen. Timo., Pelliniemi, Quti., and M. Quinn. Bernadette., (Lab. of Phys. Chem. and Electrochemistry, Helsinki Univ. of Technogy, FIN – 02015 HUT Helsinki, Finland), *J. of the American Chemical Society* 128(44), 14341 – 14346, **2006.**

[166] Tanaka. Akinori., Imamura. Masaki., and Yasuda. Hidehiro. (Dept. of Mech. Eng., Faculty of Eng. Kobe Univ. Nada - Ku, Kobe, Japan 657-8501), *Phys. Rev., B. Condensed Mater and Materials Physics* 74(11), 11340/1- 113402/4 , **2006.**

[167] M. Sathish.,Viswanathan. B., and R. P. Viswanath., (Dept. of Chem. India Inst. of Tech. Madras, Chennai, 600 036 India). *International J. of Hydrogen Energy* 31(7) , 891 – 898, **2006.**

[168] Weeraman. Champika., K. Yatawara. Achani., N. Bordenyuk. Andrey., and V. Benderskii. Alexander., (Dept. of Chem. Wayne State

Univ., Detroit, MI 48202 USA). *J. of the American Chemistry Society* 128(44), 14244 – 14245, **2006.**

[169] Sun. Yuan., I. Frenkel. Anatory., Isseroff. Rebecca., Cheryl. Shonbrun., Forman. Michelle., Shin. Kwanwoo., Koga.Tadanori., White. Henry., Zhang. Lihua., Zhu. Yimei., H. Rafailovich. Miriam., and C.Sokolov. Jonathan., (Dept. of Materials Sci. and Eng., State Univ. of New York at Stony Brook, Brook, NY 11794 – 2275 USA). *Langmuir* 22(2), 807-816, **2002.**

[170] J. Solla – Gullon., F. J. Vidal – Iglesias., E. Herrero., J. M. Feliu., and A. Aldaz., (Dept. de Quimica – Fisica, Inst. de Electroquimica, Univ. de Alicante, Spain 03080). *Electrochem. Communication* 8(1), 189 – 194, **2006.**

[171] Li. P., J. Liu., N. Nag., P. A. Crozier., (TEM Lab., Dept. of Earth and Planetary Sciences, Univ.of New Mexico, Albuqueque, NM 87131 USA). *Surface Sci*. 600(3), 693 – 702, **2006.**

[172] Matsumoto. Kazuaki., Tsuji. Ryotaro., Yonemushi.Yoshiharu., and Yoshida.Tatsushi (Adv. Polymer Materials Res. Laboratories, Advanced Polymer Materials R & D Center, Corporate Res. & Development Division, KANEKA Corporation, 5 – 1 -1 Torikai – Nishi Settsu, Osaka, J.566 0072), *J. of Nanoparticle Res*. 6(6), 649 – 659, **2004.**

[173] Dan. Zhang., Song. Ximing., Zhang. Rongwei., Ming. Zhang., and Liu. Fengqi (College of Chemistry, Jilin Univ, Changchun, Peop.Rep. China 130023). *European J. of Inorganic Chem.,* (9), 1643 – 1648, **2005.**

[174] A. Correa – Durate. Miguel., M. Luis Liz. Marzan., (Dept. de Quimica Fisica, Universidade de Vigo, Spain 36310). *J. of Materials Chemistry*, 16(1), 22 – 25 , **2006.**

[175] Anant. Mathur., Brown. Ari. David., and Jonah. Erlebacher., (Dept. of Materials Sci. and Eng. and Dept. of Chemical and Biomolecular Engineering Johns Hopkins Univ.Baltimore, MD 21218 USA), *Langmuir* 22(2), 582 – 589, **2006.**

[176] Aryal. Santosh., B. K. C. Remant., N. Dharmaraj., Narayan. Bhattarai., Kim. Chi. Hun., and Kim. Hak. Yong., (Dept. of Bionanosystem Eng., Chonbuk National Univ., Jeonju, 561 – 756 S.Korea). *Spectrochimica Acta , Pat A, Molecular and Biomolecular Spectroscopy* 63A(1), 160 – 163, **2006.**

[177] Li. Ziyou., Yuan. Jun., Yu. Chen., E. Richard. Palmer., and P.Jess Wilcoxan., (Nanoscale Physico Res. Lab., School of Physics and Astronomy, Univ. of Birmingham, UK, B15 2TT), *Advanced Materials Weinheim, Germany*, 17(23),2885 – 2888, **2005.**

[178] Zhou. Yong., Ji. Qingmin., Masuda. Mitsutoshi., Kamiya. Shoko., Shimizu. Toshimi CREST, Japan Sci. andv Tech., Agency JST, Ibaraki, J.305 – 8562). *Chem. of Materials*, 18(2), 403- 406, **2006.**

[189] S. Calvin., S. X. Luo., C. Caragianiis – Broadbridge., J. K. Mc Guinness., E.Anderson., A. Lehman., K. H. Wee., S. A. Morrison., and L. K. Kurihara., (Sarah Lawrence College, Bronxville, NY 10708 USA). *Applied Phys.Letter*, 87(23), 233102/1 – 233102/3, **2005.**

[180] Mallick. Kaushik., J. Mike Witcomb., and S. Mike Scurrell., (Molecular Sci. Inst, School of Chemistry, Univ.of the Witwatersrand,

WITS 2050 S. Afr.). *Materials Sci. & Eng., C, Biomimetic and Supramolecular Systems* 26(1), 87 – 91, **2006.**

[181] J. Toudert., S. Camelio., D. Babonneau., M. - F. Denanot., T. Girardeau., J. P. Espinos., F. Yubero., and A. R. Gonzalez – Elipe., (Lab.de Metallurgie Phys., Unite Mixte de Recherche UMR, Centre National de la Res. Scientifique CNRS 6630 – Univ. de Poitiers, 86962 Futuroscope Chasseneul, Fr.). *J. of Appied Physics*, 98(11), 114316/1- 114316/10, **2005.**

[182] Yang. Hanmin., Yang. Ming., and Guo. Rong. (Wuhan Polytechnics Univ, Wuhan, Peop. Rep. China). *J. of Dispersion Sci. and Tech*., 26(4), 477 – 482, **2005.**

[183] K. Lim. Sung., S. Ik. Chun., S. Ki. Ban., S. Chong. Yoon., K. Chang. Kim., H. Young. Kim., (Division of Materials Sci. and Eng., Hanvang Univ., Seoul, 133 – 791 S. Korea). *J. of Colloid and Interface Sci.,* 295(1), 108 – 114, **2006.**

[184] Kuo. Ping. Liang., Jyh. Wuu., and Fu - Yu. Wang., (Dept. of Chem. Eng., National Cheng Kung Univ., Tainan, Taiwan 0101). *Colloid and Polymer Sci.* 284(4), 435 – 442, **2006.**

[185]Van. Herrikhuyzen. Jeroen., A. J. Rene. Janssen., E. W. Meijer., C. J. Stefan. Meskers., P. H. J. Albertus. Schenning., (Lab., of Macromolecular and Organic Chem., Eindhoven Univ., of Tech., 5600 MB Eindhoven, Neth), *J. of the American Chemcal Socity*,128(3), 686 – 687, **2006.**